Titre: Title:	Axial convection enhanced laser CVD of carbon rods
Auteur: Author:	Ram Kiran Goduguchinta
Date:	2006
Type:	Mémoire ou thèse / Dissertation or Thesis
Référence: Citation:	Goduguchinta, R. K. (2006). Axial convection enhanced laser CVD of carbon rods [Ph.D. thesis, École Polytechnique de Montréal]. PolyPublie. https://publications.polymtl.ca/8513/

URL de PolyPublie: PolyPublie URL:	https://publications.polymtl.ca/8513/
Directeurs de recherche: Advisors:	
Programme: Program:	Unspecified

UNIVERSITÉ DE MONTRÉAL

AXIAL CONVECTION ENHANCED LASER CVD OF CARBON RODS

RAM KIRAN GODUGUCHINTA
DÉPARTMENT DE GÉNIE MÉCANIQUE
ÉCOLE POLYTECHNIQUE DE MONTRÉAL

THÈSE PRÉSENTÉE EN VUE DE L'OBTENTION
DU DIPLÔME DE PHILOSOPHIAE DOCTOR
(GÉNIE MÉCANIQUE)
DÉCEMBRE 2006

Your file Votre référence
ISBN: 978-0-494-24539-2
Our file Notre référence
ISBN: 978-0-494-24539-2

UNIVERSITÉ DE MONTRÉAL

ÉCOLE POLYTECHNIQUE DE MONTRÉAL

Cette thèse intitulée :

AXIAL CONVECTION ENHANCED LASER CVD OF CARBON RODS

Présentée par : GODUGUCHINTA Ram kiran
en vue de l'obtention du diplôme de : Philosophiae Doctor
a été dûment acceptée par le jury d'examen constitué de :

M. FORTIN Clément, Ph.D., président
M. PEGNA Joseph, Ph.D., membre et directeur de recherche
M. MUREITHI Njuki W, Ph.D., membre
M. WILLIAMS Kirk L, Ph.D., membre

ACKNOWLEDGEMENTS

I recall reading quite a while ago that a person's current position is influenced by the path he/she has trodden. I truly believe it applies to any endeavor, for every decision taken during the course of any project has an effect on its outcome. In hindsight, when I look back at my decision to move to Canada to pursue my doctorate degree, I have nothing but satisfaction. This, I believe is due in large part to my advisor Dr. Joseph Pegna. I thank him for his support throughout the course of this work, the confidence he expressed in me which I myself lacked at times, and most of all, for being a nice human being. I can still recall all the weekends we spent working together in the lab trying to learn and build the LCVD system together. I finally thank him for making me a decent handyman.

I thank Dr. Mats Boman for being a source of support and inspiration over the last 6 years. I also express my gratitude to Ana and Patricia for their moral support during their stay at polytechnique. They have always been there to lend a ear to vent my anxiety.

Over the course of this work, many individuals extended their support in different ways. I thank Mr. Jean-Paul Levesque for the technical support and advice he extended on demand. I thank Mr. Sylvain Simard for his assistance in LABVIEW programming. My kudos to the National Instruments community for their wonderful technical support. I extend my thanks to all our industrial suppliers (Newport, Specialty Glass Products, Polycontrols etc). A special mention is due to Mr. Josef Slanik (Technospin) for the verve he brought to discussions and for building the pickup system. Finally, I thank our office staff, in particular Ms. Jeanne Daunais for her exuberance and quick handling of paperwork.

On a personal front, life in Montreal wouldn't have been memorable, if it was not for my friends: Purushotham, Keerthi, Karthikeyan, Jocelyn, Christophe, Samy, and many

more. I thank all my colleagues at Pavilion J.-Armand Bombardier who have made work a pleasure. I would also like to thank all the support staff of Pavilion Bombardier.

Last, but not the least, I am greatly indebted to my parents and my brother. As much as it may seem clichéd, they have always been there to support me unconditionally. I do not have words to express my gratitude to them. Finally, I thank all my extended family members: grandparents, uncles, aunts and cousins for being such a wonderful family.

RÉSUMÉ

Une nouvelle technique de croissance de bâtonnets de carbone par *déposition de vapeurs chimiques assistée par laser (LCVD pour l'acronyme Anglais du nom courant du procédé « Laser Induced Chemical Vapor Deposition »), amplifiée par convection coaxiale* a été démontrée pour la première fois à l'air libre. Cette nouvelle approche ouvre la voie à un contrôle en temps réel des diamètres et taux de croissance à partir de d'images en temps réel de l'extrémité du bâtonnet prises sur une longueur d'onde de 656 nm, correspondant à la signature de la première transition de l'hydrogène émis durant la pyrolyse du précurseur. Ces mesures indiquent une forte variation des taux de croissance transitoires dans la focale. Une analyse approfondie des propriétés variationelles des taux de croissance en régime transitoire a permis de mettre au point une méthode intrinsèque d'identification du plan focal et de caractériser l'efficacité énergétique linéaire et molaire du procédé. Cette approche a permis la réalisation du tout premier contrôle en boucle fermée d'un système de croissance de bâtonnets par déposition de vapeurs chimique assistée par laser. Cette réalisation s'est concrétisée par la génération des plus longs filaments de carbone jamais obtenus par une technique de LCVD.

La précision qu'apporte cette nouvelle technique a rendu possible une étude scientifique détaillée de l'influence de la position du front de croissance dans la région focale sur la microstructure et les propriétés mécaniques des bâtonnets. L'intégration informatique des différents sous-systèmes a permis de réaliser un système entièrement automatisé.

Les techniques de dépositions par LCVD sont utilisées depuis plusieurs années pour déposer une grande variété de bâtonnets et de structures tridimensionnelles plus complexe dont les dimensions vont de quelques millimètres à une fraction de micron. Toutefois l'extrême sensibilité du procédé aux températures de déposition a toujours représenté une barrière à la reproductibilité des caractéristiques microstructurelles. Nos travaux ont permis, d'une part une meilleure connaissance de la phénoménologie du

procédé, et d'autre part ont été mis en œuvre dans la création d'un contrôle en boucle fermée du procédé.

La convection axiale forcée des précurseurs est assurée par une conception utilisant des micro tubes coaxiaux au filament; ce qui a permis de démontrer une amplification des taux de croissance du carbone. Les taux de croissance enregistrés sont les plus importants observés à date pour une pression de 1 bar. Qui plus est, la convection axiale semble éliminer les limitations du taux de croissance avec l'augmentation de la puissance laser observée dans les travaux antérieurs.

Le taux de croissance en LCVD est fortement dépendant de la température et influence la microstructure du dépôt obtenu. Or ces taux de croissance n'ont été mesurés en temps réel que par des méthodes optiques impliquant une intervention humaine, ou qu'à posteriori en mesurant l'accrétion de matériau. Nous savons maintenant qu'il est critique d'obtenir une mesure précise du taux de croissance en temps réel afin d'établir une relation fiable avec la microstructure. Dans la première partie de nos travaux (*ARTICLE 1: Position dependence of growth rate in convection enhanced laser CVD of carbon rods*) des bâtonnets de carbones furent obtenus dans une configuration à deux écoulements concentriques. L'écoulement intérieur fournit le précurseur chimique (éthylène) alors que l'écoulement périphérique délivre un écran d'Argon destiné à encapsuler la réaction et la protéger de l'air ambiant. L'émission à 656 nm de l'hydrogène alpha produit par la réaction a permis une observation précise en temps réel du diamètre et du taux de croissance du bâtonnet le long de son axe. Ces observations ont permis d'établir pour la première fois une relation entre le taux de croissance et la position du front dans la région focale.

Un système de trois écoulements coaxiaux présenté dans le second article (*ARTICLE 2: On the importance of focus tracking in LCVD growth of carbon rods*) a permis d'éliminer toute ambiguïté introduite par le mélange des fluides dans un système à deux

écoulements. Il nous a permis de conclure de façon décisive quant a l'existence d'un régime transitoire dans la région focale. L'absence d'une croissance uniforme dans la région focale met en lumière l'importance de maintenir le front de croissance en position constante dans la région focale afin d'assurer que les propriétés physiques du dépôt soient reproductibles.

Une série d'expériences furent conduites durant lesquelles les différents paramètres du procédé furent perturbés, tels que la distance du front au tube, la puissance laser, et la position relative du tube et de l'optique. Les résultats de ces expériences et l'analyse des résultats sont consignés dans notre troisième article. Notre analyse débouche sur une méthode qui permet la détermination de la position du plan focal intrinsèque au procédé. Les mesures permettent alors de montrer que les taux de croissances maximaux sont obtenus bien en avant de la focale, a une distance environ un ordre de grandeur de plus que la longueur de Raleigh. Ce résultat est particulièrement surprenant et va à l'encontre d'une hypothèse répandue dans la littérature relative au LCVD, qui veut que le taux de croissance soit maximal sur le plan focal. Une analyse variationelle des résultats permet de quantifier l'efficacité énergétique du procédé et démontre son importante variabilité sur une distance de l'ordre de dix fois la longueur de Raleigh en avant de la focale.

La variabilité importante des taux de croissance et de l'efficacité énergétique soulignent l'importance que revêt un contrôle en boucle fermée de la croissance des bâtonnets. Le système développé permet de maintenir le front de croissance à une position constante dans la focale qui produit le taux désiré. Des images du front de croissance capturées en temps réel ont permis de maintenir ce front en position constante alors que le filament était tiré en continu. *Les filaments de carbone ainsi obtenus sont les plus longs jamais produits*. Le contrôle réalisé représente une première tentative de développement d'un système de production de filaments et bâtonnets entièrement automatisé. L'intégration informatique des divers sous systèmes réduisent l'intervention d'opérateurs et améliore

la précision et la répétitivité des mesures des paramètres du procédé, ce qui ouvre la voie pour la transition du LCVD du laboratoire à l'application industrielle.

ABSTRACT

A novel *Axial Convection Enhanced Laser Chemical Vapor Deposition (LCVD)* setup facilitated the growth of carbon rods in chamber-free open-air conditions. The axial convection configuration paved the discovery of a real-time in-situ rod growth rate and diameter measurement technique. The technique utilizes the 656 nm hydrogen-alpha emission during precursor pyrolysis to track the growth rate and diameter of the rod along its axis. Real-time measurement of rod growth rate along its axis points to transient growth rates that appear to vary greatly inside the growth region. An in-depth analysis of variational properties of the observed transient growth rate yielded a method to identify the focal plane intrinsic to the process and characterize its linear and molar energetic efficiency. Also, *this work marks the development of a first-of-its-kind closed-loop automated LCVD rod growth system yielding the longest LCVD carbon rods to date.* Precise control afforded by the closed-loop system can help in investigating the effect of the position of the rod growth front within the laser-induced growth region on the obtained microstructure and mechanical properties of the rods. Integration and communication between various LCVD sub-systems aided in realizing a turn-key hands-free LCVD system.

Over the years, LCVD has been used to deposit a wide variety of materials as rods and more complex 3D-structures ranging in size from millimeters to sub-microns. However, the high sensitivity of the process to deposition temperature has caused control problems in obtaining structures with reproducible microstructural characteristics. The results of this work (1) helped gain a better understanding of the process behavior which has been (2) put to use by the implementation of a closed-loop controlled growth algorithm.

Axial convection enhancement offered by the developed LCVD system's coaxial tube design was found to have a positive impact on the growth rate of the produced carbon rods. In fact, growth rates observed are the highest to date at an operating pressure of 1

bar. Furthermore, axial convection enhancement seems to eliminate growth rate saturation witnessed in prior growth rate variation plots as a function of laser power.

Growth rate---a temperature dependent process characteristic which has been found to be influential in determining the resulting deposit microstructure---has predominantly been measured either online via optical means using human intervention or offline by deposit length measurements causing uncertainties in reported growth rate values. This being said, it is crucial to obtain accurate growth rate values in-situ and in real-time to form a reliable growth rate-microstructure correlation. In the first part of this work (*ARTICLE 1: Position dependence of growth rate in convection enhanced laser CVD of carbon rods*), carbon rods were grown using a two-tube axial flow configuration that allowed the precursor (ethylene) to be delivered coaxially to the growing rod in the inner tube. Argon was delivered through the outer tube as a protective shroud to encapsulate the reaction zone from the ambient. The 656 nm hydrogen-alpha emission produced during precursor pyrolysis allowed accurate in-situ real-time monitoring of the position, growth rate, and diameter of the produced rod along its axis. Obtaining the growth rate along the rod axis essentially provides a "*growth rate map*" throughout the laser-induced growth region.

Work done with a three-tube coaxial flow system (*ARTICLE 2: On the importance of focus tracking in LCVD growth of carbon rods*) eliminated flow mixing issues encountered in the two-tube system and further bolstered the existence of an unsteady transient growth rate phenomenon witnessed in the growth region. The absence of a steady-state growth region has brought to light the importance of the need for a control system to maintain the rod growth front at a particular position in the growth region to obtain desired material properties in a reproducible manner.

Experiments conducted by perturbing different process parameters such as laser power, overhang differential of the coaxial tube exit, and position of the rod tip in the laser focal

region allowed the determination of the position of the focal plane intrinsic to the process and express positional growth rate measurements in the focal plane of the laser beam (*ARTICLE 3: Variational analysis of LCVD rod growth*). Results point to growth rates that peak ahead of the laser focus by a distance about one order of magnitude larger than the Raleigh range. This result is surprising considering the general assumption in LCVD literature that peak growth rate occurs always at the laser focus. Variational analysis also allowed quantifying the process' energetic efficiency while simultaneously highlighting the variability of the process within the first 10 Raleigh ranges ahead of the focal plane.

Results pointing to a great variability in growth rate and energetic efficiency within the laser focal region culminated in the development of a closed-loop automated LCVD rod growth system. The closed-loop system is capable of maintaining the rod growth front at a desired position (preselected from the growth rate map) in the laser focal region yielding the desired growth rate. Real-time image analysis of the 656 nm hydrogen-alpha emission was used as a feedback to position as well as maintain the rod growth front. *Carbon rod samples grown using the automated LCVD system are the longest to date.* An attempt was made to develop a turn-key LCVD system for hands-free synthesis of rods and rod based structures. Integration of various LCVD sub-systems minimized operator intervention and improved measurement accuracy and repeatability. The turn-key system marks a step forward in the metamorphosis of LCVD into an industrial tool.

CONDENSÉ EN FRANÇAIS

Le progrès technologique est souvent lié aux avancées dans les domaines des matériaux et procédés. L'un des domaines de la science des matériaux qui a été l'objet de recherches intensives durant ces dernières décennies est la science des composites. Les applications des composites sont variées et s'étendent des articles de sports, tels que les clubs de golf, à l'aérospatiale. La composante maîtresse des composites est bien souvent la *fibre*, qui confère au matériau ses propriétés physiques et mécaniques.

Au sens général, une fibre n'est jamais qu'une structure d'aspect très élancé. Mais lorsqu'elle est intégrée à une matrice elle confère à la structure résultante des propriétés recherchées. La demande croissance pour des matériaux qui soient rigides, résistants, et de faible densité justifie l'importance croissante qu'ont acquise les fibres dans un passé récent. Elle permettent d'orienter la phase de renfort et par conséquent, l'utilisation en service extrême. Les besoins futurs en matières de fibres adressent principalement trois domaines : Application structurales, génération de puissance, aérospatiale. Ces domaines d'applications demandent des fibres à haute résistance, résilientes, résistantes au fluage, résistantes à l'oxydation à haute température, chimiquement stables, de faible densité (pour les applications dans lesquelles le poids est un facteur critique). Les fibres possédant certaines ou toutes les propriétés citées sont communément appelées *« fibres à haute performance »* (ou *HPF*). En dépit des techniques bien établies pour certaines fibres d'usage courant, le développement de nouvelles HPF est une proposition onéreuse, qui requiert des investissements massifs et à long terme. Le cycle typique du développement d'une nouvelle HPF est estimé entre douze et vingt ans. L'une des approches qui semblent prometteuses pour contourner les obstacles à la fabrication conventionnelle des fibres sont les techniques de déposition de vapeur chimiques assistée par laser (ou LCVD).

Le LCVD est un procédé qui permet l'accrétion de matière sur un substrat au sein de la focale d'un faisceau laser par dissociation thermique d'un précurseur gazeux. L'état de l'art en matière de LCVD montre que ce procédé peut être utilisé pour déposer non seulement des fibres, mais aussi une gamme d'objets tridimensionnels complexes constitués d'un large éventail de matériaux. Ceci dit, il reste néanmoins bon nombre d'opportunités de recherche ouvertes dans le domaine. En particulier :

1. Il a démontré que le LCVD peut représenter une augmentation des taux de production d'un ordre de grandeur comparé aux méthodes plus conventionnelles de production de fibres. Toutefois la faible productivité associée au LCVD en a limité l'usage commercial. Une viabilité industrielle du procédé requiert donc une augmentation encore plus soutenue du taux de croissance.
2. Le LCVD est encore loin d'être suffisamment bien contrôlé. Les microstructures des fibres produites sont extrêmement sensibles aux paramètres du procédé. Si le LCVD doit un jour revêtir un caractère industriel pour la production de fibres, un contrôle approprié de la croissance sera nécessaire.
3. Les longueurs de fibres communément produites par LCVD sont limitée en général à 0.5 cm. De plus, il n'existe aucune démonstration que la synthèse de fibres en continu par LCVD est possible. Si le procède doit revêtir un jour un caractère industriel, il est critique de démontrer son aptitude à produire des mono filaments continus.

Deux approches sont présentées dans la littérature pour améliorer le taux de croissance des fibres en LCVD. (1) Une augmentation de la pression du réacteur et, (2) l'utilisation d'un jet de précurseur forcé pour stimuler le transport. Une quantité importante de recherches ont versé sur le dernier point. Nos travaux présentent une nouvelle approche dans laquelle l'apport de précurseur est assuré par un écoulement forcé coaxial à la fibre et orientée dans sa direction de croissance. Le raisonnement soutenant ce concept est fondé sur une hypothèse de travail développée à partir d'indications expérimentales et

d'analyses théoriques présentées au chapitre 2. L'hypothèse de travail peut être formulée ainsi :

« La convection forcée de précurseur le long de la fibre dans sa direction de croissance peut résulter en un accroissement des taux de croissance tout en supportant la fibre extrudée. »

L'utilisation d'un écoulement coaxial à la fibre a permis de confirmer le potentiel d'amélioration du procédé. Deux types d'expériences furent conduits :

1. Étude des variations des taux de croissance à pression et débit constant en fonction de la puissance laser; et
2. Étude des variations du taux de croissance en fonction du débit à pression et puissance constante.

Des observations intéressantes ont pu être faites en étudiant la variation du taux de croissance en fonction de la puissance laser à pression et débit constants sous convection axiale :

1. Alors que toutes les expériences en réacteur statique rapportent une augmentation exponentielle du taux de croissance avec la puissance, suivie par une saturation, ce comportement n'apparaît pas dans nos expériences. A sa place nous observons une augmentation linéaire du taux de croissance, avec augmentation de la pente après 1400mW.
2. Les taux de croissance rapportés sont les plus hauts jamais enregistrés pour la déposition de carbone à 1 Bar.

Plusieurs explications sont possibles pour expliquer les différences induites par la convection axiale : un changement de la morphologie ou de la microstructure du dépôt, ou bien un changement dans les mécanismes de la déposition. Comme suggéré dans notre hypothèse de travail l'écoulement axial de précurseur doit permettre de mieux évacuer les produits de réaction. La situation est très différente dans le cas d'un environnement statique puisque l'évacuation des produits de réaction est en compétition

avec la diffusion du précurseur. Un autre effet non négligeable de l'écoulement axial forcé est qu'il réduit l'épaisseur de la couche limite comparé à un réacteur statique, et par conséquent améliore le transport du précurseur dans la zone de réaction. Les forts taux de croissance observés ainsi que l'absence de saturation sont des indicateurs sûrs des avantages de la convection axiale forcée.

Les résultats obtenus en variant la vitesse d'écoulement à puissance laser constante montrent qu'il existe un régime optimum pour lequel la production est maximale.

Les contributions scientifiques principales de cette recherche sont rapportées sous forme de trois articles, inclus aux chapitres 3, 4, et 5 de cette thèse. Dans les travaux de recherches antérieurs aux nôtres, la température, et par conséquent le taux de croissance, a été relié à la microstructure obtenue. Il est par conséquent essentiel de pouvoir mesurer le taux de croissance en temps réel si on souhaite implémenter un contrôle en boucle fermée.

Les travaux rapportés au chapitre 3 représentent une première. C'est en effet la toute première fois que le taux de croissance et le diamètre du filament sont mesurés in-situ et en temps réel. C'est la configuration du réacteur couplée à l'utilisation des émissions de l'hydrogène atomique à 656 nm qui ont rendu ces mesures possibles. Les résultats obtenus montrent que les taux de croissance varient amplement dans la région focale. Les recherches rapportées au chapitre 3 soulèvent une question importante : Ces variations du taux de croissance sont-elles caractéristiques de la déposition, ou sont-elles un artifice de l'écoulement mixe.

L'écoulement axial utilisé au chapitre 3 résultait d'une configuration à deux tubes coaxiaux, l'écoulement interne étant le précurseur (Ethylène) et l'écoulement externe un gaz écran inerte (Argon). Afin de discerner l'origine des variations enregistrées au chapitre 3, une nouvelle configuration à trois tubes a été mise à l'essai. L'écoulement

central et périphérique restant respectivement précurseur et gaz inerte, un écoulement intermédiaire de précurseur fut introduit pour prévenir la diffusion d'argon dans la zone de réaction. Les mesures des taux de croissance axiaux et volumétriques dans cette nouvelle configuration sont rapportés au chapitre 4 et confirment l'existence d'une variation importante de la déposition dans la région focale. Ces nouveaux résultats mettent une nouvelle emphase sur l'importance de contrôler la position du front de croissance dans la focale afin de maintenir une microstructure uniforme. Cette découverte montre que l'hypothèse très répandue d'une croissance uniforme dans la focale est en fait fausse.

L'analyse variationelle de la croissance rapportée au chapitre 5 est une nouveauté. Pour la première fois, une étude fut conduite de la réponse du phénomène à une perturbation des paramètres du procédé. Cette analyse a contribué une nouvelle méthode permettant de déterminer la position du plan focal de façon intrinsèque au procédé (alors que jusqu'ici une telle mesure ne pouvait qu'être faite hors-ligne). Les observations qui ont pu être dérivées sont frappantes :

1. Non seulement les taux de croissances varient énormément dans la région focale, mais nous pouvons affirmer maintenant que le maximum de la croissance est obtenu, non pas au plan focale comme on le croyait jusqu'ici, mais bien en avant de celui-ci, à une distance de l'ordre de 10 fois la longueur de Raleigh. Le taux de croissance décroît rapidement depuis ce maximum, se stabilise à la traversée du plan focal, puis reprend une lente décroissance.
2. Une mesure de l'efficacité énergétique du procédé consiste à évaluer le nombre de moles déposées par unité d'énergie. Cette mesure montre une variabilité importante sur une distance de l'ordre de 10 fois la longueur de Raleigh en avant du plan focal. À titre d'exemple, l'efficacité énergétique baisse de deux ordres de grandeurs à 1 Watt entre son maximum et le plan focal.
3. De même, une analyse variationelle de la croissance indique que la température décroît rapidement entre la région de croissance maximale et le plan focal. Elle

se stabilise à la traversée du plan focal, pour continuer de décroître lentement après la focale.

Si les chapitres 3 à 5 exposent les contributions scientifiques de cette thèse, le chapitre 6 est consacré aux contributions au génie. L'imagerie de la réaction à 656 nm a été utilisée comme signal d'entrée à un contrôle en boucle fermée. Le système de contrôle est un instrument virtuel dans LABVIEW conçu pour contrôler la position du front de croissance en temps réel. Afin de tester l'efficacité du système, plusieurs expériences ont été conduites, soit en maintenant la position à différentes positions à puissance laser constante, soit en maintenant la position du front constant à puissance laser variable. L'asservissement ainsi réalisé présente plusieurs particularités :

1. Il représente le tout premier système de croissance LCVD entièrement automatisé.
2. Il a permis d'obtenir les plus longs filaments de carbone par LCVD jamais produits.

Finalement, un prototype fut produit qui représente la première tentative de réacteur LCVD autonome pour la production de filaments. Ceci fut possible en intégrant les différentes composantes informationnelles du LCVD : puissance laser, débits, vision, contrôle. Le système permet à l'opérateur de spécifier les caractéristiques voulues (Diamètre, longueur, profile) du filament voulu. Dans le mode de démarrage, le système mesure les paramètres du procédé (taux de croissance et diamètre pour différentes position du front) en fonction des paramètres de croissance (puissance laser, débit de précurseur). Toutes les données acquises sont enregistrées au format approprié (Word ou Excel) pour l'usage ultérieur de l'opérateur. Somme toute, ce système représente une avancée importante vers l'exploitation industrielle du LCVD pour la production de filaments.

Les contributions originales et conclusions de cette thèse peuvent se résumer comme suit :

1. Un nouveau procédé de LCVD amplifié par un écoulement axial pour la production à la demande de filaments à l'air libre. *Des filaments de carbones furent obtenus pour la première fois à l'air libre (Chapitre 2).*

2. La configuration avec écoulement coaxial au filament a *produit les taux de croissance les plus hauts enregistrés* à pression atmosphérique. L'étude de la variation du taux de croissance en fonction de la puissance laser semblent indiquer une augmentation soutenue de la vitesse. *Pour toutes les puissances laser testées, aucune saturation n'a été observée (Chapitre 2).*

3. *Pour la première fois, des mesures de diamètre et taux de croissance ont pu être faite en temps réel et in-situ.* La technique de mesure développée a permis pour la première fois la détermination de la vitesse de croissance axiale de façon précise et non ambiguë. Cela a non seulement réduit les erreurs de mesure sur le taux de croissance, mais a aussi amélioré la répétitivité des mesures (Chapitre 3).

4. Contrairement à une idée reçue qui a souvent cours dans les milieux du LCVD, il n'y a pas de région de croissance stationnaire. Le taux de croissance varie de façon importante dans la région focale. Ce nouveau résultat souligne la nécessité de contrôler la position du front de croissance avec précision si l'on souhaite obtenir des microstructures qui soient reproductibles.

5. Une analyse variationelle du procédé a mis en lumière l'extrême variabilité du procédé. Cette analyse a aussi permit d'identifier la position du plan focal de façon intrinsèque au procédé. Contre toute attente, la courbe des taux de croissance n'est pas symétrique par rapport au plan focal. Ces résultats renforcent la conclusion que l'efficacité énergétique de la croissance LCVD varie très rapidement dans région focale. *Si les raisons de ce comportement ne sont pas encore comprises, les résultats démontrent clairement l'importance du contrôle de la position du front (Chapitre 5).*

6. Un algorithme de contrôle a été développé afin de réaliser le premier système de croissance par LCVD asservi. *Cette approche permet une opération semi autonome et a permit d'obtenir les plus longs filaments de carbone par LCVD (Chapitre 6).*
7. Une tentative de produire le premier prototype de croissance de filaments par LCVD entièrement automatisée est rapportée.

Les résultats obtenus dans le cours de nos recherches nous ont permiS non seulement d'obtenir un meilleure compréhension des phénomènes en jeux lors de la déposition par LCVD, mais aussi d'ouvrir de nouvelles avenues pour avancer l'état de la technologie.

1. L'absence de saturation du taux de croissance noté au chapitre 2 montre clairement l'avantage de notre type de réacteur. Afin de mieux comprendre les raisons de ce comportement, les recherches suivantes seraient souhaitables :
    a. Une simulation numérique de la zone de réaction entourant l'extrémité de la fibre pour quantifier les effets de la convection axiale forcée.
    b. Une étude permettant de relier le taux de croissance à la microstructure.
    c. Une étude spectroscopique de l'émission pour mieux comprendre les mécanismes de réaction à différentes puissances laser.
    d. Mesures de températures de la zone de réaction afin de la corréler au taux de croissance, la microstructure, et le spectre d'émission.
2. Identification et optimisation des débits de précurseurs pour chaque puissance laser.
3. L'analyse variationelle du chapitre 5 a mis en relief la nature asymétrique de la croissance et de son efficacité massique, molaire, ou volumétrique par rapport au plan focal. Une étude expérimentale plus approfondie est nécessaire pour identifier les raisons de cette asymétrie. La même analyse a révélé que la température en bout de filament décroît à mesure que le front s'approche du plan focal. Des mesures de températures combinées avec des spectrométries de la

zone de réaction seraient nécessaires pour corroborer indépendamment nos découvertes.

4. Le contrôle en boucle ouverte réalisé dans le cours de nos travaux est un prototype et nécessiterait une optimisation.
5. Le champ de vision de la camera est légèrement distordu par l'optique et le tube de quartz. Afin d'améliorer la qualité des mesures, il serait nécessaire de procéder à une calibration à la fois du CCD, et de l'image.
6. Bien que le système autonome décrit au chapitre 6 représente une avancée importante vers l'automatisation, il reste de nombreuses améliorations possibles. Par exemple, le positionnement du substrat, l'alignement du laser avec l'axe du réacteur. Ces opérations doivent maintenant être performée manuellement, ce qui augmente considérablement le temps de préparation. L'automatisation des opérations d'initialisations peut représenter un gain de temps important pour la rentabilisation d'un outil de production potentiel.
7. La qualité du contrôle que nous avons développé peut être exploité avantageusement pour :
    a. Corréler la position du front de croissance à la microstructure du produit.
    b. Corréler la position du front de croissance aux propriétés mécaniques.
8. A notre connaissance, il y a peu de résultats publiés sur la densité des filaments produits. Une corrélation entre la position du front de croissance dans la focale et la densité permettrait de développer une relation expérimentale et vérifier la qualité du matériau produit.

TABLE OF CONTENTS

LIST OF TABLES

LIST OF FIGURES

CHAPTER 1: INTRODUCTION

Technological progress of human civilization is very often linked to advances in the materials and processing used. Starting from the *Stone Age* where the material of choice for man was stone, to the present, where the choice of materials is enormous, we have made great progress. This being said, the demand for new and improved materials continues to grow by the day. One of the interesting areas of materials science that has been the focus of extensive research over the past few decades is the science of composites. Application areas for composites can range from sporting goods such as golf clubs to space crafts. Materials enthusiasts can refer to Peters et al [1] for an introduction to this exciting area of research.

1.1 Fibers, their applications, and future needs

An integral part of composites are *fibers* that contribute to the composite's physical and mechanical properties. A fiber in a very general sense can be defined as a structure having a high aspect ratio. Fibers in the recent past have achieved significant importance with an ever increasing demand for strong, stiff, and low density materials for incorporation in composite matrices as reinforcements. As part of reinforcements, they control the orientation of the reinforcing phase, thereby allowing the composite material to be used in extreme work environments. A substantial amount of research carried out over the past 40 years has resulted in the development of a wide variety of fibers [2-3]. The predominant thrust for research on advanced fibers is provided by the area of Ceramic Matrix Composites (CMC) and Metal Matrix Composites (MMC). A general consensus exists in the literature [4-7] regarding the requirements for fibers of the future. Future needs of fibers seem to be driven by three principle areas: structural applications, power generation, and aerospace. Applications in these areas require fibers with high strength, toughness, oxidation resistance at elevated temperatures, chemical stability, low density (for weight-sensitive end uses), and good creep resistance. Fibers possessing some or all of the above-mentioned qualities are more commonly referred to

as *High Performance Fibers (HPF)* [8]. A detailed discussion of the applications of fibers is beyond the scope of this work. For a comprehensive review of fiber applications (present and intended), reviews [1-2, 4-6, 9-10] and references therein are suggested. Some examples of fibers undergoing development and beginning to be commercially available, along with their application area, are summarized in Table 1.1.

Table 1.1 Developmental and commercially available HPF [4-5]

Trade Name	Prime Composition	Form	Modulus (GPa)	Cost ($)/kg	Current Production/yr	Applica -tion
Saphikon	Single crystalline (S.C) alumina	Filament	470	66,000	50 lbs Developmental fiber	CMC, MMC
Sylarmic	SiC, TiB_2	Fiber	380	6,700	Developmental fiber	CMC
Tyranno Lox E	Si-Ti-C-O	Fiber	NA	10000	Developmental fiber	CMC
SiBN(C)	$SiBN_3C$ with 1-3% O	Fiber	358	NA	Developmental fiber	CMC
Hi-Nicalon-S	Si-C	Fiber	420	6900	Developmental fiber	CMC
SiC fibrils	SiC S.C. fibrils	Filament	580	NA	Developmental fiber	CMC

As an example to illustrate the demand and cost of HPF, consider this: The US Department of Defense recently called for a Small Business Innovation Research (SBIR) proposal* to demonstrate the synthesis of mono-filament Tantalum Carbide (TaC) fibers. The intended application of these fibers is in the fabrication of nozzle throats for solid

* US DEPARTMENT OF DEFENSE. 2006. SBIR/STTR Interactive Topic Information System (SITIS). In the site *DoD SBIR Resource Center*. [On Line]. http://www.dodsbir.net/sitis/archives_display_topic.asp?Bookmark=28703 (Page Consulted on 17 August 2006)

rockets using highly aluminized propellants. Expected operating conditions of the nozzles are predicted to be in excess of 3315 °C and 2000 Psi. The proposed budget for the first phase of the proposal offered by SBIR is $100,000 USD, with the deliverable being ten 0.0003", 10" long TaC fibers. If one were to make a preliminary cost estimate taking into consideration the density* of TaC (14.5 g/cm^3) and the budget for the first phase of SBIR funding, the cost of synthesizing 1 kg of mono-filament TaC fibers comes to approximately $34 billion USD. It is important to note that the cost estimate was done without considering economies of scale and other important influencing factors; the primary purpose behind such an estimate is to drive home the importance and need for new HPF. To the author's knowledge, scant literature exists regarding preliminary development cost of new HPF. Any available information is normally classified and limited exclusively to the fiber manufacturer. Astounding as it (34 billion USD) may seem, if one were to assume that the cost can be reduced by 6 orders of magnitude once a reasonable volume of production is reached, the cost of 1 kg of TaC fibers would still be around $34,000 USD. The assumption of a decrease in cost by 6 orders of magnitude is typical in the case of the microelectronics industry, where growth has followed the Moore's law†.

1.2 Fiber production methods, development of new fibers, and hurdles

A variety of fiber production methods exist. Vapor phase methods include Metal Catalyzed Chemical Vapor Deposition [11], Hot Fiber Chemical Vapor Deposition [12], Chemical Vapor Infiltration (CVI) [13], Plasma Enhanced Chemical Vapor Deposition (PECVD) [14], and *Laser Chemical Vapor Deposition (LCVD)* [15]. Liquid phase

---

* PIERSON, Hugh O. 1996. *Handbook of Refractory Carbides and Nitrides: Properties, Characteristics, Processing and Applications.* [On Line]. Westwood, NJ: William Andrew Publishing/Noyes. 340p. http://www.knovel.com/knovel2/Toc.jsp?BookID=238 (Page consulted on 17 August 2006)

† U.S. Congress, Office of Technology Assessment, Microelectronics Research and Development – A Background Paper, OTA-B P-C IT-40, Washington, DC: U.S Government Printing Office. 35p. http://books.google.com/books?vid=ISBN1428923055&id=cs0g5VZndIcC&pg=PP1&lpg=PP1&ots=FvxTk_ZkLN&dq=Microelectronics+Research+And+Development&sig=nnq9jKMxXF0-1l28sXHEc9Ct9IA (Page consulted on 17 December, 2006)

methods include Down-drawing from preforms [16], Drawing from bushing tips [17], Updrawing from melts [18], Fiber formation in a containerless laser melt process [19], and Laser heated float zone growth [20]. Sol gel processing [21], Yajima process [22], Pyrolysis and radiation curing [23] are some of the several techniques that exist for the production of fibers from solid phase precursors.

As shown in Figure 1.1 [24], the *first phase* in the development of new fibers (or any advanced material) is the identification of the *material of interest* and the development of a suitable technology to produce it. The second phase involves the scale up of the process/technology developed in the first phase.

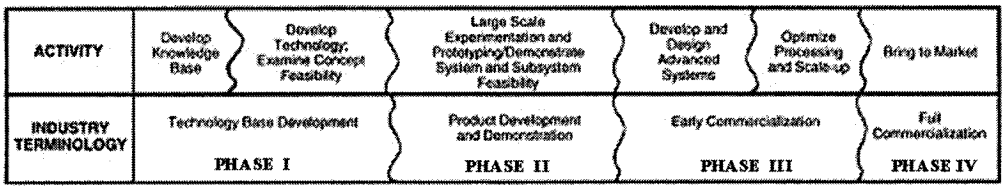

Figure 1.1 Phases in the commercialization process of a new fiber or advanced material (Modified and redrawn from [24])

To begin with, fiber development (completion of phases I and II) using existing technologies is a risky proposition for the fiber developer as it involves a large initial investment in the form of fixed costs [2, 4]. This is partly due to the complexities involved in preparing the fiber precursor and spinning the precursor to fiber form which necessitate expensive and process-specific machinery. Additional costs are incurred to deposit interfacial coatings on the produced fibers by processes such as Chemical Vapor Deposition (CVD). The fixed cost overhead can be offset if the production volume is high, which unfortunately is not the case for the fiber-in-development. This means that the fiber manufacturer would have to under-sell the new product until its feasibility is evaluated, and ultimately put to use by the end-user—typically a composites manufacturer. The whole process of development and commercialization of a new fiber

is normally 10-12 years as shown in Figure 1.2 [24]. The lack of any return on investment to the developer/manufacturer for a considerable period of time is the primary deterrent towards the development of advanced fibers. Recommendations upon survey by various committees [4, 6, 24] propose the *need for the development of a cost-effective technology requiring minimum investment in the form of fixed costs.* They also point to a glaring *deficiency of a technology that can produce small volumes of samples on an on-demand basis.* In other words, there is a necessity for a *technology that can rapidly prototype new, yet different fibers* for evaluating their feasibility in a particular application of interest.

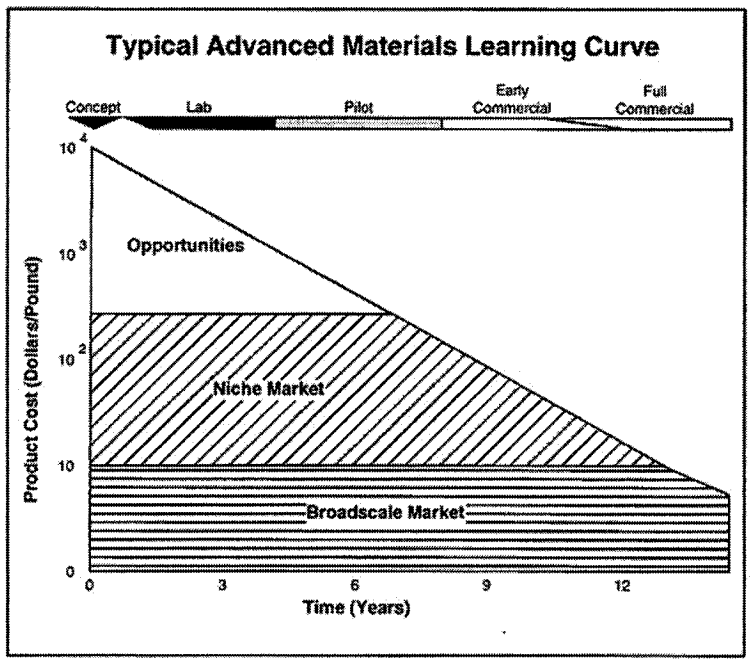

Figure 1.2 Time span for commercializing a new fiber (Modified and redrawn from [24])

1.3 Laser Chemical Vapor Deposition: Introduction

Laser Chemical Vapor Deposition (LCVD) maybe defined as a process in which a laser beam is used to dissociate a precursor (usually in gas phase) into a product of desired form. Depending on the configuration of the laser beam with respect to the substrate

and the dissociation scheme, LCVD can be classified into *Photolytic LCVD,* and *Pyrolytic LCVD* [25]. In photolytic LCVD, a precursor is chosen such that its absorption wavelength matches the wavelength of the laser beam. Furthermore, the substrate surface is parallel to the laser beam, thereby rendering the process its non-thermal nature. Photolytic LCVD is used to deposit films and is out of scope of the following work.

In Pyrolytic LCVD, the subject of this research, mass deposition takes place at the laser focus by thermal dissociation of the precursor gas at or in the vicinity of the substrate surface (Figure 1.3). Hereafter, any mention of LCVD in the remainder of this document refers to Pyrolytic LCVD.

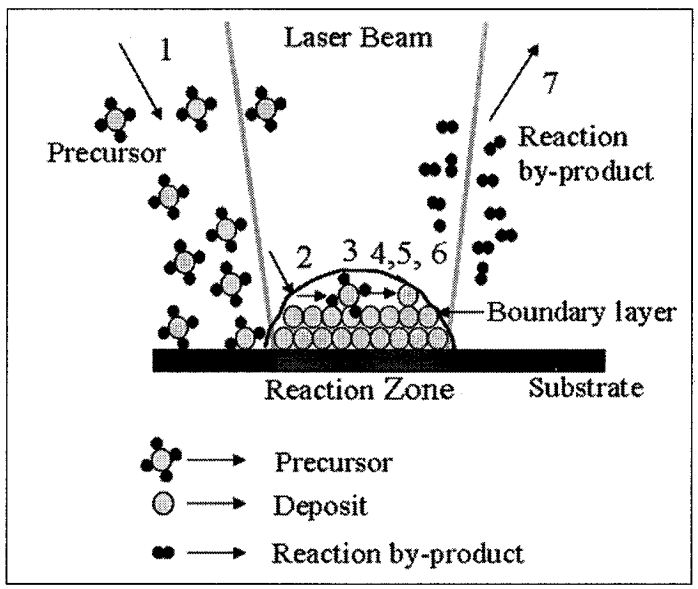

Figure 1.3 Fundamental steps of LCVD (Modified and redrawn from [26])

1.3.1 Fundamental steps of LCVD

The fundamental steps of LCVD are the same as those in CVD, except that in the former, the hot zone (defined by the laser focus) is confined to a much smaller area. This reduction in the size of the reaction zone manifests itself via increased growth rate

as a result of the 3-D diffusion pathway created by the laser focused spot, as opposed to the 1-D diffusion occurring in CVD. The fundamental steps [26] are:

1. Transport of precursor to the vicinity of the reaction zone
2. Diffusion of precursor through the boundary layer on to the substrate surface
3. Adsorption of precursor on the substrate surface
4. Chemical reaction
5. Nucleation
6. Desorption of reaction by-products
7. Transport of gaseous reaction by-products away from the reaction zone

The slowest of these seven steps determines the nature of the process. If steps 3, 4, 5 and/or 6 are rate limiting, then the process is said to be in the *"kinetic regime"*, and if steps 1, 2 and 7 are rate limiting, then the process is termed as *"mass transport limited"*. In the kinetic regime, the growth rate of the deposit can be characterized by the Arrhenius relationship (1.1).

$$k = k_0 \, Exp\left(\frac{-E_a}{RT}\right) \tag{1.1}$$

where

k is the reaction rate constant (μm/s)

k_0 is the temperature-independent pre-exponential factor (μm/s)

E_a is the activation energy (kJ/mol)

R is the gas constant (J/mol.K)

T is the temperature (K)

1.3.2 General LCVD process parameters

The process parameters of LCVD can be summarized as shown in Table 1.2. For a comprehensive introduction to the subject background, one can refer [25, 27].

1.4 LCVD: State-of-the-art

LCVD has come a long way since the first carbon fiber was grown by Nelson et al [15] in 1972. The first carbon fibers were produced from natural gas at 833 mbar with a CO_2 laser focused to 500 μm with a power of 10 watts. Carbon fibers of diameter 500 μm were obtained with a growth rate 8.3 μm/s.

Table 1.2 LCVD process parameters

Influenced parameter → / Process parameter ↓	Growth rate	Size of reaction zone	Laser power density	Initiation of deposit	Temperature of deposit growth front	Size and/or shape of deposit	Precursor concentration	Heat transfer	Reaction mechanism	Microstructure of deposit	Focal spot size
Laser Power	X		X		X	X		X	X	X	
Focal spot size		X	X			X					
Laser wavelength				X							X
Substrate properties	I			X	I	I		I			
Deposit properties	X			X	X	X		X		X	
Precursor pressure	X					X	X	X	X	X	
Precursor flow rate	X				X	X	X	X	X		
Precursor composition	X						X			X	

I - Influence active only during initial stages of growth

1.4.1 Materials deposited by LCVD

The versatility of LCVD lies in its ability to deposit any material, provided its precursor is available in gaseous form. In principle, any material deposited by CVD can be deposited by LCVD. Comprehensive literature reviews [28-29] and texts [25, 27] can be referred for a complete list of materials deposited. Over the years, LCVD has been used to deposit *metals/metal oxides* (Aluminum [30], Alumina [31], Copper [32], Gold [33], Molybdenum [26], Nickel [34], Platinum [35], Rhodium [36], Titanium [37], Tungsten [26]), *non-metals and semi-metals* (Boron [38], Carbon [15], Germanium [39], Silicon [40]), *binary alloys* (Boron Nitride [41], Gallium Arsenide [42], Manganese-Gallium

[43], Cobalt-Gallium [43], Nickel-Iron [44], Silicon Carbide [39], Silicon Nitride [39], Titanium Carbide [45], Titanium Nitride [46], Titanium disilicide [47], Tungsten Carbide [26]), and *ternary alloys* ($B_xN_yC_z$ [48]). A quick glance at the materials deposited reveals the capability of LCVD to produce materials of proven and potential importance.

1.4.2 Structures deposited by LCVD

A variety of structures such as lines [30], fibers [26], helical coils [40], antennas [49], micro-solenoids [40], trussed structures [50], microtweezers [51], linear micromotors [51], photonic bandgap structures [53], microtubes [52], and 3-D freestanding structures [53] have been realized by LCVD. More recently, functional objects such as micro-turning lathe [54] for contact-free trapping and machining of micron sized particles; micro-cage [55] for contact-free trapping, handling and transfer of polarizable micro-sized neutral particles; and microcoil heaters [56] for gas thrusters in nano satellites have been developed. Realization of such complex structures brings to the fore the ability of LCVD to rapidly prototype 3-D micro-scaled objects not possible by any other means.

1.5 LCVD for fiber development: Advantages and Possibilities

As mentioned in section 1.2, the two major hurdles in the rapid and economical development of new HPF are:

1. Exorbitant costs involved in the development of new fibers using existing technologies.
2. Absence of a suitable method to rapidly prototype small volumes of *fibers of interest.*

Most of the conventional fiber production technologies are tailored to suit the material being produced. This customization leads to an increase in the investment in the form of specialized equipment for precursor processing, fiber handling, and heat treatment. For example, purification required to spin carbon pitch into carbon fibers can raise the cost of raw material (pitch) from dollars/ton to dollars/pound [4]. On the other hand,

equipment designed for LCVD operations can be used to produce a variety of fibers by merely changing the precursor gas. Gaseous LCVD precursors require no further processing and can be used directly for fiber production. These advantages in using LCVD manifest themselves into considerable savings in investment.

Before new fibers can be developed and introduced into the market, it is imperative that they be tested for their feasibility to the specific application in hand. To do so, one needs to have a method capable of producing the desired fibers in small quantities at minimum expense. Furthermore, some high-end applications might require fibers only in small volumes. Conventional fiber development technologies fall far short in this regard as identified by surveys [4, 6, 24]. LCVD has proven itself to be an efficient tool at rapid prototyping short fibers (<1.5 cm long) and 3-D micro-objects [57]. One can therefore utilize LCVD to produce small quantities of fibers for evaluation prior to large scale production.

Other advantages of LCVD that make it a production-worthy candidate for fiber synthesis are:

1. LCVD's unique *ability to tailor the microstructure* can be used to produce materials that are amorphous, crystalline, polycrystalline, metastable, or functionally graded by simply adjusting its process parameters as demonstrated in [38, 58].
2. With its *ability to deposit multiple materials simultaneously* [41-47] and tailor the deposit microstructure, LCVD appears to be a route capable of producing interesting material combinations such as Si-B-C-N, SiC-TiB_2, and continuous, single crystalline fibers as listed in Table 1.3
3. *Growth rates* demonstrated *by the High-Pressure LCVD (HP-LCVD) process are at par with some commercialized fiber production technologies* [39]. This supports the use of LCVD as a tool for rapid prototyping fibers in small volumes.

4. *LCVD is a containerless process.* In most of the existing fiber production methods, the final product at one stage or another is exposed to fiber or precursor handling equipment leading to a possible contamination or degradation of fiber quality. LCVD on the other hand is capable of producing fibers of high chemical, structural, and optical purity since the growing fibers are not in contact with any foreign materials.

Table 1.3 Materials of the future by LCVD (Redrawn from [2])

Proposed Single Crystalline fiber	Melting point (°C)	Service temperature (°C)	Bulk density (g/cm^3)	Youngs Modulus (GPa)
TaC	3880	<2715	13.9	496
ZrC	3532	<2472	6.7	455
HfN	3305	<2313	13.8	476
TiN	3290	<2303	5.4	684
HfB_2	3100	<2170	10.5	345
TiC	3067	<2147	4.9	496
HfC	3000	<2100	12.2	414
SiC	2830	<1981	3.2	427
HfO_2	2765	<1942	9.7	296
ZrO_2	2710	<1897	5.7	253
Al_2O_3	2054	<1434	4.0	443
Diamond	3550	<1000	3.5	1000

1.6 LCVD for fiber development: Challenges

Despite the proven ability (section 1.4) and advantages (section 1.5) of LCVD as a potential candidate for fiber production, there are still a number of issues that need to be addressed with regard to the process itself.

1.6.1 Process control and automation

A process is never complete until it is controlled. LCVD is a highly temperature-dependent process. Owing to the gaussian profile of the laser beam, the induced temperature rise varies by orders of magnitude between the center and edge of the laser spot. It has been documented in literature [59] that the temperature, and in turn the growth rate, affects the microstructure of the produced fiber. Microstructure in turn is related to the strength and overall quality of the fiber as demonstrated by [60]. Unless growth occurs at identical focal conditions, uniformity of microstructure cannot be guaranteed. To realize uniform focal conditions throughout fiber growth, two different approaches have been followed in the literature.

The first approach [61] involved the control of the position of the focal lens with respect to the fiber growth front by monitoring the motion of the emission during deposition using a position-sensing diode. Although this approach was successful in ensuring identical focal conditions and in being able to obtain axial growth rate measurements during fiber growth, it has key limitations:

1. Accurate in-situ axial growth rate measurements were limited to a specific laser power (induced temperature) range, probably due to position sensor constraints. Outside of this range, axial growth rate measurements were made by the operator using a microscope objective.
2. Typical length of fibers grown was 1 mm, and the maximum fiber length was dictated by the travel range of the focusing lens and the position sensor, as well as the size of the reaction chamber.

The second approach [62] focused on maintaining the temperature constant throughout the fiber growth. This was accomplished using a thermal imaging camera to monitor the temperature in the reaction zone and to control the laser power in real-time to maintain the temperature constant. The position of the focusing lens and substrate was kept

constant during fiber growth. Barring the improvement in temperature measurement accuracy, this method too has its set of drawbacks namely:

1. Inability to obtain axial growth rate measurements in-situ; growth rate measurements were made offline by dividing the length of the fiber with the time required for deposition of that length.
2. The typical length of fibers grown was less than 1mm, and the maximum fiber length was limited by the size of the reaction chamber.
3. Thermal imaging is an extremely expensive option.

The majority of LCVD on-line growth rate measurements reported to date are operator-specific. These measurements are obtained by measuring the time taken for the fiber growth front to traverse a specific distance (typically 20 to 40 μm) within the field of view of the microscope objective. Focus tracking is achieved by the operator manually pulling back the fiber growth front after it traverses the said distance. Measurements such as these are prone to error. This is more so at high growth rates when tracking and maintaining the position of the fiber growth front becomes increasingly difficult, as reported by [59].

LCVD has historically been open-loop, partly because of the absence of a method to compute the axial growth rate in-situ and in real-time. Focusing on temperature control using thermal imaging techniques to control the process is an expensive option. Moreover, this method does not yield real-time information on growth rate. If one were *to achieve closed-loop control of the LCVD process, it is imperative for the control scheme to have 1) the axial growth rate, and 2) position of the fiber growth front as inputs* to maintain the fiber growth front at the same position relative to the focus. Furthermore, *accurate axial growth rate measurements are necessary for characterizing the reaction rate.*

LCVD process control and automation can eliminate growth rate measurement inaccuracies caused by human error and realize uniform microstructure throughout the length of the produced fiber. Moreover, automation of the LCVD process is a step ahead towards making it a competent fiber production technique. In conclusion, *central to the idea of achieving LCVD process control and automation is the need to determine the axial growth rate and fiber growth front position in-situ and in real-time.*

1.6.2 Continuous fiber synthesis

An interesting observation that can be made from the discussion in section 1.6.1 is that irrespective of the control approach taken, the maximum fiber length was limited to the size of the reaction chamber. This can be attributed to the design limitation of the chambers used. A survey of literature reveals the typical length of LCVD fibers produced to be less than 0.5 cm. The only exception to this seems to be the work done by Wallenberger et al., [2, 39, 57] where they propose that fibers can be grown indefinitely if one were to design a spooling system that can take up the grown fiber at one end of the reaction chamber. Using a semi-continuous process that yielded 1.4 cm long fibers, they report to have grown 2 meter long Boron fibers in sections of 1.4 cm [57].

To the author's knowledge, no demonstration of continuous fiber growth using LCVD has been made. If LCVD is to make inroads into being a commercial fiber production technique, it is essential for it to be able to synthesize continuous fibers.

1.6.3 Growth rate improvement

Achieving improved growth rate can pave the way for LCVD to enter into the commercial arena. Two schemes have been proposed to improve the growth rate: 1) to increase the reactor pressure and 2) to use a forced precursor jet to aid mass transport into the reaction zone.

Wallenberger [2] was the first to investigate the effect of using high reactor pressures up to 10 bars. Growth rates were found to increase exponentially with pressure. This observation was later confirmed by Maxwell et al and Williams et al [58, 63]. Indeed, Williams et al [63] report to have increased reactor pressures up to 11 bars and grown carbon rods using ethylene at growth rates as high as 13 cm/s. It has also been documented that HP-LCVD yields fibers with better mechanical properties when compared to Low Pressure-LCVD (LP-LCVD). As a matter of fact, carbon fibers grown using LP-LCVD at 1 bar by Longtin et al [64] had a Youngs modulus of 20 GPa in comparison to a Youngs modulus of 180 GPa for carbon fibers grown using HP-LCVD at 10 bars by Wallenberger et al [57]. At identical laser powers, increasing the reactor pressure increases the growth rate [57]. Microstructural analysis of LCVD carbon rods by Fauteux et al [59] has attributed production of amorphous structures to increased growth rate. Amorphous carbon fibers are known to be mechanically superior compared to polycrystalline carbon fibers [57]. The excessive grain boundaries in polycrystalline fibers results in a poor Youngs modulus. Moreover, HP-LCVD carbon and boron fibers have demonstrated tensile strengths of 3 GPa and 7.5 GPa [2], values that are on par with commercially available carbon and boron fibers.

In their patent, Maxwell et al [65] proposed the use of a forced jet of precursor to aid the mass transport of precursor into the reaction zone, and thereby improve the growth rate. Duty et al [66] experimented with a nozzle to deliver the precursor at an angle towards the reaction zone. In this configuration, the direction of precursor flow is opposite to the fiber growth direction. The angled jet of precursor flow was found to impede the growth rate due to convection cooling. Furthermore, the forced convection enhancement was found to be beneficial only when the deposition was severely mass transport limited. *It remains to be seen if the decrease in growth rate due to forced convection is an artifact of the angle of precursor flow with respect to the fiber growth direction rather than a real phenomenon at work.*

1.7 Objectives of the Thesis

An attempt has been made to gain a better understanding of the LCVD process, which in turn could lead to a better process control. The objectives of the thesis are as follows:

Scientific Contributions:

1. Develop an axial convection enhanced LCVD setup to study the effect of forced axial convection on the growth rate.
2. Gain a better understanding of the process by devising a method to determine the axial growth rate and position of the fiber growth front in real-time.

Engineering Contributions:

3. Develop an automated closed-loop control system for fiber growth.
4. Devise a means of producing long/continuous fibers.

The identified scientific contributions will help to advance the LCVD state-of-the-art. The engineering contributions on the other hand will aid in the realization of LCVD as a reliable industrial tool for fiber synthesis.

1.8 Organization of the Thesis

This thesis is divided into 7 chapters. Chapter 1 gives an introduction to fibers, their applications, and production techniques. It then provides an introduction to LCVD and LCVD state-of-the-art before delving into the advantages of LCVD as a fiber production technique. Finally, the chapter discusses the challenges facing LCVD and objectives of the thesis.

Chapter 2 focuses on the proposed hypothesis supporting the flow of precursor in the same direction as the growing fiber/rod. Theoretical arguments and experimental observations are provided to support the use of axial convection enhancement. Results of experiments conducted at varying laser power, constant precursor flow; and varying flow, constant laser power are reported.

Chapters 3, 4, and 5 are presented in the form of 3 articles. Chapter 3 introduces a real-time in-situ growth rate and rod diameter measurement technique. The technique allows the measurement of rod growth rate along its axis during a stationary laser focus and substrate experiment. Results in chapter 3 allowed the quantification of growth rate variation within the laser-induced growth region. Chapter 4 reports the results obtained with a three-tube coaxial flow system. Real-time in-situ growth rate measurements confirm the great variation in transient growth rates along the rod axis. Chapter 5 presents the variational analysis of rod growth conducted by a systematic perturbation of LCVD process parameters.

Chapter 6 introduces the algorithm developed to build a closed-loop automated LCVD system. It then describes the turn-key LCVD system developed to produce rods and rod based structures using minimum operator intervention. Finally, it describes the advantage of the proactive approach of closed-loop control compared to open-loop methodologies followed in literature.

Chapters 2 through 5 address the objectives identified as scientific contributions of the following work. Chapter 6 focuses on the engineering contributions of the work. Finally, Chapter 7 presents the discussion of the obtained results, conclusions of the thesis, and suggests avenues for future work.

CHAPTER 2: AXIAL CONVECTION ENHANCED LCVD

2.1 Motivation for Convection Enhanced LCVD

One of the most important hurdles in transforming LCVD into a commercially viable technology for fiber production is the throughput of the process. Despite the documented *"order of magnitude increase in growth rate using LCVD"* compared to Hot-Wire CVD, the throughput of LCVD is significantly lower than the latter. It must be noted, however, that HW-CVD essentially produces sheath-core fibers. For example, HW-CVD boron fibers are produced by coating a thick layer of boron on a small diameter tungsten filament [12]. In contrast, LCVD can produce fibers without the inner support core. This results in improved "specific properties". For instance, LCVD boron fibers with diameters 0.06-0.04x and strength 1.6x (~7.6 GPa compared to 4.8 GPa) that of HW-CVD boron fibers have been demonstrated [67]. *Improved material properties such as those reported in [67] are sufficient motivation to improve the LCVD process.*

Of the two approaches presented in literature to improve the growth rate: *1) increasing the reactor pressure and 2) using a forced precursor jet to aid mass transport*, considerable amount of work has been done on the former.

Scant literature exits on the investigation of the effect of aiding the mass transport of precursor into the reaction zone using a forced precursor jet. A vast majority of LCVD work to date has used a static reactor fill approach, wherein the reaction chamber is filled to a desired pressure of the precursor before the start of LCVD operations. Maxwell et al [65] were the first to propose the use of a forced jet of precursor to aid the mass transport of precursor into the reaction zone to improve the growth rate. Duty et al [66] experimented with a nozzle at 45° to the fiber growth direction (Figure 2.1).

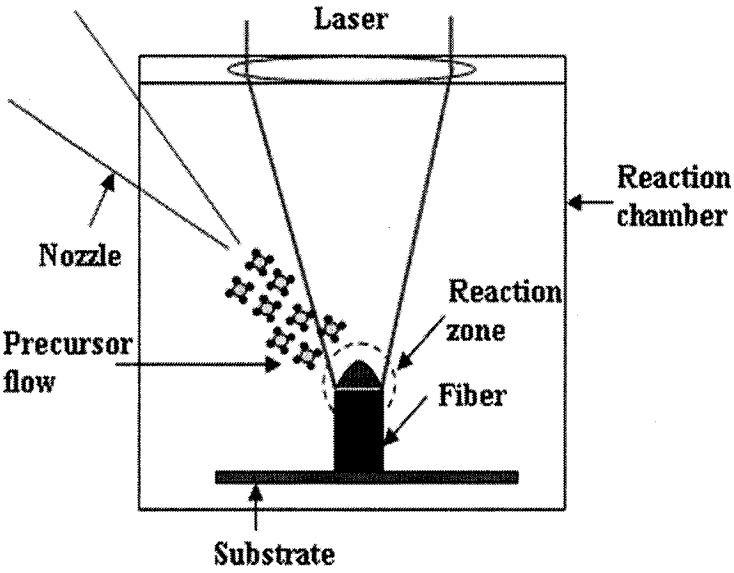

Figure 2.1 Schematic of a forced precursor jet system

In this configuration, the precursor is directed at an angle towards the reaction zone with the direction of precursor flow opposite to the fiber growth direction. Modeling results in [66] showed forced convection enhancement to be beneficial only when the deposition was severely mass transport limited. No experimental data regarding the effect of laser power (or temperature) on the growth rate was reported for the angled jet LCVD system of [66]. This being said, *it remains to be seen if the decrease in growth rate due to forced convection is an artifact of the angle of precursor flow with respect to the fiber growth direction rather than a real phenomenon at work.* The reduction in surface temperature with increasing precursor flow rate [66] is not surprising and neither is the growth rate decrease with increased precursor flow rate. To study the true influence of a forced precursor jet, it therefore seems more appropriate to study the effect of laser power on the growth rate at different precursor flow rates. Ideally speaking, *if convection enhancement were to have a positive impact on the growth rate, then it would have the effect of pushing farther the mass transport limit (growth rate saturation) experienced at high laser powers* [58] as in static fill reactors (Figure 2.2).

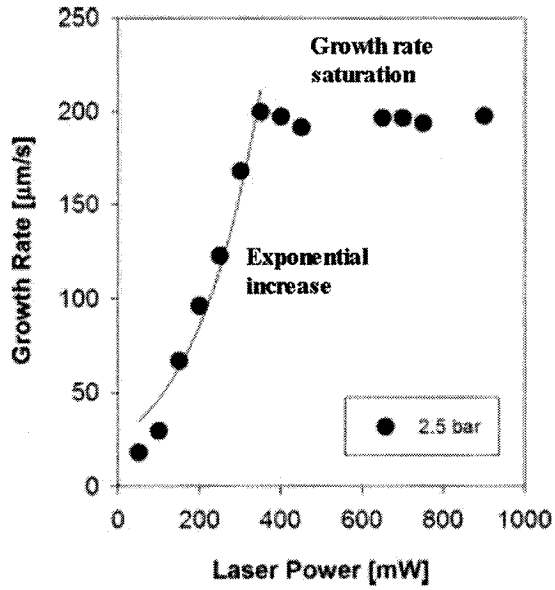

Figure 2.2 Effect of laser power on growth rate at constant pressure in a static fill reactor (modified from [58])

2.2 Development of work hypothesis

The majority of modeling works on LCVD are based on the hemi-spherical diffusion model of Ehrlich et al [68]. They modeled the reaction zone at the laser focus as a hemisphere acting as a sink for the diffusing precursor. From this model, they were able to calculate the concentration of the precursor as a function of time by assuming the surface reaction rate to be proportional to the density of precursor molecules at the surface of the hemisphere. In summary, Ehrlich et al [68] took into consideration only the diffusion of the precursor into the reaction zone while neglecting the convection due to the molar change of species.

Copley [69], however, considered the convection due to molar change of species by modeling it as a radial outflow of an incompressible gas from a point source. Deposition flux values were estimated for a model considering diffusion of precursor alone (as in [68]), and compared to a model considering both diffusion and convection. Deposition flux values predicted by the diffusion model were found to be greater than the diffusion

plus convection model. This reduction was attributed to the convective outflow of the reaction by-product. Moreover, reactant pressures predicted by the diffusion plus convection model were not equal to the diffusion model because of the influence of the convective outflow of by-products on the diffusion of the precursor into the reaction zone. Finally, the variation in total pressure witnessed in the diffusion model was eliminated by the convective flow in the diffusion plus convection model.

Experimental observations [58] point to strong convection currents during fiber deposition in a static fill setup even without the use of a forced precursor jet. Moreover, these currents were found to occur along the fiber axis into the laser beam. Fluid velocities greater than 10 m/s were measured near the reaction zone using Particle Imaging Velocimetry (PIV). The analytical and experimental observations in [69, 58] therefore raise an interesting remark: *"If a convective outflow of reaction by-products indeed exists, then it seems appropriate to have the precursor flow in the same direction as the by-product flow."*

In conclusion, the work hypothesis for the development of an axial convection enhanced LCVD system can be stated as follows:
"Forced convection of precursor gas along fiber growth direction contributes to enhanced growth rate and better support of the growing fiber."

2.2.1 Supporting argument for the proposed hypothesis

Let us consider an LCVD fiber tip geometry (Figure 2.3) with its origin at point O at the end of the fiber's steady-state diameter, and beginning of the fiber tip. The fiber tip geometry is assumed to have symmetry of revolution. Hence, we shall only consider a radial plane in which the tip profile is parametrized with angle θ ($0 \le \theta \le \frac{\pi}{2}$) measured between the tip local normal and the fiber's axis. A local point on the fiber tip has

coordinates $z[\theta]$ and $r[\theta]$ in a frame with origin at O, and with z-axis corresponding to the fiber axis.

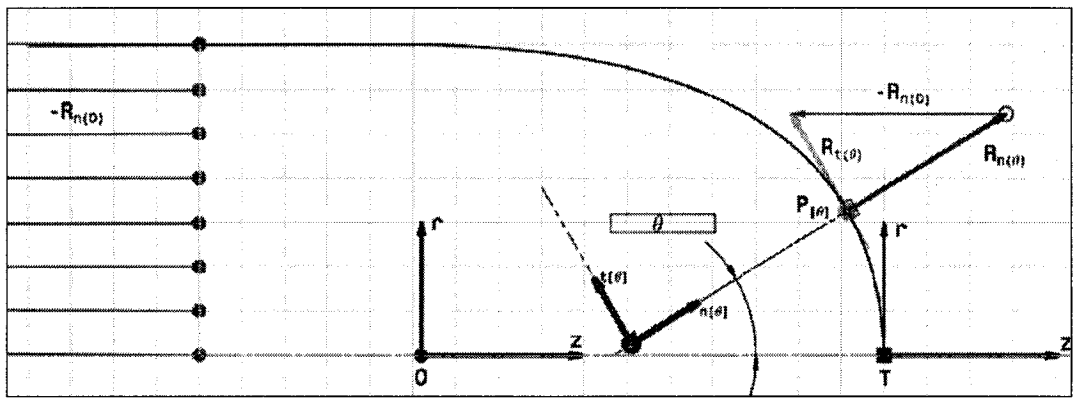

Figure 2.3 Kinematic fiber tip growth model

Let $R_n[0]$ denote the fiber's axial growth rate (m/s). From a pure kinematics consideration, one can derive the normal and tangential rate of motion at a point $P[z[\theta], r[\theta]]$ on the fiber tip. The normal growth rate at θ is denoted by $R_{ng}[\theta]$ (m/s), while the tangential growth rate at the point $P[\theta]$ is $R_{tg}[\theta]$. The subscript "g" stands for "geometric."

By starting from a kinematics viewpoint, we can place ourselves in a reference frame in which the tip is stationary with its apex T along the fiber's axis. The unit vector along the fiber's axis in the direction of its growth is denoted $\vec{z}$ and the unit vector in the radial direction is denoted $\vec{r}$. The origin of the reference is at point O—the boundary where the steady-state diameter of the fiber ends and the tip region starts. The fiber is assumed to be pulled back along its axis with a velocity $-R_n[0]$ such that the tip T is stationary. The unit outward normal $n[\theta]$ to the tip at an arbitrary point $P[\theta]$ makes an angle θ with the fiber's axis. The tangent direction to the tip at that point is denoted

$t[\theta]$. The angle θ may then serve as a parameter to the tip geometric description provided the relationship of θ to $P[\theta]$ is one to one.

Regardless of the cause of growth, let us assume for now that the tip front would expand normal to itself in such a way that its geometry remains stationary. Hence, if we let $R_{ng}[\theta]$ denote the normal growth rate at point $P[\theta]$, the resulting velocity $R_{tg}[\theta]$ at $P[\theta]$ can only be the vector addition of the relative velocity $R_{ng}[\theta]$ and the pull or entrainment velocity $-R_n[0]$. Since the tip geometry is stationary, it can only be that the resulting velocity vector $R_{tg}[\theta]$ is tangent to the tip profile at $P[\theta]$. The consequence of this observation is that the tip shape is the result of the velocity distribution at the tip. A relation between the normal, tangential and axial growth rates can therefore be obtained:

Normal velocity $R_{ng}[\theta] = R_n[0]Cos[\theta]$ (2.1)

Tangential velocity $R_{tg}[\theta] = R_n[0]Sin[\theta]$ (2.2)

Furthermore, radial and axial velocities associated to $P[\theta]$ can be defined using

Radial velocity $R_{rg}[\theta] = R_n[0]Sin[\theta]Cos[\theta]$ (2.3)

Axial velocity $R_{ag}[\theta] = -R_n[0](Sin[\theta])^2$ (2.4)

Letting $\rho[\theta]$ denote the radius of curvature of the tip profile at $P[\theta]$ and $s[\theta]$ denote the arc length measured on the tip profile from T to $P[\theta]$, one can obtain the following relations.

$ds = R_{tg}[\theta]dt = \rho[\theta]d\theta$ (2.5)

From (2.5), we can obtain

$$\partial_t\theta = \frac{R_{tg}[\theta]}{\rho[\theta]} = R_n[0]\frac{Sin\theta}{\rho[\theta]} \quad (2.6)$$

Consequently, the fiber diameter Φf can therefore be obtained by the following expression

$$\Phi f = 2\int_0^{\frac{\pi}{2}} R_{rg}[\theta]\,dt = 2R_n[0]\int_0^{\frac{\pi}{2}} \frac{Sin[\theta]Cos[\theta]}{\partial_t \theta} d\theta = 2\int_0^{\frac{\pi}{2}} \rho[\theta]Cos[\theta]d\theta \tag{2.7}$$

The volumetric growth rate can be obtained from the product of the fiber axial growth rate $R_n[0]$ and its cross-sectional area. The geometric growth rate imposes the integral volumetric growth rate

$$V_o \text{ as } V_o = R_n[0]\frac{\pi\Phi f^2}{4} \tag{2.8}$$

If one were to assume that the fiber growth happens in the kinetic regime (as is the case in this work as demonstrated by the results in section 2.4), then the growth can be characterized by the well-known Arrhenius relationship. The growth rate $R_n[\theta]$ at any arbitrary point on the fiber tip, and temperature at the same point $T[\theta]$ can be related by

$$R_n[\theta] = kC[\theta]^n\, Exp\left[-\frac{E_a}{RT[\theta]}\right] \tag{2.9}$$

where

k is the pre-exponential constant

n is the reaction order

$C[\theta]$ is the precursor concentration around the fiber tip

E_a is the activation energy of the reaction, and

R is the perfect gas constant.

By relating the growth rate at an arbitrary point θ to the growth rate at the center of the fiber tip, we obtain (2.10)

$$\frac{R_n[\theta]}{R_n[0]} = \left(\frac{C[\theta]}{C[0]}\right)^n Exp\left[-\frac{E_a}{R}\left(\frac{1}{T[\theta]} - \frac{1}{T[0]}\right)\right] = Cos\theta \tag{2.10}$$

While it is true that the precursor concentration around the fiber tip strongly depends on the temperature around the fiber tip, quantification of the concentration gradient as a function of the temperature distribution is extremely difficult. For the sake of simplicity, if one were to assume that the concentration around the fiber tip is constant, then the concentration distribution $C[\theta]$ can be decoupled from the temperature and one can solve for the temperature distribution around the fiber tip. This assumption reduces (2.10) to

$$\frac{T[\theta]}{T[0]} = \frac{1}{1 - \frac{Log[Cos[\theta]]}{\frac{E_a}{RT[0]}}}. \tag{2.11}$$

An elliptical tip with unit radius and a major axis equal to twice the radius was used to model the fiber tip. By assuming an activation energy of 244 kJ/mol [61] and tip temperatures ranging logarithmically from 773 K (innermost curve – displayed blue in the electronic version of the thesis) to 4273 K (outermost curve – displayed red in the electronic version of the thesis) scaled to 4273 K, the normalized temperature distribution around the fiber tip takes the form in Figure 2.4 as shown in the normal offset plot.

One can observe from Figure 2.4 that the higher the temperature at the center of the fiber tip, the steeper is the temperature distribution at the tip. Conversely, experimental observations in [70] provide evidence to poorly conducting materials yielding sharper fiber tips (owing to steeper temperature distribution) and vice versa. Good thermal conductors dissipate the input thermal energy of the laser beam more effectively causing

a broader temperature distribution as opposed to the steep distribution induced by a poorly conducting material.

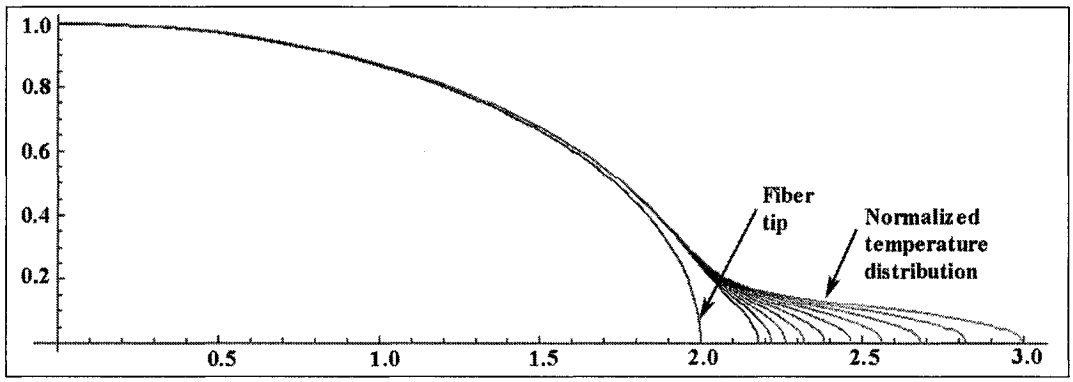

Figure 2.4 Normal offset plot of normalized temperature distribution around fiber tip for various tip temperatures

Now that we have an idea of the temperature distribution around the fiber tip, we can now focus on modeling the deposition of carbon around the fiber tip. To achieve this, one can start by obtaining carbon volumetric deposition rates in $(m^3/s)/m^2$, before moving on to obtain the mass and the molar deposition rates of carbon. If one were to consider the thermal expansion of deposited carbon, then the carbon volumetric deposition rate (corrected for thermal expansion) at an arbitrary position on the fiber tip making an angle θ to the fiber axis can be obtained by

$$RnC[\theta] = (1+3\alpha C[r[\theta]](T(\theta)-T_r)R_n[\theta] \qquad (2.12)$$

where

$RnC[\theta]$ is the volumetric deposition rate of carbon corrected for thermal expansion

$\alpha C[r]$ is the coefficient of thermal expansion of carbon as a function of fiber radius

$T(\theta)$ is the temperature at an arbitrary position making an angle θ to the fiber axis

T_r is the reference room temperature

$Rn[\theta]$ is the normal growth rate at θ

Using (2.11), (2.12) can be written as

$$RnC[\theta] = (1+3\alpha C[r[\theta]](\frac{T[0]}{1-\frac{Log[Cos[\theta]]}{\frac{E_a}{RT[0]}}} - T_r))R_n[0]Cos[\theta]. \quad (2.13)$$

Carbon fibers produced by LCVD were found to be non-homogeneous [71], consisting of a pyrolytic graphite core and an amorphous carbon outer layer. This being the case, using the coefficient of thermal expansion of a standard homogeneous material such as pyrolytic graphite or graphite cannot yield accurate results. However, the average coefficient of thermal expansion of a non-homogeneous LCVD carbon fiber cannot be beyond the range of values obtained for homogeneous carbonaceous materials such as a graphite ($\alpha : 1.18\times10^{-6}\ ^{o}K^{-1}$), polycrystalline graphite ($\alpha : 1.18\times10^{-6}\ ^{o}K^{-1}$), diamond ($\alpha : 1.18\times10^{-6}\ ^{o}K^{-1}$), and polycrystalline diamond ($\alpha : 1.18\times10^{-6}\ ^{o}K^{-1}$) [72]. An order of 10^{-6} for the thermal expansion coefficient plays a negligible role when inserted into (2.13). One can therefore approximate $RnC[\theta]$ to $R_n[\theta]$. LCVD carbon fibers being non-homogeneous, it follows that the density of the fiber will be dependent on the dominant microstructure. By assuming a uniform average density of $1.65\times10^{3}\ kg/m^{3}$ over the fiber cross-section

$$\rho C[r] = \rho C = 1.65\times10^{3}\ kg/m^{3}. \quad (2.14)$$

Now, the mass deposition rate of carbon can be represented as

$$\mu C[\theta] = R_n[\theta]\rho C \quad (2.15)$$

The molar deposition of carbon $MC[\theta]$ can now be obtained from

$$MC[\theta] = \frac{\mu C[\theta]}{C_m}. \quad (2.16)$$

where C_m is the atomic weight of carbon ($12.011\times10^{-3}\ kg/mol$).

Therefore, the deposition rate of carbon in various forms (normal, volumetric, mass, molar) can be written as

$$\frac{R_n[\theta]}{R_n[0]} = \frac{RnC[\theta]}{RnC[0]} = \frac{\mu C[\theta]}{\mu C[0]} = \frac{MC[\theta]}{MC[0]} = Cos[\theta]. \tag{2.17}$$

Representing the fiber tip again as an ellipse with unit radius and a major axis equal to twice the radius, carbon non-dimensional deposition rate in all forms mentioned in (2.17) can be plotted as shown in Figure 2.5.

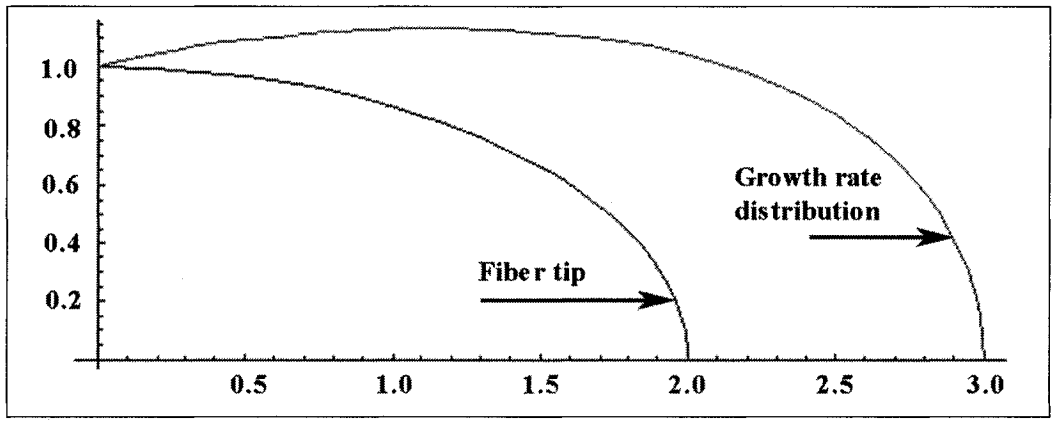

Figure 2.5 Carbon deposition rate normal offset plot around fiber tip

LCVD being a highly temperature-dependent process, the obtained growth rate along the fiber tip is dependent on the temperature distribution around the tip. This means that the growth rate at the center of the fiber tip must be larger than at the tip's periphery. The steep temperature distribution profiles in Figure 2.4 would therefore indicate that gaseous reaction by-products (atomic hydrogen, hydrogen, and/or intermediate radicals) should be emitted in larger quantities from the center of the fiber tip owing to higher reaction rates. To obtain the distribution of the emitted hydrogen by-product, one will need to know:

1. The stoichiometry of the reaction
2. The yield ${}_{t}C[\theta]$ of the deposition where ${}_{t}C[\theta]$ represents the fraction of deposited carbon
3. The fraction $\beta(T)$ of atomic hydrogen emitted at temperature T
4. The temperature T of the emitted hydrogen.

While it is acknowledged that many elementary reactions happen during carbon deposition from ethylene, for the sake of simplicity, ethylene pyrolysis stoichiometry can be expressed as

$$C_2H_4 \rightarrow 2C_{(s)} + 4\beta H + 2(1-\beta)H_2. \tag{2.18}$$

The stoichiometric ratio expressing the number of moles of each species (atomic hydrogen and molecular hydrogen) emitted per mole of deposited carbon is:

$$S'[H] = 2\beta$$

$$S'[H_2] = 1-\beta.$$

Knowledge of molar deposition rate of carbon $MC[\theta]$ and its yield ${}_{t}C[\theta]$ can aid in determining the emission rates of the by-products. The molar rate of atomic and molecular hydrogen ($M[H,\theta], M[H_2,\theta]$) can then be obtained from the following expressions

$$M[H,\theta] = \frac{2\beta[T]M[C,\theta]}{{}_{t}C[\theta]} \tag{2.19}$$

$$M[H_2,\theta] = \frac{(1-\beta[T])M[C,\theta]}{{}_{t}C[\theta]}. \tag{2.20}$$

Using the molar rates of emission of atomic (2.19) and molecular hydrogen (2.20), one can proceed to obtain volumetric emission rates of atomic hydrogen (2.21) and molecular hydrogen (2.22) by taking into account the molar volume v_0 of hydrogen at 273 K under the assumption that the emitted hydrogen by-product behaves like a perfect gas.

$$R_n[H,\theta] = v_0\, M[H,\theta]\frac{T[\theta]}{T[0]} = v_0\,\frac{2\beta[T]M[C,\theta]}{{}_tC[\theta]}\frac{T[\theta]}{T[0]} \tag{2.21}$$

$$R_n[H_2,\theta] = v_0 M[H_2,\theta]\frac{T[\theta]}{T[0]} = v_0\,\frac{(1-\beta[T])M[C,\theta]}{{}_tC[\theta]}\frac{T[\theta]}{T[0]}. \tag{2.22}$$

One can non-dimensionalize the equations (2.21) and (2.22) by taking the ratio with respect to emission rates of atomic and molecular hydrogen at $\theta = 0$, to obtain (2.23) and (2.24)

$$\frac{R_n[H,\theta]}{R_0[H,0]} = \frac{\frac{\beta[T]}{\beta[0]}\frac{T[\theta]}{T[0]}Cos[\theta]}{\frac{{}_tC[\theta]}{{}_tC[0]}} = \frac{\frac{\beta[T]}{\beta[0]}\frac{Cos[\theta]}{1-\frac{Log[Cos[\theta]]}{\frac{E_a}{RT[0]}}}}{\frac{{}_tC[\theta]}{{}_tC[0]}} \tag{2.23}$$

$$\frac{R_n[H_2,\theta]}{R_0[H_2,0]} = \frac{\frac{1-\beta[T]}{1-\beta[0]}\frac{T[\theta]}{T[0]}Cos[\theta]}{\frac{{}_tC[\theta]}{{}_tC[0]}} = \frac{\frac{1-\beta[T]}{1-\beta[0]}\frac{Cos[\theta]}{1-\frac{Log[Cos[\theta]]}{\frac{E_a}{RT[0]}}}}{\frac{{}_tC[\theta]}{{}_tC[0]}} \tag{2.24}$$

While not entirely true, an assumption is made that the yield is uniform around the fiber tip. In reality, however, the yield or reaction rate is dependent on temperature in the kinetic regime. The assumption simplifies (2.23) and (2.24) to

$$\frac{R_n[H,\theta]}{R_0[H,\theta]} = \frac{\beta[T[\theta]]}{\beta[T[0]]}\frac{Cos[\theta]}{1-\frac{Log[Cos[\theta]]}{\frac{E_a}{RT[0]}}} \tag{2.25}$$

$$\frac{R_n[H_2,\theta]}{R_0[H_2,\theta]} = \frac{1-\beta[T[\theta]]}{1-\beta[T[0]]}\frac{Cos[\theta]}{1-\frac{Log[Cos[\theta]]}{\frac{E_a}{RT[0]}}}. \tag{2.26}$$

Experimental observations (chapters 3, 4 and 5) indicate that the atomic hydrogen emission signal at 656 nm is limited to a very small region around the tip. Optical emission spectroscopy of the fiber tip and at various distances away from the fiber tip

could yield qualitative, if not quantitative information on the availability of atomic hydrogen away from the fiber tip. A recent study* of the light emission during LCVD of Yttria-stabilized Zirconia (YSZ) films confirms the dominance of ionic species confined close to the reaction zone. Furthermore, a detailed analysis of the thermodynamics of ethylene pyrolysis at various temperatures is needed to understand the reaction step yielding atomic hydrogen. Until further quantitative information is available, if one were to make the assumption that the yield of atomic hydrogen is minimum compared to molecular hydrogen, then the expression for obtaining the volumetric emission rate of molecular hydrogen (2.26) becomes

$$\frac{R_n[H_2,\theta]}{R_0[H_2,\theta]} = \frac{Cos[\theta]}{1-\frac{Log[Cos[\theta]]}{\frac{E_a}{RT[0]}}}. \tag{2.27}$$

If we were to again take an elliptical tip with unit radius and a major axis equal to twice the radius and plot the emission rate of hydrogen at temperatures ranging from 1273 K to 4273 K, scaled to the maximum temperature, the normalized molecular hydrogen emission distribution around the fiber tip takes the form presented in Figure 2.6.

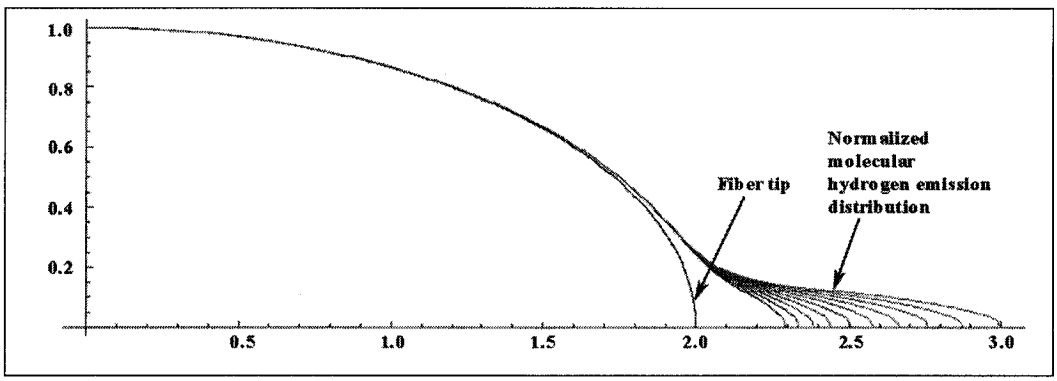

Figure 2.6 Normal offset plot of normalized hydrogen emission distribution around fiber tip

* H. Miyazaki, T. Kimura, T. Goto. J: Jpn. J. Appl. Phys. 42, L316-L318 (2003)

At this venue, it is acknowledged that the supporting argument indeed made many simplifying assumptions as an in-depth modeling of the fiber tip is beyond the scope of this study. The main objective behind the fiber growth model was to get a qualitative idea of what could be happening at the fiber tip. It must be noted, however, that despite the simplifying assumptions, experimental observations (section 2.2.2) augment the proposed hypothesis. Going back to Figure 2.6, if by-products indeed were emitted with such a steep gradient at the fiber tip as shown in the figure, then one should be able to experimentally observe the by-product jet or the convection currents induced by the jet in the vicinity of the reaction zone.

2.2.2 Experimental evidence of the by-product jet

Results from static fill HP-LCVD experiments done at the Institute for Micro-manufacturing, Louisiana Tech University [73] report observing a particle jet, evidenced as a series of bright spots emanating from the reaction zone and moving towards the laser beam along the fiber growth axis (Figures 2.7a and 2.7b). Formation of carbon dust/soot at high laser powers in both HP-LCVD and LP-LCVD has been reported in the literature [2, 74]. In all likelihood, the bright spots witnessed in the LCVD setup of [73] are a result of the so-formed carbon soot cutting across the laser beam. Differential image analysis (Figure 2.7c) of consecutive image frames in Figures 2.7a and 2.7b clearly indicate the direction of travel of the bright spots. It must be noted, however, that the data presented in Figure 2.7 neither provides information on the velocity of the particle jet nor tracks the individual particles as they move across the field of view of the camera. It merely lends proof to the existence of a particle jet. Using a different viewing hardware configuration, experiments of [73] also provide evidence to the existence of a luminous jet at the reaction zone during fiber growth as shown in Figure 2.8.

Recent experimental results with a static fill setup [58] corroborate the presence of a luminous jet along the laser axis during fiber deposition. In fact, it reports that the

luminous jet follows the reaction zone as the fiber grows. Furthermore, strong convection currents were observed in the vicinity of the reaction zone along the fiber axis, and into the laser beam.

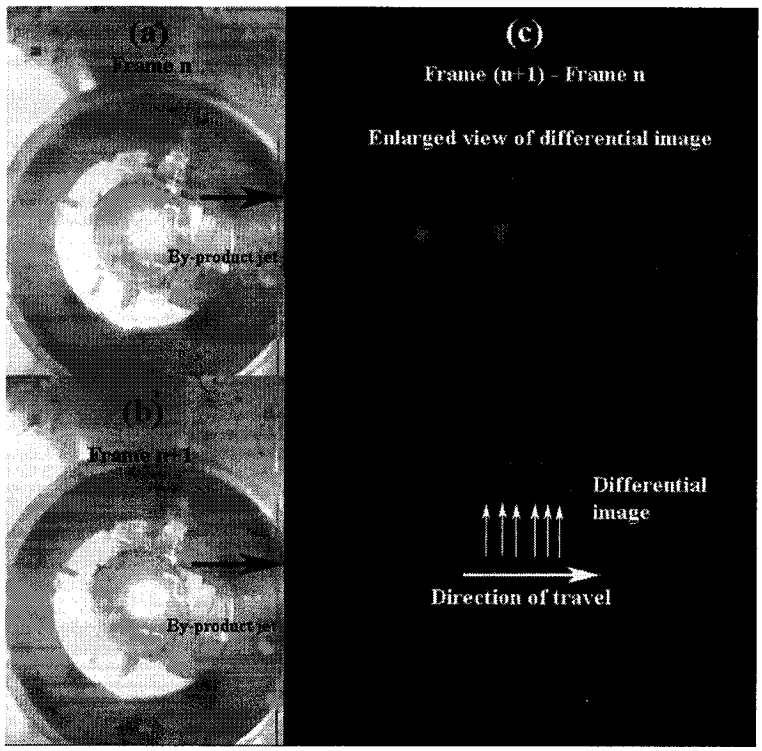

Figure 2.7 Differential imaging of by-product jet images [73]

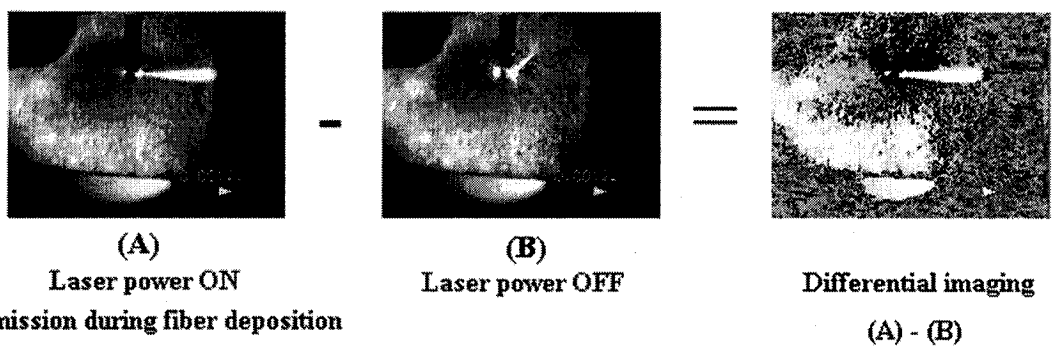

Figure 2.8 Differential imaging of LCVD video footage [73]

PIV measurements yielded velocities as high as 10 m/s near the reaction zone. The observed velocities are astoundingly high considering the fact that the experiments were done in the absence any externally induced flow.

The results of [58, 73], while providing sufficient evidence to the presence of a flow emanating from the reaction zone; raise the question of finding the source causing this flow. *To find the source, one need not look any further than the by-product jet.*

2.2.3 Conclusions from theoretical argument and experimental evidence

Based on the argument described in section 2.2.1 and experimental evidence presented in section 2.2.2, it can be hypothesized that momentum transfer caused by the by-product jet is sufficient to explain the strong convection currents observed in the vicinity of the reaction zone during fiber deposition. A schematic of the proposed by-product jet phenomena is shown in Figure 2.9. It can be noticed that the schematic does not include any additional directed flow of precursor (via a nozzle) as in Figure 2.1. In other words, Figure 2.9 can be considered as a static fill experiment, wherein the only evident flow in the form of convection currents is caused by the by-product jet.

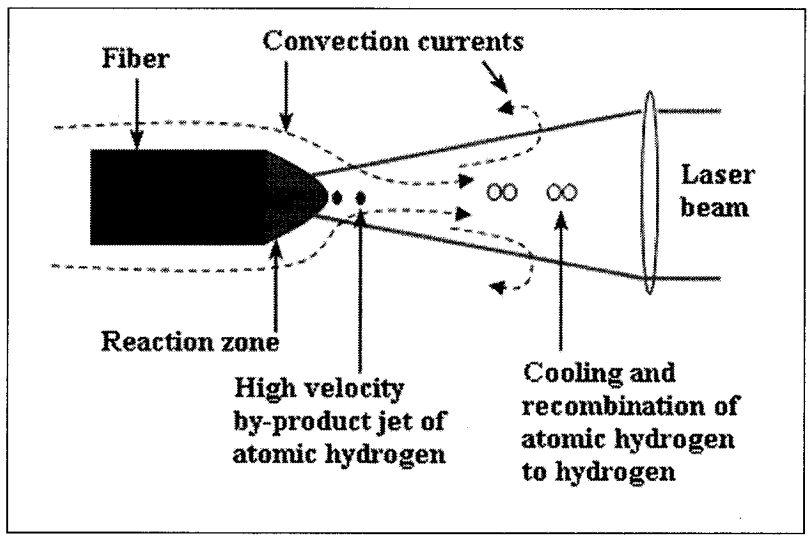

Figure 2.9 Schematic of proposed by-product jet phenomena

From Figure 2.9, it can be hypothesized that the thermal decomposition of precursor (methane/ethylene in the case of carbon deposition) at the tip of the fiber produces a concentrated by-product jet, which by momentum transfer produces a strong convection current that forces the surrounding precursor gas to move in the growth direction of the fiber. The carbon dust/soot follow the induced convection currents while crossing the laser beam path, yielding the streaking pattern witnessed in Figure 2.7. Another likely event that can occur is the cooling and recombination of the atomic hydrogen to form hydrogen. The recombination process can lead to a sudden decrease in volume creating an entrainment that exerts a suction effect on the precursor (causing the precursor to be pulled along the fiber axis). The effect of the momentum transfer and a probable entrainment is three-fold.

1. It brings in fresh precursor to the reaction zone thereby aiding the deposition process.
2. It improves heat transfer between the reaction zone and surrounding ambient. This in-turn can have two effects:
    a. Enhanced cooling rate resulting in smaller diameter fibers
    b. Enhanced cooling rate can extend the limits of the kinetic regime
3. It provides adequate support to the growing fiber from the buckling force created by the by-product jet. More recently, highly flexible carbon fibers that bent freely due to the convective bulk fluid forces during HP-LCVD from ethylene (using a static reactor setup) were observed [58].

In light of the discussion presented, the following conclusions can be drawn.

1. It appears that the generally accepted hemi-spherical model for LCVD growth [68] is inappropriate to describe the transport of precursor and its by-products. The model does not consider the convective outflow of by-products; it over-estimates the growth rate and does not represent the true situation during fiber growth. While Copley's work [69] better represents the fiber growth, both models consider isotropic diffusion in and out of the hemisphere.

2. In the case of a static reactor [73], the flow of by-products is directed into the laser beam. The anisotropic evacuation of by-products constitutes a micro-jet that entrains the surrounding gas and replenishes the reaction zone. However, this pumping effect is only driven by the jet. In the case of an axial convection enhanced system, the by-product jet is focused even more along the axial direction and the supply of fresh precursor can be enhanced by the forced precursor flow. In other words, an axial convection enhancement might contribute to an enhanced growth rate.
3. It can be concluded that a forced precursor jet in any direction other than the axial growth direction of the fiber would actually impede the growth rate by obstructing the self-sustained supply of precursor maintained by the momentum transfer imparted by the by-product jet. Published work reporting the decrease in growth rate using an angled jet convection enhanced system [66] lends support to the conclusion.
4. The viscous force of the precursor delivered coaxial to the growing fiber can bolster the fiber against the reaction force induced by the by-product jet. The reinforcement would be more pronounced at high reactor pressures.

2.3 Axial convection enhanced LCVD experimental setup

Before going any further, it is essential for a clarification to be made regarding the nomenclature of the produced deposit in the remainder of the following work.

According to literature [2], LCVD structures with diameter less than 100 μm are typically addressed as *fibers* while those larger than 100 μm are classified as *rods.* Although structures of different diameters (from ~25 μm to ~400 μm) have been deposited in the course of this work, we choose to address the deposited structures as rods in the context of the following research.

To experimentally investigate the work hypothesis, it is necessary to have a system that satisfies the following criteria

1. Ability to direct the precursor gas to flow coaxially to the deposited rod.
2. Ability to closely monitor the growth so as to obtain growth rate and positional information regarding the rod growth front.

A simplified schematic of the experimental setup is shown in Figure 2.10. The setup consists of an argon-ion laser operating in the TEM_{00} mode with an output beam diameter of 3.97 mm and a maximum power output of 5 watts in the multi-wavelength mode. The laser beam is focused to a 10 μm spot atop a 75 μm diameter tungsten wire substrate coaxial to the laser beam. The tungsten substrate is itself located in a stainless steel tube. Two different tube configurations were tried: the work in chapter 3 was done with a two-tube coaxial system, and the work in the remaining chapters was done with a three-tube coaxial system. In both configurations, the tungsten substrate is in the innermost tube of the coaxial configuration while argon gas is supplied through the outermost tube as a protective shroud to enclose the reaction zone from the ambient.

Flow rates of ethylene (precursor) and argon are controlled by a combination of precision flow meters and metering valves interfaced with a LABVIEW data acquisition system by means of a National Instruments PCI-6251 multi-function DAQ card. The emission from the reaction is monitored by a SONY XCD-X710 IEEE 1394 digital camera fitted with a 35X objective and a borescope that allows viewing only the region of interest. A 656 nm bandpass filter with 10 nm bandwidth placed between the objective lens and the CCD sensor allows viewing only emission centered at 656 nm. Positional growth rate information on the growing rod is obtained by tracking the centroid of the emission spot. The "field of view" of the borescope (32^0) is adjusted to encompass the effective growth inducing region of the laser beam. In the case of our experimental setup, the length of the focal region defined by the Raleigh range of optics is 160 μm.

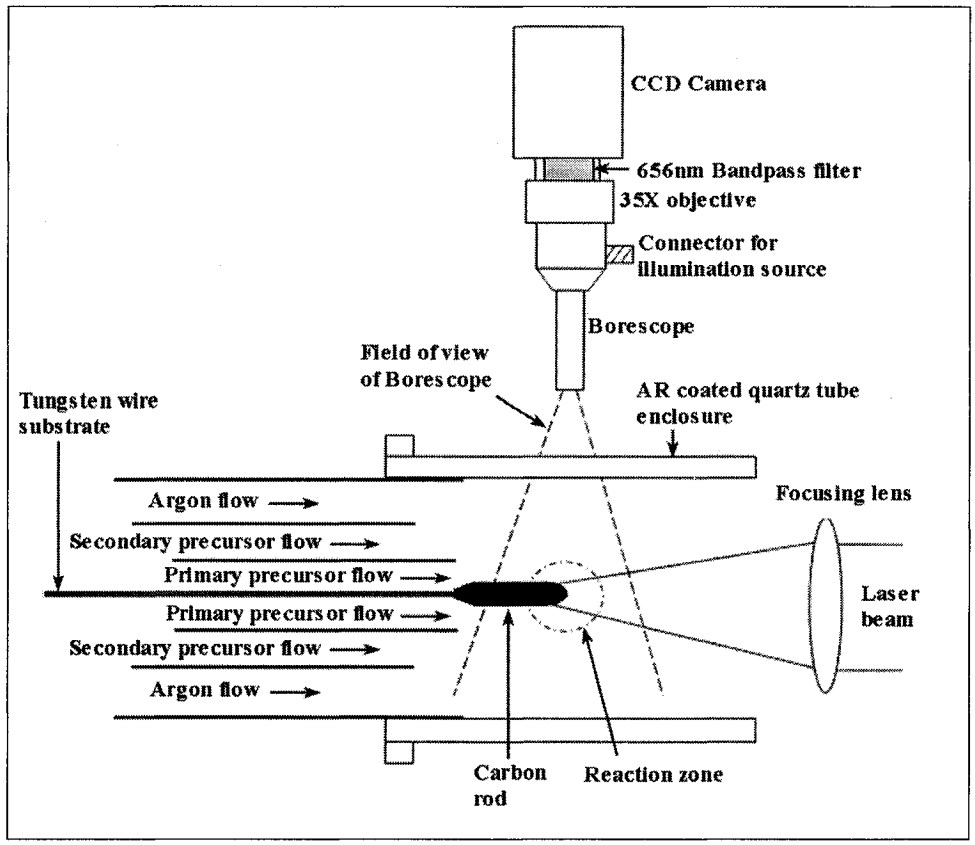

Figure 2.10 Schematic of axial convection enhanced LCVD setup

It is important to remember that rod growth can be sustained to lengths up to 4 mm using a stationary laser focus and substrate setup, at laser powers greater than 1.4 W. It is interesting to note that the length of the laser-induced growth region can be an order of magnitude greater than the Raleigh range of the optics. Rod growth happens in a chamber-less open-air environment wherein the reaction is restricted to the cloud of ethylene at the exit of the inner coaxial tube(s). To the author's knowledge, this work represents the first time rod growth using LCVD has been demonstrated in an open-air environment. Open-air LCVD of carbon coatings however have been demonstrated by Kwok et al [75].

2.4 Study of the effect of convection enhancement on growth rate

To test the designed axial convection enhanced LCVD setup, two different studies were conducted:

1. Studying the effect of laser power on the rod growth rate at constant precursor flow conditions.
2. Testing the effect of precursor flow rate on the rod growth rate at constant laser power.

2.4.1 Effect of laser power on growth rate at constant precursor flow rate

The objective of the axial convection enhanced flow configuration afforded by the proposed LCVD setup is to provide the reaction by-products such as atomic hydrogen and their ilk a free passage away from the reaction zone, while simultaneously replenishing it with fresh precursor injected from behind. The expected consequence of having the precursor to flow in the natural flow direction of the system is an improved growth rate and a possible extension of the limits of the kinetic regime. Previous work [66] on convection enhanced LCVD using a precursor directed at 45^{o} to the growing rod axis (Figure 2.1) does not report on the effect of increasing temperature (or laser power) on the rod growth rate at constant flow conditions.

A number of rods were grown at varying laser powers starting from 400 mW to 1800 mW in increments of 200 mW, while maintaining constant precursor flow conditions. Each rod was grown using a stationary substrate and laser focus. Positional growth rate curves (Figure 2.11) along the length of each rod was obtained using the image analysis procedure presented in chapter 3. The centroid of the emission spot is tracked during rod growth to measure the growth rate of the rod as well as the position of the rod growth front.

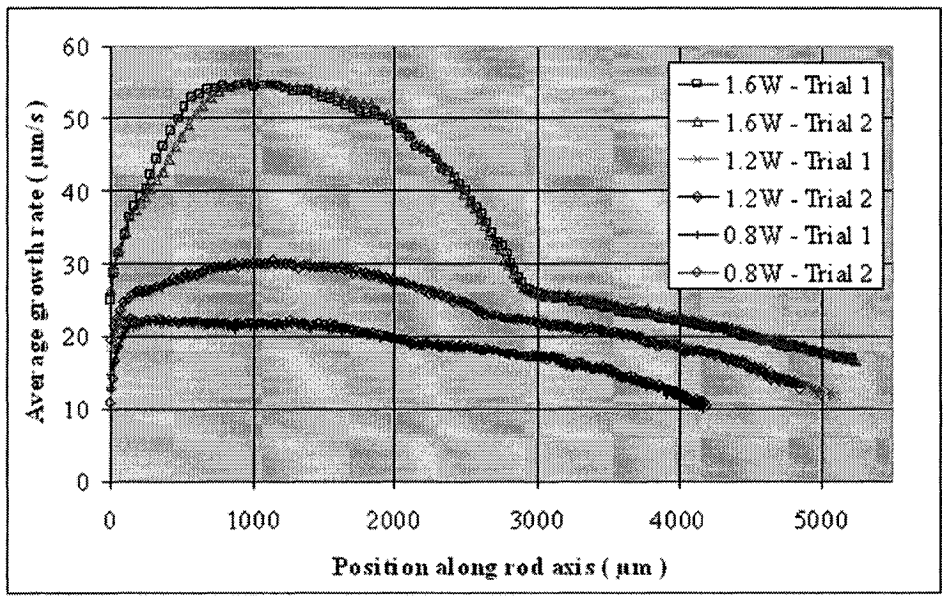

Figure 2.11 Repeatability of growth rate measurements

The maximum growth rate observed at each laser power is obtained from the corresponding growth rate curve and plotted in Figure 2.12. The repeatability of growth rate measurements (trial 1 vs. trial 2 in Figure 2.11) afforded by the image processing algorithm used in this work is worth noting. Also of interest is the consistent transient behavior of growth rate in the growth region, which is amplified with an increase in laser power.

A couple of interesting observations can be drawn from Figure 2.12:

1. The pattern of exponential increase in growth rate at lower laser powers followed by growth rate saturation witnessed in static reactor setups (Figure 2.2 as at 2.5 bars) is absent. Instead, the growth rate seems to follow a linear trend, with an increased slope at laser powers higher than 1400 mW.
2. A survey of LCVD literature reveals that growth rates obtained in Figure 2.12 are the highest recorded for carbon deposition at an operating pressure of 1 bar.

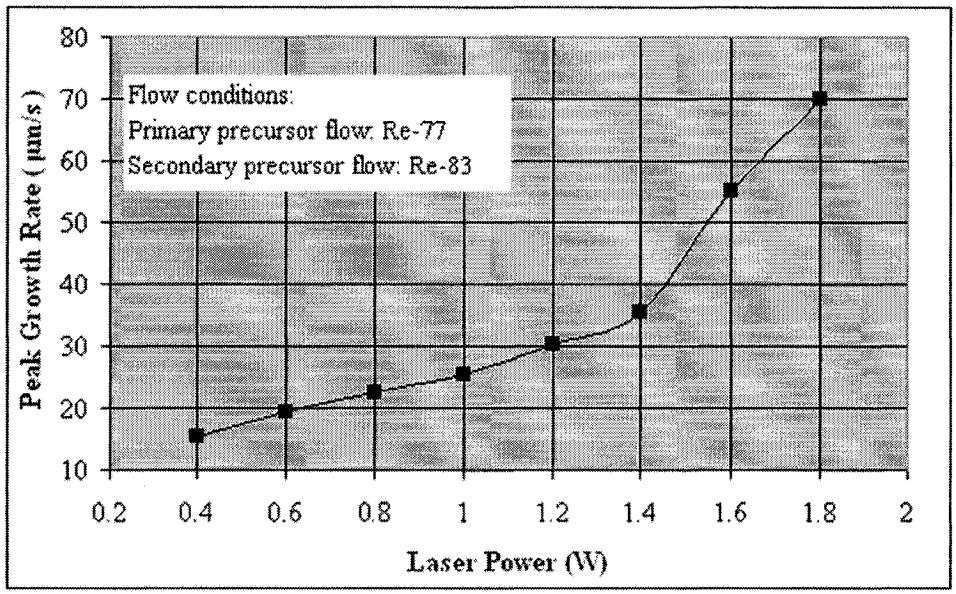

Figure 2.12 Effect of laser power on growth rate at constant flow rate

While we agree that there is no proportional relationship between laser induced temperature rise and laser power used, our inability to measure temperature makes it difficult to correlate the growth rate with temperature. Nevertheless, assuming a proportionality between laser power and laser induced temperature rise can allow one to get a pseudo Arrhenius plot (Figure 2.13) by plotting the inverse of laser power and logarithm of the growth rate on the X and Y axes respectively.

The results in Figures 2.12 and 2.13 are intriguing in that the growth rate trend observed goes against the commonly witnessed pattern of an exponential growth rate increase followed by saturation. The results can be explained in terms of convection enhancement, morphology change in rod microstructure, and/or a change in reaction mechanism.

A possible phenomenon that could have led to the continuously increasing growth rate pattern is the convection enhancement provided by the axial precursor flow of the LCVD setup. As proposed in the hypothesis, the axial precursor flow must be providing

a free passage to the by-products which is not the case in a static setup where the exit of by-products from the reaction zone is impeded by the incoming diffusive flow of precursor.

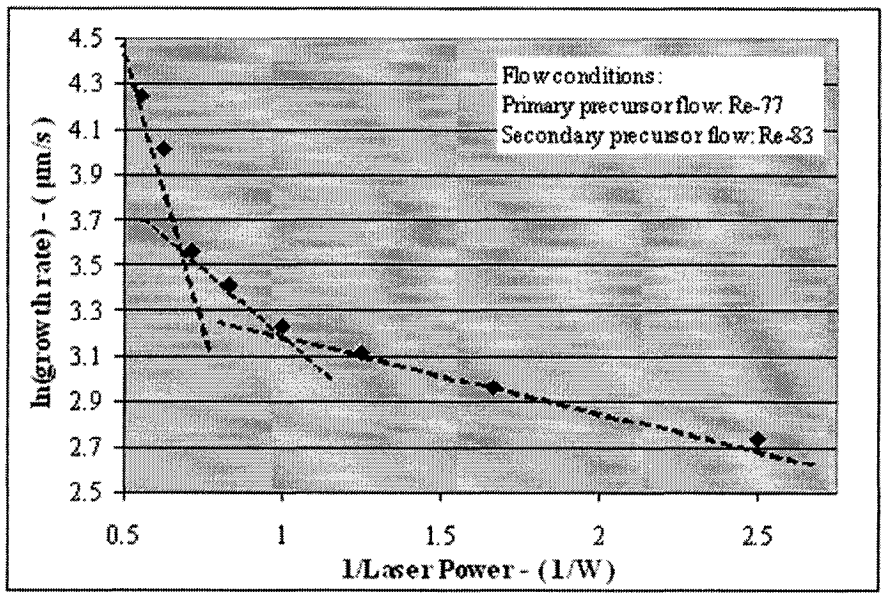

Figure 2.13 Pseudo Arrhenius plot

It appears that at lower laser powers from 400 mW to 1400 mW, the effect of convection enhancement far outweighs the laser induced temperature rise. This could explain the smaller slope of the curve from 400 mW to 1400 mW. After 1400 mW however, the laser induced temperature rise seems to dominate the effect of convection. A sudden change (increase) in temperature can explain the abrupt change in slope of the growth rate curve after 1400 mW. If the process is in the kinetic regime, the observed growth rate is extremely sensitive to the temperature, and any increase in temperature influences the growth rate significantly. Another possible effect of axial convection enhancement is the thinning of the boundary layer relative to a static setup, which can lead to improved mass transport. Though the reasons mentioned above provide a logical explanation to the witnessed experimental results, further computational and experimental studies are essential to corroborate and quantify the effect of axial

convection enhancement. Nevertheless, the *high growth rates coupled with the absence of growth rate saturation* observed in Figure 2.12 *is a clear indication of the positive impact of the axial convection enhancement* provided by the LCVD setup.

Another phenomenon that could be responsible for the growth rate pattern witnessed (Figure 2.12) is the change in rod microstructure with an increase in the laser induced temperature rise. It is documented in literature [76] that a change in the microstructure of the deposit (from amorphous to crystalline and vice versa) can influence the reaction mechanism. A morphology change on the surface of the growing rod can increase the surface area and lower its reflectivity [77]. A reduction in reflectivity in turn raises the temperature. If the process is kinetically limited, an increased surface area and lower reflectivity causes an increase in growth rate. The increase in the slope of the growth rate curve from 1400 mW suggests a possible change in the microstructure of the rod. Comparison of microstructures of rods produced at laser powers on either side of the transition point (1400 mW) can shed light on whether microstructural changes influenced the growth rate values.

The growth rate curve (Figure 2.12) can also be explained by a possible change in the reaction mechanism, which in turn is influenced by elementary reactions happening at a particular temperature. It is possible that a change in the laser induced temperature rise can affect the elementary step. It is proposed in [78] that the following two reactions are important during the decomposition of ethylene at high temperatures

$$C_2H_4 + H \rightarrow C_2H_3 + H_2 \tag{2.28}$$

$$C_2H_4 + M \rightarrow C_2H_2 + M + H_2, \tag{2.29}$$

where M is a non-reacting body.

An increase in reaction temperature can favor the abundance of atomic hydrogen in the reaction zone due to thermal diffusion [61]. This can lead to (2.28) being the elementary reaction step. An increase in atomic hydrogen concentration around the reaction zone

reduces the growth rate [61]. As reported in [2, 74], homogeneous reactions can also become important at high temperatures. Homogeneous reactions generate solid particles such as carbon dust that can lead to (2.29) being the elementary step. In fact, as observed in [58, 73], a particle jet and plume along the rod axis was clearly evident at high laser powers (≥1400 mW). Homogeneous reactions can also produce intermediate species such as CH_2 that can result in more efficient kinetics. Better kinetics manifests itself into improved growth rate. Identifying species emitted at the rod growth front and at different points in the plume by Optical Emission Spectroscopy (OES) can aid in achieving a better understanding of the reaction mechanism influencing the growth rate. Finally, temperature measurement of the reaction zone can assist in developing a correlation between emission spectra and reaction temperature.

In conclusion, a multitude of factors (temperature, microstructure, and/or reaction mechanism change) exist to explain the growth rate trend in Figure 2.12. Substantiating the actual factor(s) responsible for the witnessed trend however requires further study of the by-product emission signature, microstructure, temperature measurement of the reaction zone, computational, and experimental investigation of the effects of convection enhancement.

2.4.2 Effect of precursor flow rate on growth rate at constant laser power

To study the effect of precursor flow rate on the growth rate, several rods were grown at a constant laser power, but varying primary precursor flow rate. Each rod growth experiment was conducted with a stationary laser focus and substrate. As in section 2.4.1, the maximum growth rate at each laser power and primary precursor flow condition was obtained from their corresponding growth rate curve. Figure 2.14 plots the variation of growth rate at three different laser powers 800 mW, 1200 mW and 1600 mW at varying primary precursor flow rates.

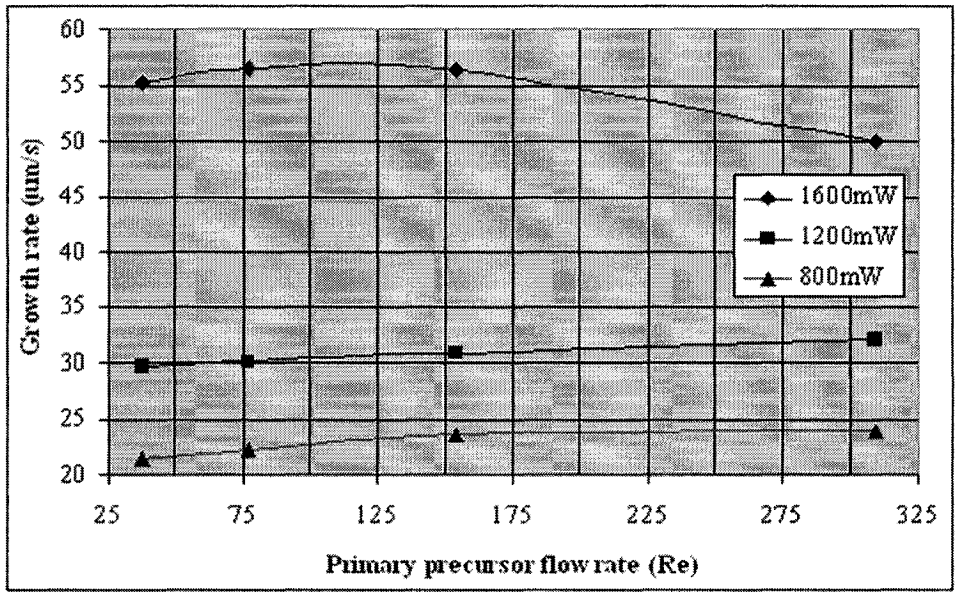

Figure 2.14 Effect of primary precursor flow on growth rate at constant laser power

The observations that can be drawn from the graph are as follows:

1. As in Figure 2.12, at all flow conditions used, the growth rate increase for the same laser power increment is noticeably higher at higher laser powers (Figure 2.15). This further reinforces the trend (absence of growth rate saturation) noticed in Figure 2.12.
2. At the highest laser power 1600 mW, the growth rate seems to reach an optimum value (between flow conditions Re: 75 and Re: 155) after which it experiences a downward trend. Surprisingly, the growth rates at lower laser powers do not reach their optimum value at the same flow conditions as 1600 mW. Within the available flow conditions tested, the growth rates at 800 mW, and 1200 mW marginally improve with an increase in flow rate. It remains to be seen if further experiments at 800 mW and 1200 mW at flow rates greater than Re: 309 will yield an optimum growth rate value followed by a decreasing trend as witnessed at 1600 mW.

3. At flow rates above Re: 154, irrespective of laser powers used, excessive flickering of the speckle pattern* (produced during rod growth) was observed. Even though the speckle pattern does not influence the growth rate, the instability of the speckle pattern can be used as an indicator for noticing the drop in growth rate at 1600 mW. A contrasting observation (marginal increase in growth rate with increasing flow) at lower laser powers 1200 mW and 800 mW is unexplained at this time. The drop in growth rate at 1600 mW after Re: 154 could also be due to enhanced cooling.

It must be noted that all the experiments reported in Figure 2.14 were done using a constant secondary precursor flow of Re: 83. Prior experiments identified Re: 83 to be the optimum flow for the secondary precursor syringe.

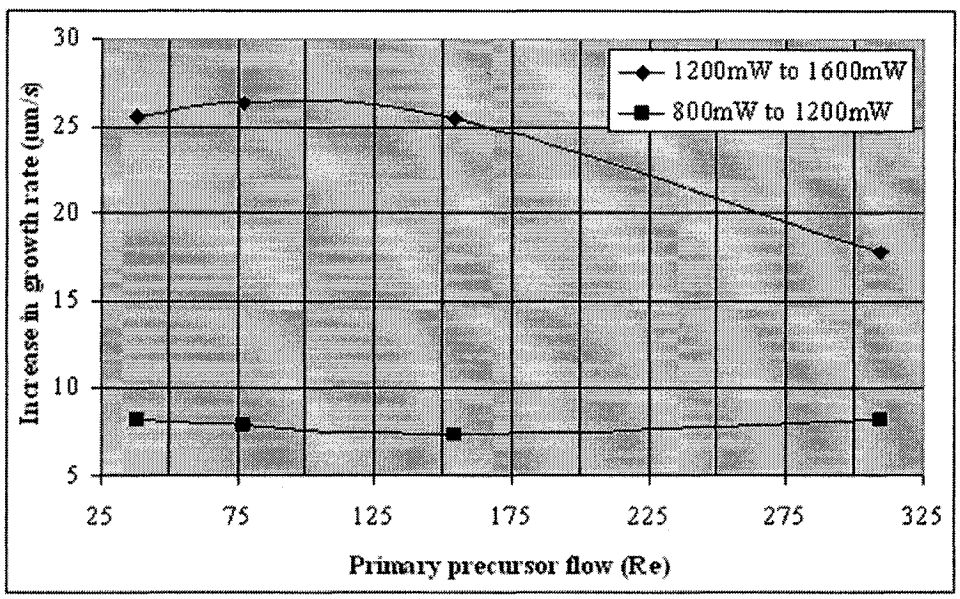

Figure 2.15 Effect of laser power increments to higher and lower laser powers at constant primary precursor flow

* Readers can refer to J.L. McLaughlin, Appl. Opt. vol.18, no.3, pp.1042-1045, 1979.

2.4.3 Conclusions on axial convection enhanced LCVD

In conclusion, the following comments can be made on the work reported in this chapter.

1. A first-of-its kind axial convection enhanced LCVD setup was realized.
2. The absence of saturation in the witnessed growth rate trend (Figure 2.12) lends evidence to the positive impact of axial convection enhancement on the growth rate. Further computational, microstructural, emission signature, and temperature measurement studies are essential to interpret the observed growth rate trend. The growth rates recorded are the highest to date for deposition of carbon rods at 1 bar.
3. Primary precursor flow variation studies point to the need for flow optimization to obtain optimal growth rates.

CHAPTER 3: ARTICLE 1 - POSITION DEPENDENCE OF GROWTH RATE IN CONVECTION ENHANCED LASER CVD OF CARBON RODS

One of the deterrents (identified in section 1.6, chapter 1) in advancing the use of LCVD as a fiber/rod development and production tool is poor process control. As identified earlier, temperature and consequently the produced growth rate is crucial to the obtained deposit microstructure. It is therefore essential to be able to determine the axial growth rate in-situ and in real-time. The obtained axial growth rate value can then be used to drive a feedback loop to position and control the rod growth front.

To the author's knowledge, this work represents the first time the axial growth rate and diameter of the produced rod along its axis have been determined in-situ and in real-time. This was made possible by the use of a 656 nm filter to monitor the atomic hydrogen emission during precursor pyrolysis. Obtained positional growth rate information can be beneficial in building a closed-loop control that can position and maintain the rod growth front at points of known growth rates, thereby yielding reproducible microstructures. Results also point to growth rates that appear to vary greatly inside the laser-induced growth region. It remains to be determined if the observed growth rate trend is not just an artifact of flow mixing.

POSITION DEPENDENCE OF GROWTH RATE IN CONVECTION ENHANCED LASER CVD OF CARBON RODS

R. Goduguchinta*, J. Pegna

Freeform Fabrication Laboratories, École Polytechnique de Montréal, Box 34, Pavillon J.-Armand Bombardier, 2900 Edouard Montpetit, Montréal H3T 1J4, Québec, Canada.

Submitted to: Applied Physics A on 11/09/2006

3.1 Abstract

The ability to closely monitor LCVD rod growth in the laser-induced growth region is demonstrated in the context of the first open-air axial convection enhanced micro-reactor. It was used to monitor carbon rod growth inside coaxial cylindrical flows of ethylene and argon. Monitoring and subsequent image analysis of the 656 nm atomic hydrogen emission from ethylene pyrolysis allowed real-time in-situ determination of axial growth rate and diameter along the axis of the produced carbon rods for the first time. Growth rates appear to vary greatly inside the growth region. This experiment raises questions about published qualitative models of LCVD rod growth that favor a uniform steady state regime. If the trend demonstrated in our experiments is not just an artifact of flow mixing, then it would indicate that published registered growth rates may just be an average value in the case of stationary substrate and laser focus experiments; or an artifact of focus tracking in the case of moving focus/substrate experiments. The results therefore point the way to experiments that would allow discrimination between the effect of flow mixing and the true nature of LCVD rod growth in the growth region.

PACS 81.16.Mk; 81.10.Bk; 81.05.Uw

---

* corresponding author: tel: +01-5143404711 x 7408; fax: +01-5143405282; email: ramkiran.goduguchinta@polymtl.ca

3.2 Introduction

Laser Chemical Vapor Deposition (LCVD) has been used to deposit rods of different materials [28-29] ever since the first rod growth demonstration was published by Nelson and Richardson in 1972 [15]. Excellent reviews [25, 27] provide an introduction to the subject. Maxwell et al [79] propose that growth occurs in three different regimes for rods initiated on perpendicular planar substrates without focus tracking: *Transient Regime,* where nucleation and growth rate of the deposit are influenced by the substrate properties; *Steady-State Regime*, where the growth rate is uniform and independent of substrate properties, and the diameter of the resulting rod is uniform as well, provided the laser power density is sufficient to sustain the growth rate; and *Tail Regime,* where the growth rate continuously drops as the rod tip gradually grows farther away from the laser focus.

The general approach followed in the literature [62, 80] for determining the axial growth rate of rods in a stationary substrate and laser focus experiment is to visually monitor the distance traversed by the rod tip over a certain time. Unless the measured growth happened in a region of identical focal conditions that can be ensured by either maintaining a constant laser power density [62, 79] or by always maintaining the rod growth tip at the laser focus [38], this system of measurement is likely to be insensitive to variation in growth rate with position of the rod tip in the growth region. To the authors' knowledge, this work represents the first attempt to quantify the axial growth rate in-situ and in real-time at different points along the axis of the produced rod. LCVD rod growth is known to be strongly dependent on temperature in the kinetic regime (following an Arrhenius relation). It has been demonstrated [59] that the temperature (and in turn the resulting deposition rate) affects the microstructural properties of the resulting rod. Microstructure in turn is related to the strength and overall quality of the rod as demonstrated by [60]. Knowledge of growth rate that yields the optimum material characteristics will help in building a control algorithm that can continuously maintain the deposition (rod growth front) at a position yielding the desired rate. Also, a

survey of literature provides no mention of rod growth in an open-air/chamber-free environment using LCVD and this marks the beginning of the same.

3.3 Experimental

The setup (Figure 3.1) consists of an Argon-ion laser operating in the TEM_{00} mode with an output beam diameter of 3.97 mm and a maximum power output of 5 watts in the multi-wavelength mode. The laser beam is focused to a 10 μm spot (measured using knife-edge technique) atop a 75 μm diameter tungsten wire substrate coaxial to the laser beam. The tungsten substrate is itself inside an inner tube with inner diameter 800 μm through which the precursor (Ethylene gas – 99.5% pure) is injected. The substrate overhangs from the inner coaxial tube by about 1 mm.

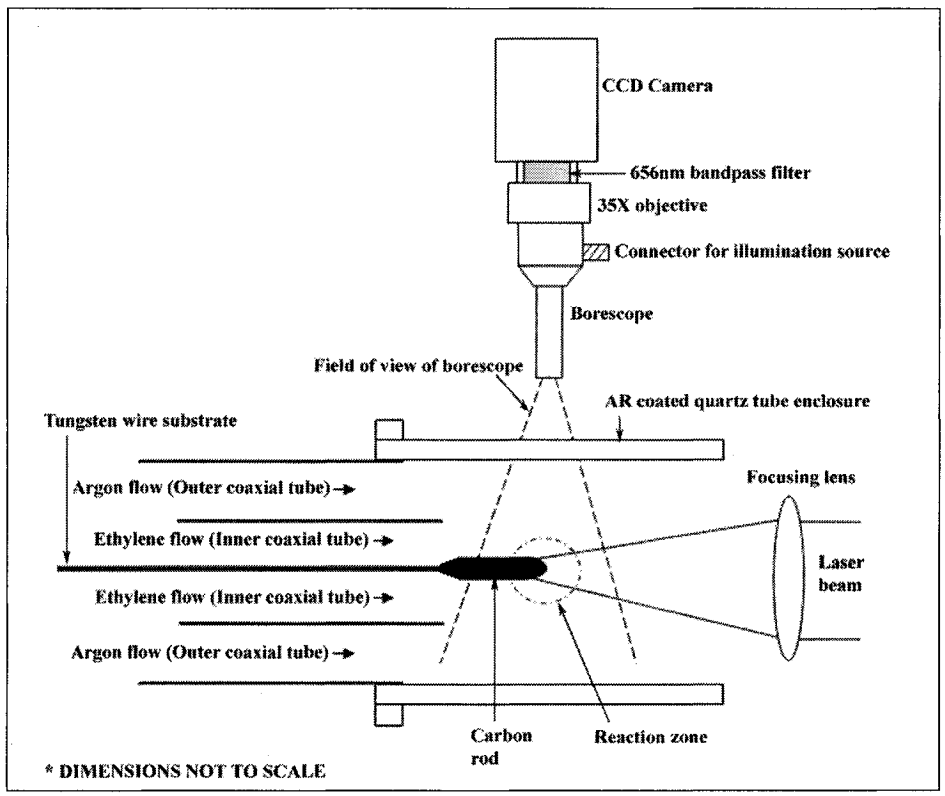

Figure 3.1 Experimental setup

The reaction zone is shielded from the ambient by a coaxial flow of argon that is delivered through an outer tube with inner diameter 4.57 mm. Flow rates of ethylene and argon are controlled by a combination of precision flow meters and metering valves interfaced with a LABVIEW data acquisition system by means of a National Instruments PCI-6251 multi-function DAQ card. The emission from the reaction is monitored by a SONY XCD-X710 IEEE 1394 digital camera fitted with a 35X objective and a borescope that allows viewing only the region of interest. A 656 nm bandpass filter with 10 nm bandwidth placed between the objective lens and the CCD sensor allows viewing only emission centered at 656 nm. The "field of view" of the borescope (32^{o}) is adjusted to encompass the laser-induced growth region.

Rod growth happens in a chamber-less open-air environment wherein the reaction is restricted to the jet of ethylene at the exit of the inner coaxial tube. Flow modeling of the experimental setup was conducted using FLUENT 6.1.22 for rod overhangs at 1, 2 and 3 mm and tip temperatures at 291 and 2500 K. The resulting mole fraction and molar concentration maps are shown in Figure 3.2. They clearly indicate that overhang and tip temperature have an influence over concentration in the region of interest. These numerical results also show that beyond 5 mm from the nozzle exit, in the worst case, mixing is almost complete.

The minimum distance at which mixing is complete (>80% argon molar concentration) thus effectively defines the micro-reactor chamber as a cylinder 1mm in diameter by 5 mm long. This numerical simulation further demonstrates that the micro-reactor effective length shortens with increasing overhang between 1 and 3 mm, and with increasing tip temperatures (Figure 3.3). Above 3 mm, neither overhang nor temperature seems to have a significant effect. The substrate is brought into the vicinity of the laser focus and once growth is initiated, the position of the laser focus and the substrate is kept unchanged. Rods grown at laser powers of 2.5 W, 1.5 W and 0.5 W

using a flow of Reynolds number, Re: 64 of Ethylene and Re: 176 of Argon are taken as representative examples for the analysis in the succeeding section.

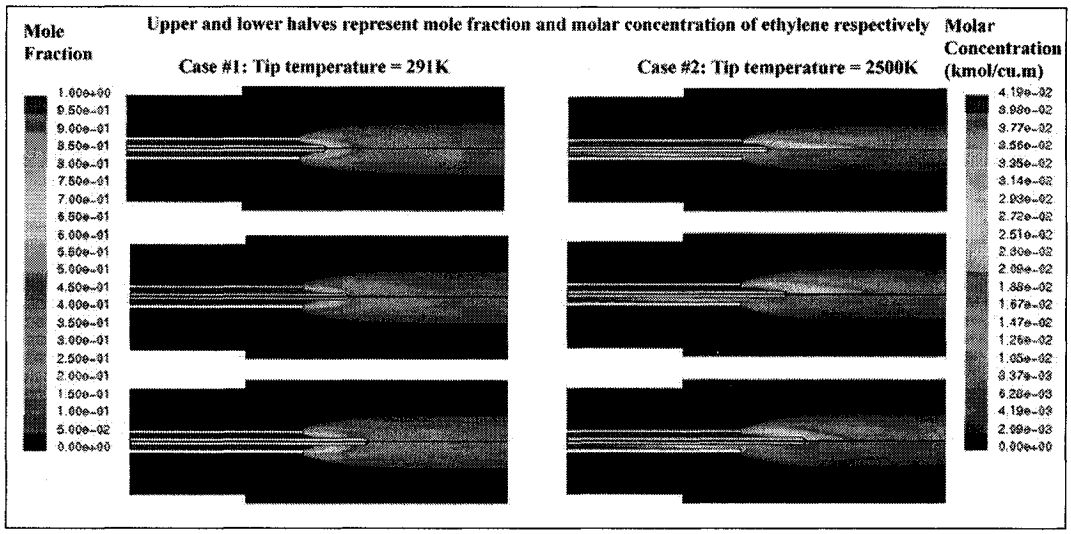

Figure 3.2 Mole fraction and molar concentration maps of ethylene in the micro-reactor for varying overhang (1, 2, and 3 mm) and assumed tip temperatures (Courtesy Jun Yu).

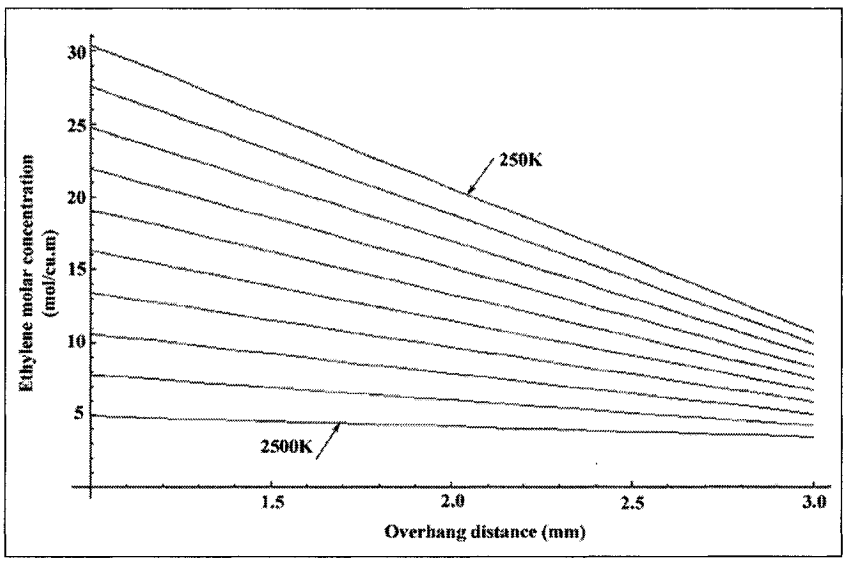

Figure 3.3 Tip concentration of ethylene as a function of overhang distance and tip temperature ranging from 250 K to 2500 K in increments of 250 K

3.4 Results and Discussion

In [79], it was proposed that the Hydrogen-Alpha line at 656 nm, representing the transition from $n = 3 \rightarrow n = 2$ in the Balmer series of atomic hydrogen is the dominant emission in the LCVD pyrolysis of ethylene. In the current work, the deposition was marked by the simultaneous appearance of a bright glow (corresponding to 656 nm) on the CCD array. "LABVIEW IMAQ for 1394 cameras" image acquisition software was used to capture a sequence of emission images in time intervals of 1 second throughout the range of rod growth. Each image was simultaneously processed by an image processing algorithm that involved the following three steps: 1) Thresholding to obtain a bitmap image 2) Emission spot centroid computation and 3) Centroid position difference measured along the rod's axis to obtain the axial growth rate. By increasing the threshold value, the effective image analysis area is confined to the hydrogen-rich region of rod growth. It is worth noting at this venue that it is legitimate to assume that the hydrogen-rich region also corresponds to the hottest region, yet thermal emission does not contribute significantly at 656 nm and thus can be neglected. Figure 3.4 with a typical image of the 656 nm emission as an inset, displays the rod grown (flow: Ethylene-Re: 64 and Argon-Re: 176, laser power: 2.5 W) as a demonstrative example to explain the positional growth rate computation scheme. Since rods at different growth parameters were sequentially deposited one on top of another, separation of the same from one another resulted in cracked top and bottom surfaces as seen in Figure 3.4.

Figure 3.5(a) shows the overlay of emission images captured every 30 seconds (t = 0, 30, 60, 90, 120, 150 and 180 sec) during the growth of the rod in Figure 3.4, and it gives a qualitative idea of the change in growth rate as the emission spot (rod growth front) travels across the CCD screen. By scanning the picture from the left to the right, one can observe that the displacement of the emission spot in each interval increases up to t = 60 sec, whereupon it slowly starts decreasing. Growth rates were measured in real time on the basis of the difference between consecutive centroid positions. The translation from image units relied on a calibration of the image acquisition system.

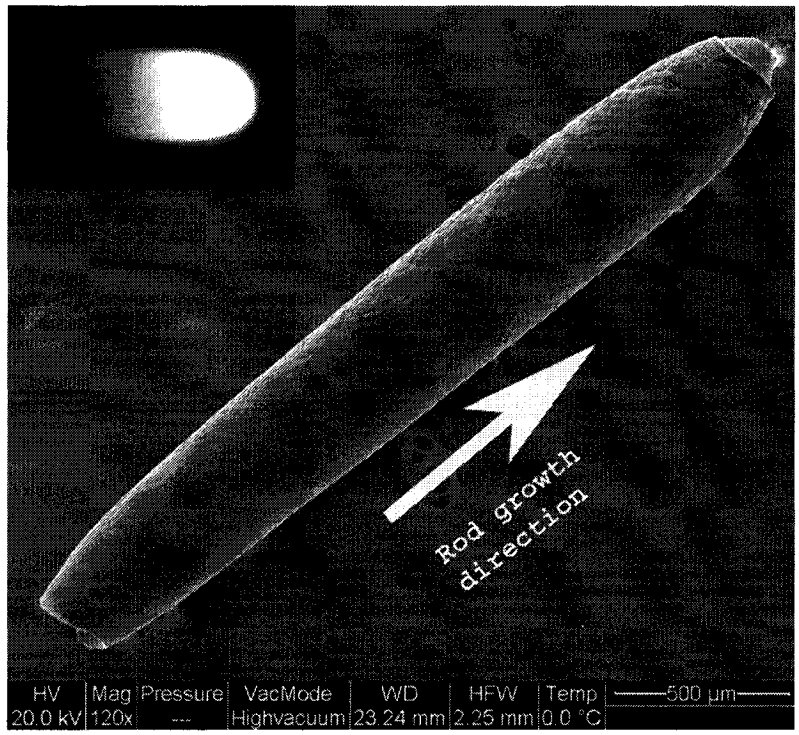

Figure 3.4 SEM image of carbon rod (inset: 656 nm emission spot)

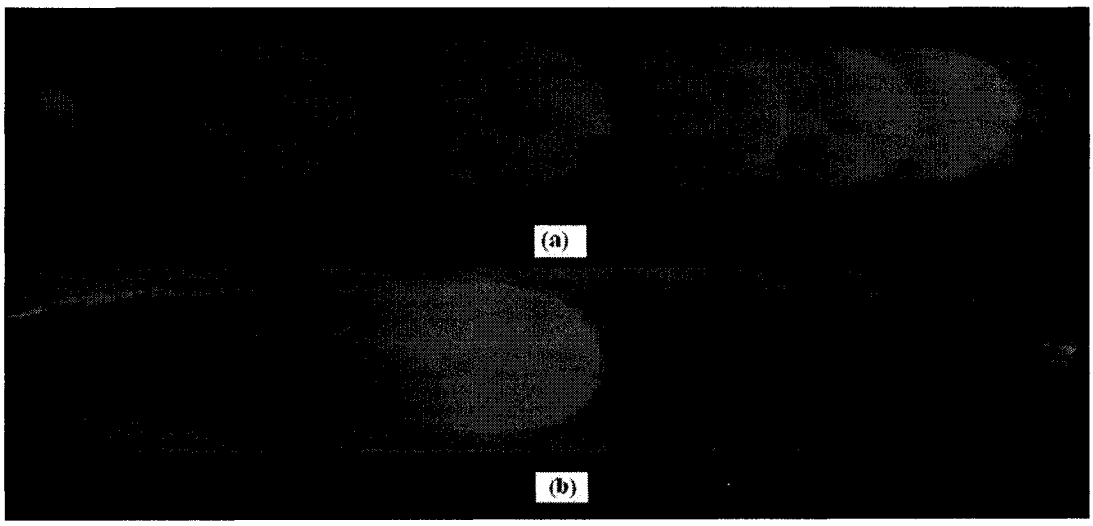

Figure 3.5 (a) Overlay of emission images captured every 30 seconds (b) Overlay of emission and rod images

Figure 3.6(a), representing the variation in growth rate (μm/s) with respect to the position along the rod axis corroborates and quantifies the observation made in Figure 3.5(a). Although all the growth curves in Figure 3.6(a) reach their peak growth rate at approximately the same position along their length, the growth curves at lower laser powers seem to exhibit a more uniform growth rate over their length. Obtaining a growth rate curve as shown in Figure 3.6(a) can be beneficial in 1) Knowing the maximum possible growth rate for a given process parameter set, as well as growth rates experienced by the rod at different points along its length or in other words, at different points in the focal region 2) Will be useful in building a feedback system that can position as well as maintain the substrate/rod growth front at points of known growth rates, yielding reproducible microstructures.

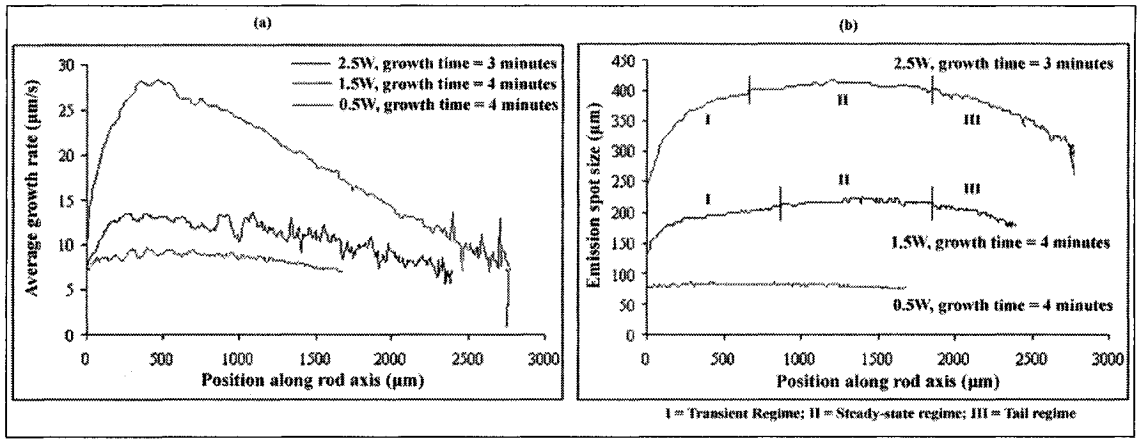

Figure 3.6 (a) Variation of growth rate with position along rod axis (b) Variation of emission spot size with position along rod axis

Another observation that was made during the course of this work is that the dimension of the 656 nm emission spot seems to correlate with the rod diameter. This discovery affords a means for making real-time in-situ rod diameter measurements. Figure 3.5(b) represents an overlay of the emission image at time t = 60 sec during growth of the rod shown in Figure 3.4, on the image of the same rod captured using the CCD camera. Measurement of the emission and rod diameters revealed a close match between the two,

with a maximum error of 5%. The size of the emission spot during the growth of the rod in Figure 3.4 was calculated in real-time by extracting the column of pixels corresponding to each centroid position obtained from the previously discussed algorithm, and calculating the length of the high intensity region in the column. The result in Figure 3.6(b) closely follows the shape of the rod in Figure 3.4. Also, it appears that with a decrease in laser power, the size of the steady-state diameter region seems to increase. Contrary to growth rates, the results concerning rod diameter in Figure 3.6(b) are consistent with the notion that three regions can be identified as in [79]. Granted our experiments differ from those of Maxwell et al [79] in terms of substrate and convection enhancement, it appears nonetheless that growth regimes identified in [79] do not agree with our observations. In light of our results, only the rod diameter appears to have a steady-state region. Growth rate, on the contrary is anything but steady. In fact, it strongly depends upon the position of the growth front inside the growth region. In other words, the axial growth rate of a rod in our reactor is anything but uniform when both substrate and focus are stationary. It remains to be determined by further experiments whether this relatively important variation in growth rate along the laser-induced growth region is an artifact of concentration variations only, or if it betrays a heretofore unrecognized characteristic of LCVD rod growth.

3.5 Conclusions

A novel LCVD micro-reactor design has allowed the monitoring of rod growth when both laser focus and substrate are stationary. Because the substrate is a wire tip coaxial with the laser and precursor flow, this configuration eliminates the flow restriction imposed by a planar substrate, while allowing the study of the effect of forced axial convection. Image analysis of the atomic hydrogen emission signal at 656 nm from ethylene pyrolysis allowed real-time in-situ determination of the axial growth rate and diameter along the axis of the rod's growth front for the first time. It brings into question whether growth rates reported in the literature to date were either averaged in the case of stationary laser focus and substrate systems, or just an artifact of the tracking

system in the case of moving focus rather than a characteristic of the deposition. Incremental knowledge provided by our rate measurement is important in securing a feedback system that allows accurate reproduction of microstructures. This knowledge is critical if one is to control the process well enough to ensure reproducible microstructures and study the effect of convection enhancement on the reaction kinetics.

Acknowledgements

Financial support for this research was provided by the National Science and Engineering Research Council of Canada under grants EQPEQ301036-04 and I2IPJ305768-03, in partnership with Technospin Inc., of Saint-Laurent, Québec. Financial support from Free Form Fibers, L.L.C is greatly acknowledged. The authors also would like to express their gratitude to Jun Yu for help with flow modeling and to Christian Fauteux and Rémi Longtin for their valuable comments on the manuscript.

CHAPTER 4: ARTICLE 2 - ON THE IMPORTANCE OF FOCUS TRACKING IN LCVD GROWTH OF CARBON RODS

The work presented in chapter 3, while presenting a technique for the real-time in-situ determination of the axial growth rate and diameter of the produced rod along its axis, also raised a question on the effect of flow mixing on the varying positional growth rate trend witnessed. A new coaxial tube system was designed wherein the primary precursor (ethylene) flow was separated from the argon flow in the outermost coaxial tube by a secondary precursor (ethylene) flow acting as a protective shroud. This flow scheme eliminates flow mixing concerns prevalent in the earlier tube system (chapter 3).

In-situ axial and volumetric growth rate measurements utilizing the technique presented in chapter 3 confirm the large variation of growth rate within the laser-induced growth region. The results reiterate the importance of controlling the position of the rod growth front relative to the focal plane to obtain microstructural uniformity.

ON THE IMPORTANCE OF FOCUS TRACKING IN LCVD GROWTH OF CARBON RODS

Ramkiran Goduguchinta*, Joseph Pegna

Freeform Fabrication Laboratories, École Polytechnique de Montréal, Box 34, Pavillon J.-Armand Bombardier, 2900 Edouard Montpetit, Montréal H3T 1J4, Québec, Canada.

Submitted to: Journal of Applied Physics on 17/09/2006

4.1 Abstract

Published LCVD literature often assumes rod growth rate to be constant within the laser-induced growth region. A novel experiment shows that it is not so. Transient growth rates appear to vary greatly inside the growth region. Hence previously published growth rates could be just average values or an artifact of focus tracking. To show this, a novel Convection Enhanced-Laser Chemical Vapor Deposition (CE-LCVD) micro-reactor was used to monitor carbon rod growth inside a dual coaxial ethylene flow, shielded with a coaxial argon flow. Real-time in-situ measurements of rod tip axial position and diameter point to a rapid variation of both linear and volumetric growth rate within the growth region. This discovery goes against published results with a stationary laser focus and substrate setup—describing LCVD growth of carbon rods as a stationary rate process within the growth region. It also points to the critical importance held by the growth front position relative to the focus as a process parameter to guarantee consistency of material properties.

PACS 81.16.Mk; 81.10.Bk; 81.05.Uw

---

* Corresponding author: tel: +01-5143404711 x 7408; fax: +01-5143405282; email: ramkiran.goduguchinta@polymtl.ca

4.2 Introduction

Results obtained with a novel convection enhanced LCVD micro-reactor appear to negate a commonly accepted view of rod growth, represented for example by Maxwell et al [62, 79, 81]. It is generally assumed that for stationary laser focus and substrate, rod growth goes through three different regimes without focus tracking: a *Transient Regime,* where nucleation and growth rate of the deposit are influenced by the substrate properties; a *Steady-State Regime*, where the growth rate is uniform and independent of substrate properties, and the diameter of the resulting rod is uniform provided the laser power density is sufficient to sustain the growth rate; and *Tail Regime* where the growth rate continuously drops as the rod tip gradually grows out of laser focus. The aforementioned view suggests that the growth rate experiences a period of uniformity over part of the rod length produced.

Determining the growth rate in real time is arduous since only optical probing is possible and the rod tip is flooded in laser, thermal, and by-product emissions. Thus, the general approach followed in determining axial growth rates in a stationary substrate and laser focus experiment is to visually monitor off-line the distance traversed by the rod tip over time [62, 81]. Unless the measured growth happened in a region of identical focal conditions that can be ensured by either maintaining a constant laser power density [62] or by always maintaining the rod growth tip at the same position in the laser focus [38], this system of measurement is likely to be insensitive to variations of growth rate with position of the rod tip within the laser-induced growth region.

Maxwell et al [79] were able to monitor volumetric deposition rates from the emission intensity of hydrogen at 656 nm. A novel reactor design allowed us to quantify the axial growth rate in-situ and in real-time at different points along the axis of the produced rod by imaging at 656 nm. The forced convection indeed produces a hydrogen emission that is confined close to the rod tip as opposed to the flame like emissions observed in static reactors.

Fauteux et al. [59] and Longtin et al. [60] have experimentally shown that temperature and deposition rates are critical to the produced microstructures and hence their properties. They indeed point to focus tracking as a critical process parameter. Focus tracking however may entail different processes depending on whether growth rate is indeed stationary or not. If it is, then it is sufficient to pull the focus away from the deposit at a rate less than or equal to the stationary growth rate. Even if one were to pull the deposit continuously at a constant rate like Wallenberger et al. [57] using the so-called *"self-regulating mechanism"* of axial growth rate, material properties of the deposit would be consistent no matter the position of the deposit relative to the focus. To our knowledge however, no investigation of the dependence of material properties upon pulling rate was ever conducted.

In contrast, and that is the focus of our paper, if growth rates were to experience large variations within the laser-induced growth region, then the conditions presiding over material deposition are strongly dependent on the position of the growth front relative to the focal plane. Rather than the pulling rate, it would therefore be that relative position which would become a critical process parameter towards controlling properties of the deposit. Granted that position determines growth rates, one should now focus on controlling the growth front position to ensure a consistent microstructure. If velocity driven focus tracking were to be used, it would have to rest on a prior knowledge of positional growth rate to secure microstructural consistency, no matter the selection of either a closed [38] or open-loop control [57].

If LCVD is to ever become an instrument for materials processing and synthesis, monitoring growth rate, growth regimes, and temperatures must be achieved. Our discovery that the growth rate varies greatly within the laser-induced growth region during rod growth is therefore an important milestone towards controlling the deposit materials properties.

On a different note, the work reported herein was conducted in an open-air reactor, and this marks the first such instance of LCVD rod growth.

4.3 Experimental

The setup (Figure 4.1) consists of an Argon-ion laser operating in the TEM_{00} mode with an output beam diameter of 3.97 mm and a maximum power output of 5 watts in the multi-wavelength mode. The laser beam is focused to a 10 μm spot (measured using knife-edge technique) atop a 75 μm diameter tungsten wire substrate coaxial to the laser beam. The tungsten substrate is itself located inside a stainless steel tube, with inner and outer diameters 310 μm and 565 μm respectively, through which the primary precursor (Ethylene gas – 99.5% pure) is injected. A second coaxial micro-tube, with inner and outer diameters 1.32 mm and 2.54 mm respectively surrounds the setup and is used to inject a secondary coaxial flow of precursor.

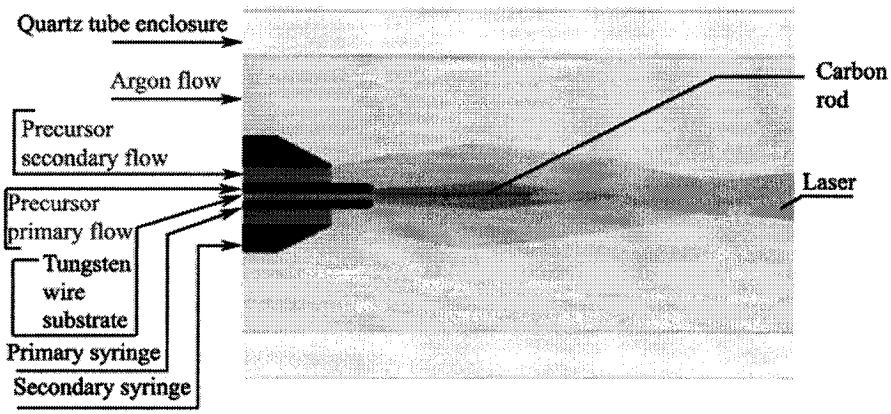

Figure 4.1 Micro-reactor schematic

In the present experimental setup, the secondary precursor is the same as the primary and is intended to provide a protective shroud preventing diffusion of species from a third coaxial flow, this time of argon, into the reaction zone. This flow of argon surrounds the whole reaction zone and is itself contained inside a 6 mm quartz tube

through which optical measurements are made perpendicular to the axis. The substrate overhangs from the inner coaxial tube by about 0.5 mm. Flow rates of ethylene and argon are controlled by a combination of precision flow meters and metering valves interfaced with a LABVIEW data acquisition system by means of a National Instruments PCI-6251 multi-function DAQ card. The emission from the reaction is monitored by a SONY XCD-X710 IEEE 1394 digital camera fitted with a 35X objective and a borescope that allows viewing only the region of interest. A 656 nm bandpass filter with 10 nm bandwidth placed between the objective lens and the CCD sensor allows viewing only emission centered at 656 nm. The "field of view" of the borescope (32^{o}) is adjusted to encompass the laser-induced growth region. Rod growth happens in a chamber-less open-air environment wherein the reaction is restricted to the cloud of ethylene at the exit of the inner coaxial tubes. Flow modeling of the experimental setup was done using FLUENT 6.1.22 to assess whether the ethylene shroud from the secondary flow would prevent diffusion of argon into the reaction zone. As the top half of Figure 4.2 illustrates, this assumption was supported by numerical simulations.

The substrate is brought into the vicinity of the laser focus and once growth is initiated, the position of the laser focus and the substrate is kept unchanged. Rods were grown at laser powers of 1.6 W, 1.4 W, 1.0 W and 0.6 W. The mean flowrates of all experiments were 7.4 and 60 sccm for the primary and secondary precursor flows respectively. This translates to Reynolds numbers of 42 and 83 respectively, well inside the laminar flow range.

4.4 Results and Discussion

Maxwell et al. [79] proposed that the Hydrogen-Alpha line at 656 nm, representing the transition from $n = 3 \rightarrow n = 2$ in the Balmer series of atomic hydrogen is the dominant emission in LCVD pyrolysis of ethylene. In the current work, the deposition was marked by the simultaneous appearance of a bright glow (corresponding to 656 nm) on the CCD array. "LABVIEW IMAQ for 1394 cameras" image acquisition software was

used to capture a sequence of emission images in time intervals of 1 second throughout the range of rod growth.

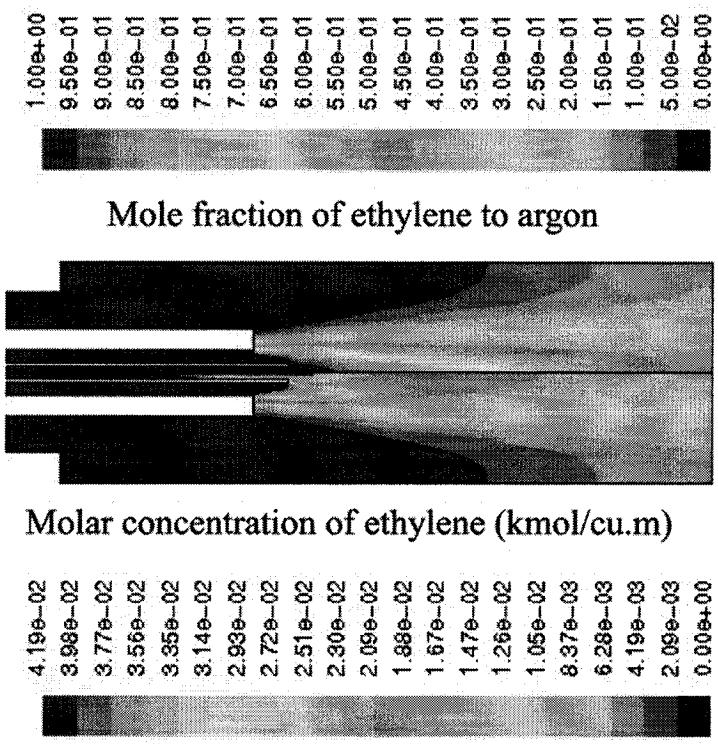

Figure 4.2 Flow simulation for stated experimental conditions and a tip temperature of 2500 K. Top half: Mole fraction of ethylene. Bottom half: Molar concentration of ethylene (kmol/m^3) (Courtesy Jun Yu).

Each image was simultaneously processed by an image processing algorithm that involved the following three steps: 1) Thresholding to obtain a bitmap image 2) Emission spot centroid computation and 3) Centroid position difference measured along the rod's axis to obtain the axial growth rate. By increasing the threshold value, the effective image analysis area is confined to the hydrogen-rich region of rod growth. It is worth noting at this venue that it is legitimate to assume that the hydrogen-rich region also corresponds to the hottest region, yet thermal emission does not contribute significantly at 656 nm and can be neglected.

Furthermore, we noted that the 656 nm image varies in size and shape during growth. To discriminate between possible influences due to size changes from those due to growth front advances, two image processing approaches were confronted. The first used the centroid position and the second used the image difference of consecutive emission fronts. Both measures gave results that were within $\pm 5\%$ of each other. Therefore, centroid position will be used for position measurement in the rest of this paper. The imaging measurement principle is illustrated in Figure 4.3, which shows a sample emission image superimposed onto the final rod. Tracking of the emission spot during growth thus provided real-time measurements of position, and axial growth rate of the deposited rod. Axial growth rates were obtained on the basis of the difference between consecutive centroid positions. The translation from image units relied on a calibration of the image acquisition system.

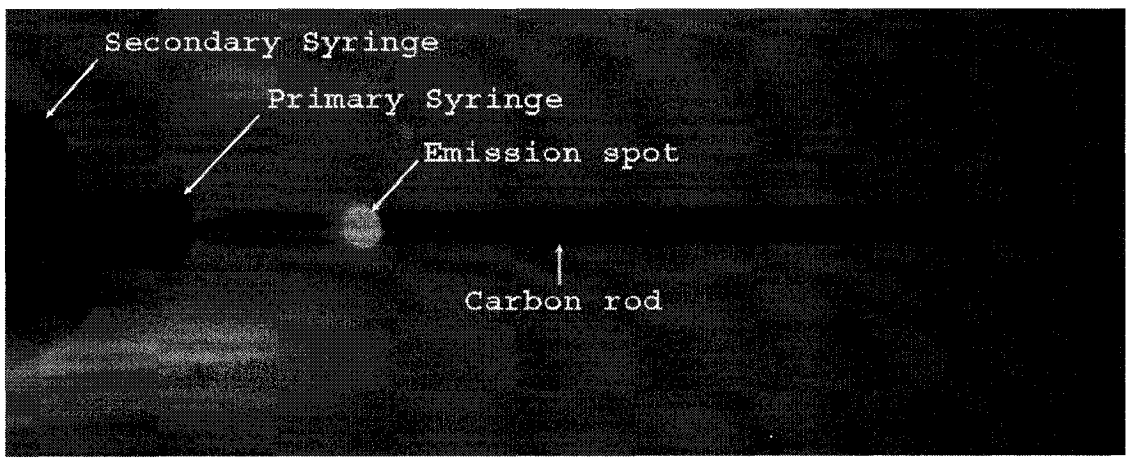

Figure 4.3 Superimposed pictures of the 656 nm emission during growth and final rod.

Rods were grown at 1 W by bringing the wire substrate to an initial position that was identical for all experiments. Growth rates versus position were recorded. The continuous curve in Figure 4.4 (Rod #1: 240 seconds) shows a sample positional growth rate curve. Positional growth rate curves were found to be reproducible within experimental noise.

Rod growth being a cumulative phenomenon, it is legitimate to question whether the observed relationship between position and growth rate indeed exists or if it is just an artifact of the cumulative nature, and therefore depends on the starting point. To discriminate between these two hypotheses, a second type of experiment was conducted wherein growth was interrupted and re-initiated from the same point. Whereas the continuous growth shown in Figure 4.4 (Rod #1: 240 seconds) was obtained over 240 seconds, a second series of rods were grown in 10 intervals of 24 seconds. After each 24 second interval, the laser power was turned off. Laser power was turned back on after a few seconds and the process was repeated.

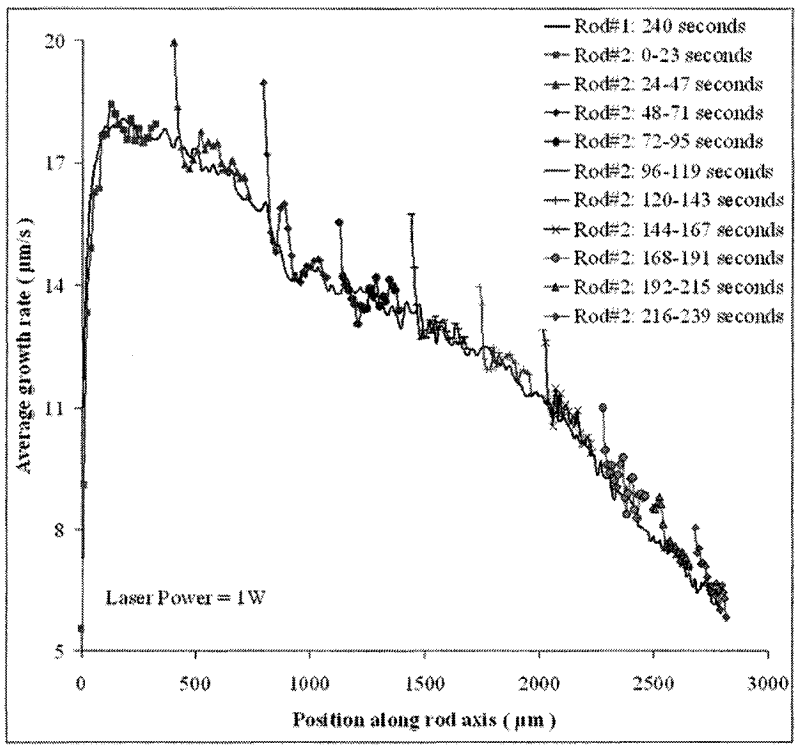

Figure 4.4 Positional axial growth rate along rod axis

Figure 4.4 now superimposes the fractional growth curves with the continuous one showing that growth rate is indeed a characteristic of position. It is however worth noting that in the case of the fractional growth experiment, growth rate experiences an

initial spike before settling to the continuous growth rate after a few oscillations. This initial surge in growth rate at the start of each fractional growth could be explained by the availability of fresh precursor just before turning on the laser power. As indicated by the plot in the lower half of Figure 4.2, the laser induced temperature rise significantly decreases the precursor molar concentration at the rod tip. Although this may contribute to the noticed drop in growth rate after the initial spike, it cannot account for the oscillatory behavior of growth rate. Moreover, note that the initial slope of the fractioned growth curves is of the order of 20 Hz. In all likelihood this would be too slow to account for a millisecond or less laser induced temperature rise. The transient behavior of fractioned growth may therefore point to more intricate interplay for which we do not have a satisfactory explanation. Finally, the shape and size of the final rod obtained at the end of all the fractional growth experiments appears to be no different from the rod of the continuous growth experiment. Needless to say, the rod growth in each of the fractional growth experiments continued from where it left off leaving no trace suggesting the intermittent nature of the experiments.

Several different combinations of precursor flow rates and laser powers were tried and all experiments exhibited growth rate profiles similar to Figure 4.4. Figure 4.5 represents the variation of linear growth rate (μm/s) along the axis of the rods grown at varying laser powers, but with the same precursor flow rates in the primary (Re: 42) and secondary (Re: 83) syringes. Although all the growth curves in Figure 4.5 reach their peak growth rate at approximately the same position along their length, the growth curves at lower laser powers exhibit a less drastic variation over their length.

The results illustrated in Figures 4.4 and 4.5 offer both scientific and engineering benefits. From a scientific viewpoint, these results dispel a heretofore implicit belief in a steady state growth rate using a stationary substrate and laser focus setup. This clarification is certainly more incisive in terms of engineering application since it

demonstrates the need to maintain growth at a given position in the focus to secure the targeted materials characteristics and facilitate reproducible microstructures.

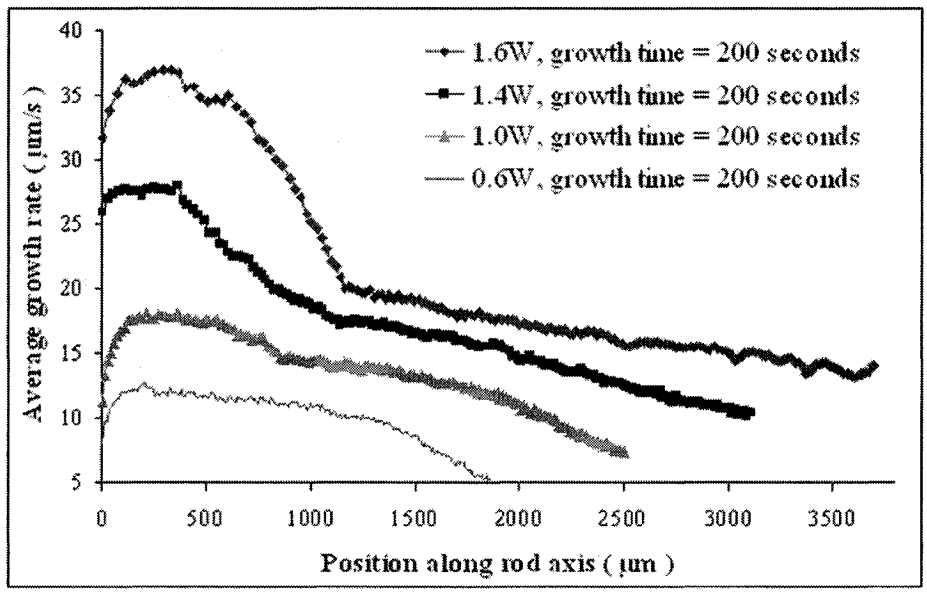

Figure 4.5 Variation of growth rate with position along rod axis at varying laser powers

Another observation that was made during the course of this work is that the dimension of the 656 nm emission spot seems to correlate with the rod diameter. This discovery affords a means for making real-time in-situ rod diameter measurements (Figure 4.6(a)). The size of the emission spot during rod growth was calculated in real-time by extracting the column of pixels corresponding to each centroid position obtained during growth rate measurement, and calculating the length of the high intensity region in the column. By combining axial growth rate information obtained from Figure 4.5 with rod diameter information from Figure 4.6(a), one can obtain volumetric growth rate information of the rod along its axis (Figure 4.6(b)). The drastic variation in both the axial and volumetric growth rates over the length of the rods is especially apparent at high powers. For example, in the case of growth at 1.6 W, the axial and volumetric growth rates drop by as much as 54% and 52% respectively within the first 1000 μm of growth. Granted our experiments differ from those of Maxwell et al [79] in terms of

substrate and convection enhancement, it appears nonetheless that growth regimes identified by them [79] are rather arbitrary. In light of our results, growth rate is anything but steady. In fact, it strongly depends upon the position of the growth front inside the laser-induced growth region. In other words, rod growth rate is anything but uniform when both substrate and focus are stationary.

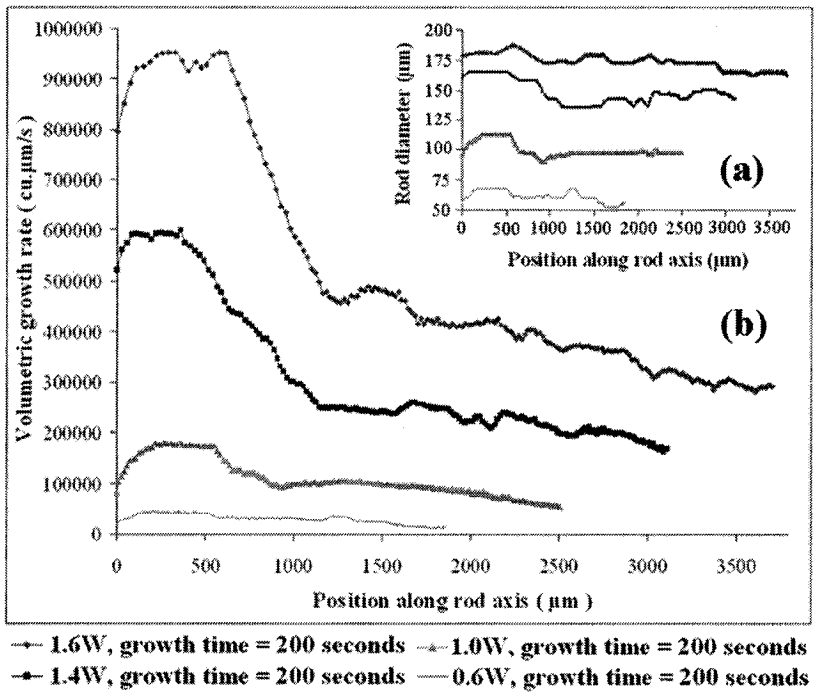

Figure 4.6 Variation of (a) rod diameter and (b) volumetric growth rate with position along rod axis

4.5 Conclusions

Measurements made possible by a novel convection enhanced LCVD micro-reactor design indicate that a commonly accepted assumption about stationary rod growth may well be incorrect. These measurements uncovered a relationship relating growth rate to position of the growth front in the laser-induced growth region, whereby, at higher laser powers, growth rates experience wide variations within the growth region.

Image analysis of atomic hydrogen emission signal at 656 nm from ethylene pyrolysis allowed real-time in-situ determination of the axial and volumetric growth rate along the axis of the rod's growth front for the first time. It also points to a weakness in growth rates reported to date to the extent that they were averaged over the growth range in the case of stationary laser focus and substrate systems, or that they may just be an artifact of the tracking system in the case of moving focus.

From a scientific standpoint, this article contributes a new vision into LCVD rod growth which dispels an implicit assumption of stationary rate. The main impact however is anticipated to be on engineering applications of LCVD rod growth as our observations point to the need to maintain position of the rod growth front during growth in order to guarantee the uniformity of microstructures and materials properties.

Acknowledgements

Financial support for this research was provided by the National Science and Engineering Research Council of Canada under grants EQPEQ301036-04 and I2IPJ305768-03, in partnership with Technospin Inc., of Saint-Laurent, Québec. Financial support from Free Form Fibers, L.L.C is greatly acknowledged. The authors also would like to express their gratitude to Jun Yu for help with flow modeling and to Christian Fauteux and Rémi Longtin for their valuable comments on the manuscript.

CHAPTER 5: ARTICLE 3 - VARIATIONAL ANALYSIS OF LCVD ROD GROWTH

The axial convection enhanced LCVD system in combination with the real-time in-situ growth rate measurement technique has yielded an effective tool to gain a better understanding of the process by closely monitoring rod growth. In the following work, the advantage offered by the measurement technique is exploited to study the effect of process parameter perturbations on the process variables. The findings of the work bring to fore the extreme sensitivity of the process. Furthermore, the results stress the importance of process control of LCVD to obtain reproducible growth characteristics, and hence reproducible microstructures.

VARIATIONAL ANALYSIS OF LCVD ROD GROWTH

R. Goduguchinta, J. Pegna*

Freeform Fabrication Laboratories, École Polytechnique de Montréal, Box 34, Pavillon J.-Armand Bombardier, 2900 Edouard Montpetit, Montréal H3T 1J4, Québec, Canada.

Submitted to: Applied Physics A on 11/09/2006

5.1 Abstract

Variational analysis of LCVD rod growth was made possible by a new axial convection enhanced micro-reactor design that lent itself to accurate in-process measurements of growth rate and position inside the growth region. The methodology follows a typical design of experiments approach where the effect of small perturbations to process parameters are measured in real-time. The findings are rather startling. They point to a growth rate that is not symmetric with respect to the focal plane. In fact, the peak growth rate is consistently recorded well in front of the focal plane, at a distance one order of magnitude greater than the Raleigh range, decreases rapidly afterward, steadies across the focus, and then decreases slowly. A measure of energetic efficiency can be derived that shows a rapid decay of the amount of material deposited per Joule. A central assumption to this analysis is that growth occurs in the kinetic domain and that was confirmed experimentally. The reason for the great variability and asymmetry observed are still unknown. However, corroboration of our results would throw into question a large body of published LCVD measurements as they would have to account for the wide variability of the measured quantities within the growth region.

PACS 81.16.Mk; 81.10.Bk; 81.05.Uw

---

* corresponding author: tel: +01-5143404711 x 4197; fax: +01-5147074644; email: joseph.pegna@polymtl.ca

5.2 Introduction

Since the early 1970 [15], there has been a growing body of works investigating LCVD rod growth. Over the years, LCVD has matured from growing simple structures such as rods [82] to more complex forms like micro-coils and solenoids [83], antennas [49], photonic bandgap structures [31] and an electric cage laser micro-turning lathe [55]. Review articles [25, 27, 28-29] can be referred for an insight into the subject. In addition to being a versatile tool for the fabrication of complex three-dimensional structures, LCVD is invaluable in understanding CVD precursor kinetics as demonstrated by [61, 84], where the variation of axial growth rate of the rod with temperature in the kinetic regime is used as a means of measuring the activation energy of the precursor. LCVD rod growth with a stationary laser focus and substrate is described by Dean et al [62] and Maxwell et al [79]. It consists of focusing a laser onto a substrate well enough to initiate rod growth and then letting growth continue as long as it can be sustained without altering experimental conditions. We shall refer to the extent of sustained growth as the *"growth region."* The size of the growth region can exceed that of the Raleigh range of the optics by an order of magnitude or more [79]. A commonly accepted view of rod growth using a stationary laser focus and substrate [62, 79] suggests that the axial growth rate of the rod undergoes a period of uniformity. This being said, it must be noted that axial growth rates reported to date were either averaged over the length of the rod in stationary laser focus and substrate experiments [62, 79, 81] or measured within a specific distance in the laser focal region in moving substrate/focus experiments [38, 61, 84]. The reported values however do not represent the true growth rate experienced by the rod at different positions along its length (in the case of stationary substrate and laser focus experiments) or in other words, at different positions within the growth region (in the case of moving focus/substrate experiments). Recent results (discussed in this work) obtained from real-time in-situ growth rate measurements point to transient growth rates that appear to vary greatly inside the growth region.

An attempt has been made in this work to investigate the variational properties of such growth, namely the response to small perturbations of the process parameters. The variational properties of interest are the linear and volumetric efficiency of the process, which we define respectively as the length and volume of deposit per joule of laser power. To measure these properties, we will perturb process parameters and gain information on process variables.

Our work claims to be the first to explore this avenue, and this was made possible through a novel reactor design allowing for axial forced convection of the precursors. This configuration indeed permits simple and repeatable observations of the reaction to monitor it in real time, and derive the variational properties of interest.

5.3 Experimental

5.3.1 Experimental Setup

The experimental setup is illustrated in Figure 5.1. It embodies a forced convection reactor that features three coaxial annular flows, the outermost one just functioning as a protective shroud. The optics consist of an argon-ion laser coaxial to the flow and operating in the TEM_{00} mode, with an output beam diameter of 3.97 mm and a maximum power output of 5 watts in multi-wavelength mode. The laser beam is focused to a 10 μm spot (measured using knife-edge technique*) onto the tip of a 75 μm diameter tungsten wire substrate coaxial to the laser beam. The tungsten wire substrate is itself located inside a stainless steel tube, with inner and outer diameters 310 μm and 565 μm respectively, hereafter called *"primary injection syringe."* The wire substrate initially overhangs the primary injection syringe by about 500 μm to 600 μm (see Table 5.2 for exact initial overhang dimensions). The primary injection syringe is contained

* Y. Suzaki, A. Tachibana, Appl. Opt. vol.14, no.14, pp.2809-2810, 1975.

inside a coaxial *"secondary injection syringe"* with inner and outer diameters 1.32 mm and 2.54 mm respectively.

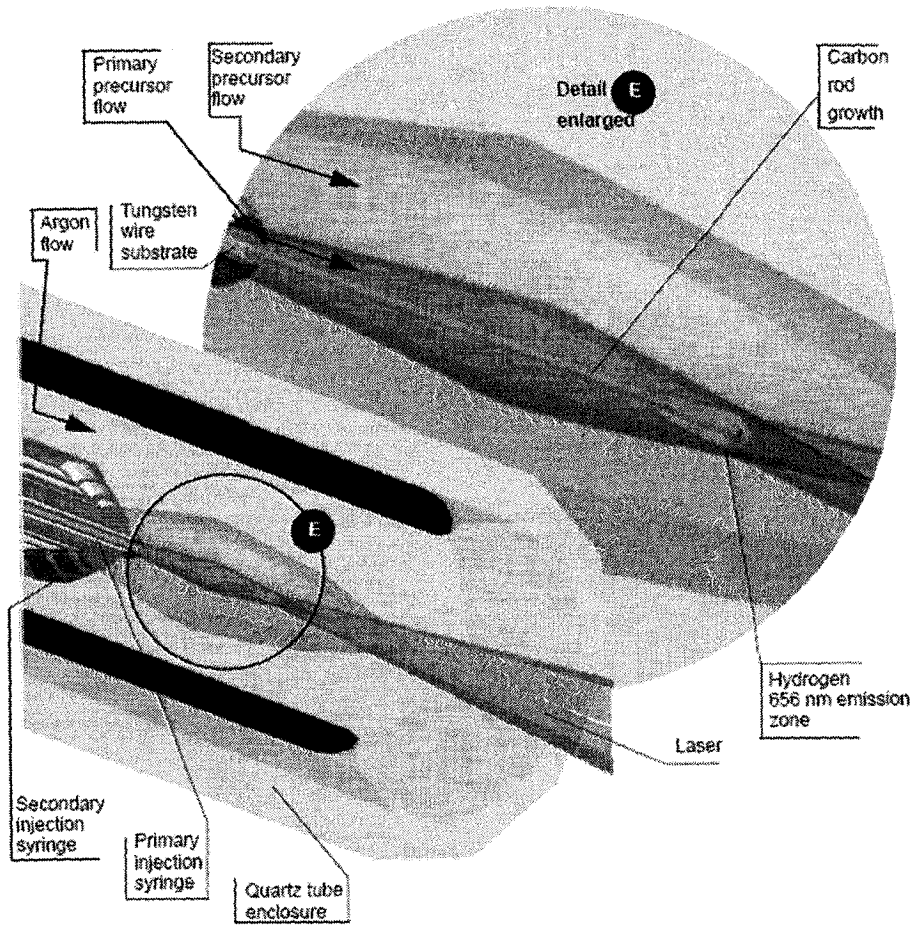

Figure 5.1 Schematic of axial convection enhanced LCVD micro-reactor

The entire syringe tube assembly is contained within a coaxial 6 mm inner diameter quartz tube. The inner most annular flow of *primary precursor* surrounds the tungsten substrate and is forced into the chamber through the primary injection syringe. The next annular flow of *secondary precursor* is forced through the secondary injection syringe. Finally, a third annular flow confines the previous two and provides a protective shroud of argon around the reaction zone. Flow rates of precursor and argon are controlled by a combination of precision flow meters and metering valves interfaced with a LABVIEW

data acquisition system by means of a National Instruments PCI-6251 multi-function DAQ card.

For the experiments described here, the primary and secondary precursors are both 99.5% pure ethylene. The purpose of the secondary precursor flow is to provide a protective shroud preventing diffusion of argon into the reaction zone. Flow modeling of the experimental setup done using FLUENT 6.1.22 confirms that the flow arrangement confines the effective LCVD chamber to a cylinder less than 2 mm in diameter and 5 mm long located at the primary syringe exit. It also confirms that the ethylene shroud from the secondary flow is sufficient to prevent diffusion of argon into the effective LCVD chamber. The quartz tube opens up directly to the atmosphere; hence the experimental setup qualifies as the first open air LCVD rod growth. The substrate is brought into the vicinity of the laser focus and once growth is initiated, the position of laser focus and substrate are kept unchanged. Rods were grown at laser powers of 1.4 W, 1 W and 0.6 W. The mean flowrates were 7.4 and 44.8 sccm for primary and secondary precursor flows respectively. This translates to Reynolds numbers of 42 and 62; respectively well inside the laminar flow range.

5.3.2 Imaging, position, and diameter measurements

In prior works such as [79] using 656 nm imaging in a static reactor, hydrogen emission from the reaction gave rise to a plume propagating into the laser axis. Imaging data in [79] could not be used beyond simple volumetric deposition rate measurements. Axial convection enhancement however eliminates the plume and confines the emission zone to a small region representative of the rod tip. This change in configuration presents us with a unique instrument for real-time measurement of rod tip shape, position and diameter. A sample image is shown in Figure 5.2(A), with unfiltered emission data plotted in Figure 5.2(B). These figures illustrate the quality of imaging data made available by axial forced convection, as well as the high signal to noise ratio. A simple thresholding filter can then be used to create a crisp image of the emission zone (Figure

5.2(C)), which in turn is used to derive real-time information about rod tip position, diameter and shape. Real-time growth rate measurements were obtained from the difference in centroid positions of consecutive emission image frames. While the image acquisition rate was 30 frames/sec, only image frames spaced one second apart were used for growth rate measurements. Rod diameter was measured in real-time by extracting the column of pixels corresponding to the centroid position of each emission image frame, and computing the length of the extracted high intensity column. Position information of the rod growth tip is obtained from centroid information as well.

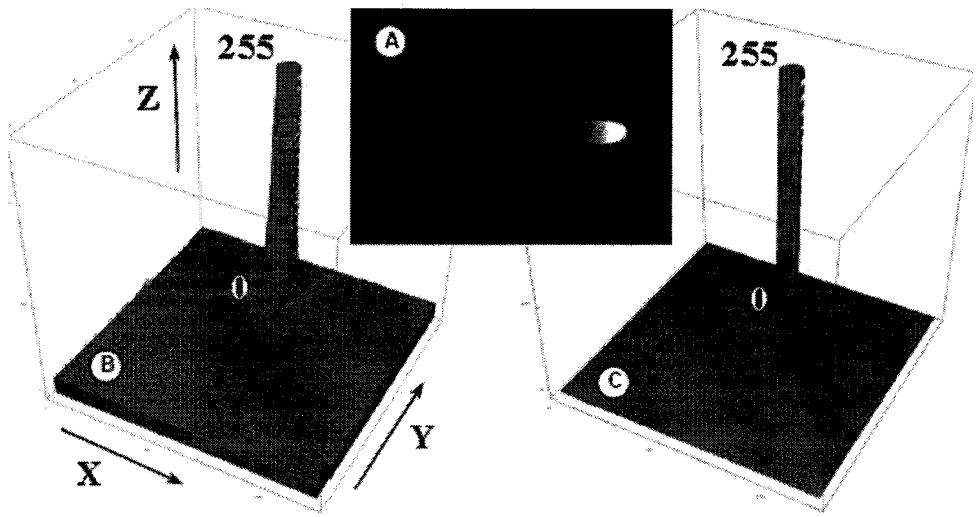

Figure 5.2 Rod tip position measurements. X and Y axes represent the captured image frame. Z axis represents the grayscale emission intensity ranging from 0 to 255 (A) Sample 656 nm emission imaging (B) Unfiltered emission intensities (C) Filtered image intensities

From a hardware point of view, the reaction is monitored by a SONY XCD-X710 IEEE 1394 digital camera fitted with a 35X objective and a Hawkeye precision borescope (Gradient Lens Corp., Rochester NY) perpendicular to the flow axis. A 656 nm bandpass filter with 10 nm bandwidth placed between the objective lens and the CCD sensor allows viewing of only the emission centered at 656 nm. The "field of view" of

the borescope (32^{o}) is adjusted to encompass the effective (growth inducing) growth region of the laser beam.

5.4 Parametrization of experiments

The purpose of this work is to relate the effect of perturbations of process parameters (flow and laser power) on the evolution of growth rate in the growth region. This objective requires that positional measurements relate to the focal plane. In practice however, this is difficult to accomplish as the focal plane position relative to the rod tip can only be known within a few millimeters. The methodology adopted here is illustrated in Figure 5.3. The focus remains unchanged throughout all experiments. All positional measurements are made relative to the frame of a reference experiment, hereafter called *experiment 0*. The series of variational experiments allow us to relate the frame of experiment 0 to the focal plane. Figure 5.3 illustrates the experiment's positional parametrization. Similarly, given the small flowrates, it would be very difficult to induce a very small perturbation to the flow of precursors by direct control of the flowmeters. Numerical flow simulations however indicate that such a small perturbation is possible by varying the amount of overhang of the rod with respect to the primary injection syringe. It is this overhang parameter that we shall use to perturb the flow around the rod tip.

At this venue, it is indicated to define our reference frames and terminology in reference to Figure 5.3. Even though we do not know the position of the focal plane with precision at the start of our experiments, let us associate a reference frame to the laser beam, which remains stationary throughout all experiments. We attach a frame L to the laser with axis $\vec{x}_L$ oriented along the laser axis, and perpendicular $\vec{y}_L$ axis in the focal plane (Figure 5.3(A)). Similarly each of the ith experiments, including experiment 0, has a local frame of reference defined by the laser axis $\vec{x}_i = \vec{x}_0 = \vec{x}_L$ and a y axis $\vec{y}_i$ defined by the initial position of the substrate, prior to initiating growth. The

accumulated growth is measured in the local frame of the ith experiment by ${}^{i}_{i}x$. Subsequent to our choice of origin, the initial value of the *accumulated growth* ${}^{i}_{i}x$ measured in the reference frame of the ith experiment is 0 (Figure 5.3(B)).

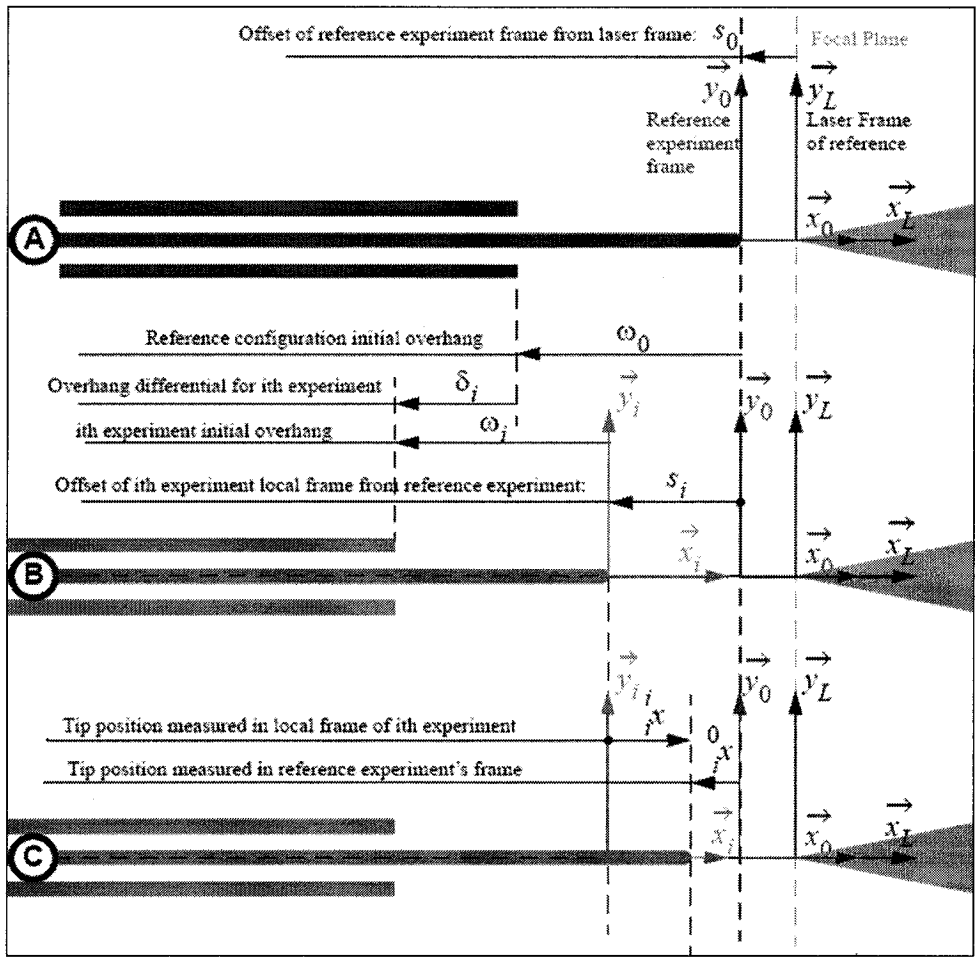

Figure 5.3 Parametrization of position measurements. (A) Reference experiment initial configuration (B) i th experiment initial configuration (prior to rod growth) (C) i th experiment parametrization (during rod growth)

Note that accumulated growth and tip position coincide only in their experiment frame. The *initial overhang* of the rod in the ith experiment is measured from the tip to the

tube end by ω_i, which makes the overhang negative with our axis convention. Hence the overhang in the ith experiment once growth is initiated will be $\omega_i + {}^{i}_{i}x$ (Figure 5.3(C)). In addition, the tube for the ith experiment can be translated with respect to the reference experiment by an amount δ_i, which we call the *overhang differential*. Thus the overhang differential allows control of flow perturbations while laser power and focal position of the rod tip remain identical.

Finally, all the local frames are related to the reference experiment's frame by measuring the initial shift s_i of the rod tip with respect to the reference experiment's frame. So the rod tip position of experiment i measured in frame 0 is given by:

$$ {}^{0}_{i}x = s_i + {}^{i}_{i}x \tag{5.1}$$

Note that in Figure 5.3(B) s_i is negative as drawn. If measurements are made in terms of tube shift and initial overhangs, then:

$$ s_i = \omega_0 + \delta_i - \omega_i \tag{5.2}$$

In summary, the setup described here provides an opportunity to focus on a reduced number of process parameters and process variables, which are summarized in Table 5.1. Flow parameters (concentration, Reynolds number-Re) can be finely perturbed by the amount of overhang, while measurements focus on the growth rate versus position for a range of laser powers.

Table 5.1 Summary of experimental process parameters and process variables

Process Parameters			Process Variables
Control	Parameter	Measurement	
Laser Power	Incident power density		Temperature Rod diameter Growth rate (linear/volumetric) Material properties
Overhang differential δ_i	Flow	Concentration Reynolds number Convection	
Accumulated growth ${}^{i}x$			

5.5 Experiments

Experiments were conducted at different laser powers and overhang differentials without modifying the optics, laser focus, or substrate position. All tip positions were reported to the frame of experiment 0, and both the growth rate and the diameter evolution during growth were recorded. Table 5.2 summarizes the perturbation parameters. Sample growth rate curves are shown in Figure 5.4, representative of each combination of perturbation parameters. Before further comments however, it is worth mentioning a remark not contained in these curves. It concerns the onset of mass transport limit. Indeed, literature [58] typically reports that growth rates reach a plateau when laser power is increased at a constant pressure. Experiments conducted at higher laser powers with the same flow conditions during this work show that forced convection delays the onset of mass transport limit. Indeed, within the range of laser powers available to us, we failed to detect any saturation of the growth rate due to increased laser power. This observation is important for the analysis presented below in Section 5.6 as it ensures that all our experiments were conducted in the kinetic domain.

In Figure 5.4, one can notice that for identical laser powers and tip positions, the overhang differential of 500 μm affects the growth rate in a consistent manner. This supports that the overhang differential affords a means for fine control of the flow conditions around the rod tip. Furthermore, reasoning indicates that the perturbations to convective heat transfer cannot be a factor in this shift, for a temperature perturbation would exhibit an exponential variation rather than the linear change observed.

Numerical simulations indicate that the main cause for such a small shift of the growth curves is a small change in precursor concentration near the tip. The consistent behavior of the process with growth rates is repeated for rod diameters as illustrated by Figure 5.5.

Table 5.2 Experiment Matrix (*Reference experiment)

Parameter	Laser Power	Overhang differential	Experiment number	Primary precursor flow/Reynolds number	Secondary precursor flow/Reynolds number	Initial Overhang	Frame Shift
Symbol	P_i	δ_i	i			ω_i	s_i
Unit	mW	μm		sccm/No	sccm/No	μm	μm
	600	0	4	7.4/636	44.8/937	-559	-20
		-500	9			-552	-527
	1000	0	2			-538	-41
			3			-565	-14
		-500	7			-586	-493
			8			-565	-514
	1400	0	0*			-579	0
			1			-579	0
		-500	5			-572	-507
			6			-586	-493

5.6 Analysis

The observation that all growth reported with forced axial convection occur in the kinetic domain underlies our analysis. Indeed, this means that we can rely on the well documented Arrhenius equation (5.3) to govern the growth, and turn it into a means of measurement.

$$k_{(P,\delta,x)} = k_0 C^n_{(P,\delta,x)} e^{\left[\frac{E_a}{RT_{(P,\delta,x)}}\right]} \tag{5.3}$$

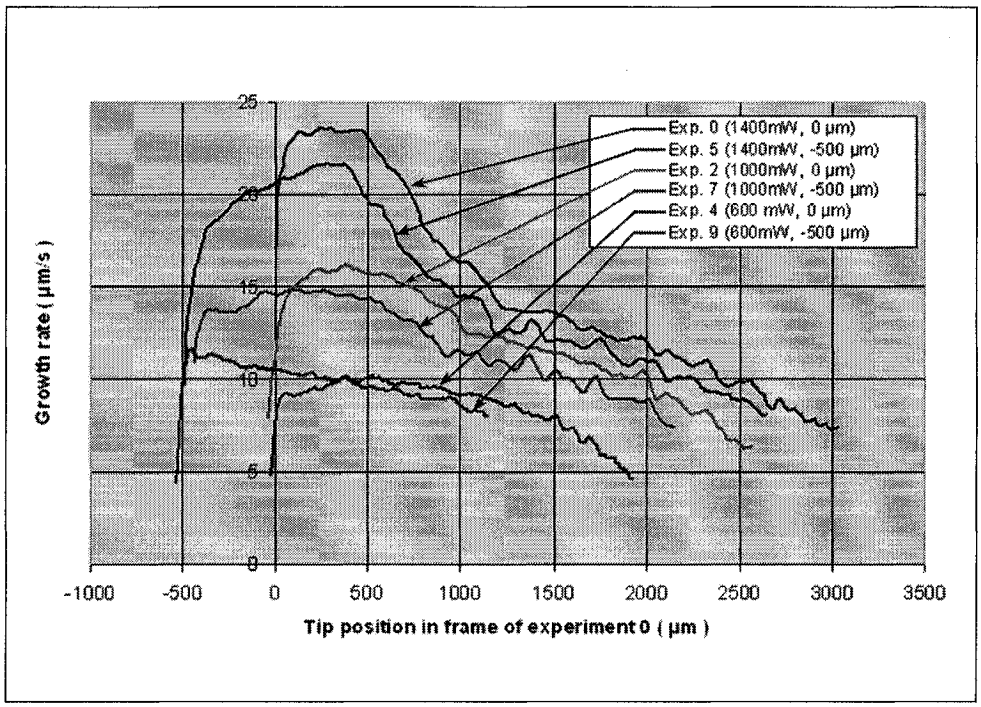

Figure 5.4 Sample growth rate vs. position curves for various laser powers and overhang differentials

Here, k is the growth rate, k_0 is the pre-exponential constant, C is the concentration at the tip, n is the reaction order, E_a is the activation energy, R is the perfect gas constant, T is the temperature, and P, δ and x are the process parameters: laser power, overhang differential and rod tip position respectively.

To further exploit this equation in the context of our experimental setup, we can now state two further hypotheses, to be tested against experimental results.

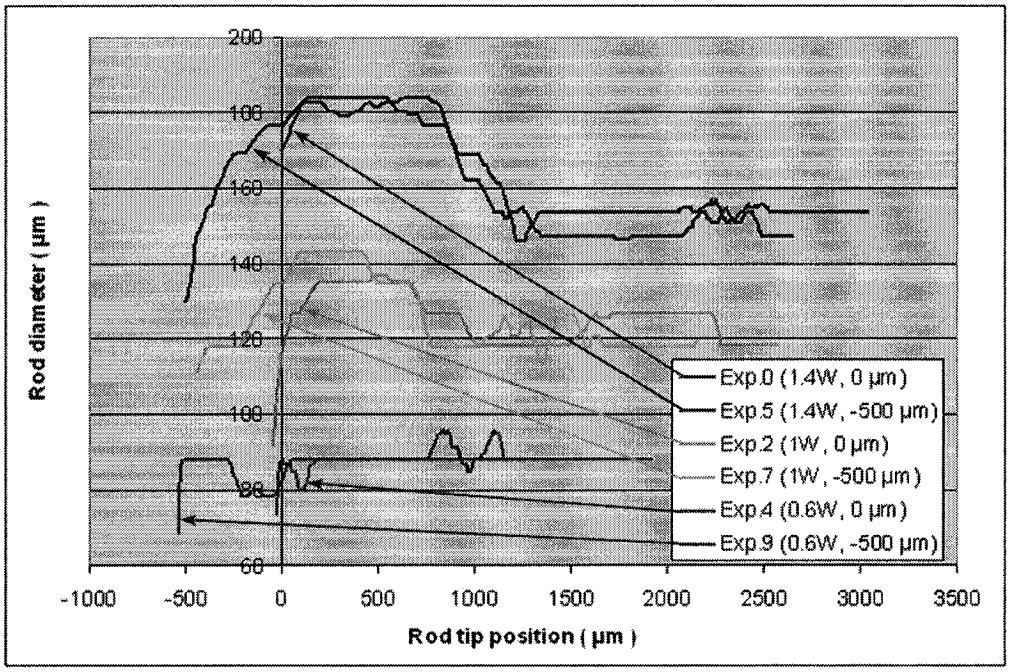

Figure 5.5: Sample rod diameter vs. position curves for various laser powers and overhang differentials

Hypothesis 1 (Concentration): Numerical flow simulations indicate that the concentration will be affected by a change in laser power, the accumulated growth, and the overhang delta. However, it is legitimate to assume that concentration, whatever it is, will have a proportional response to a change in laser power for identical tip positions. Hence whether the overhang is 0 or -500 µm, a change in laser power by 0.4 W should result in identical proportional changes in concentrations. i.e.

$$\frac{C_{(P+\Delta P,0,x)}}{C_{(P,0,x)}} = \frac{C_{(P+\Delta P,-500\mu m,x)}}{C_{(P,-500\mu m,x)}} \tag{5.4}$$

Hypothesis 2 (Temperature): Numerical simulations indicate that a change in tip temperature will effect a change on concentration at the tip. Conversely however, it appears that the change in tip temperature effected by a differential overhang of 500 µm is negligible. It seems therefore legitimate to assume that a 500 µm differential

overhang will not affect the convective heat transfer significantly. As mentioned earlier in section 5.5, if indeed the convection heat transfer was affected significantly by a differential overhang perturbation, then such a perturbation would have influenced the temperature causing an exponential variation of growth rate rather than the linear variation witnessed in Figure 5.4. Hence we can neglect the overhang differential in the expression for temperature. i.e.

$$T(P,\delta,x) = T(P,x) \tag{5.5}$$

If hypotheses 1 and 2 are correct, then the variation in growth rate for the same power input differential should be independent of the overhang. We can test the validity of this claim by comparing the growth rate ratios for 0 overhang and -500 μm overhang. If they are correct, the ratios should be identical regardless of x. Indeed, if we consider the ratio of growth rates for experiments 0 and 2 with 0 overhang and 400 mW differential power as

$$\frac{k_{(1.4W,0,x)}}{k_{(1W,0,x)}} = \left(\frac{C_{(1.4W,0,x)}}{C_{(1W,0,x)}}\right)^n Exp\left(-\frac{E_a}{R}\left(\frac{1}{T_{(1.4W,x)}} - \frac{1}{T_{(1W,x)}}\right)\right) \tag{5.6}$$

and the ratio of growth rates for experiments 5 and 7 with -500 μm overhang and 400 mW differential power (5.7), and plot the ratio of experimental values of (5.6) and (5.7), we should get 1 identically for all values of x.

$$\frac{k_{(1.4W,-500,x)}}{k_{(1W,-500,x)}} = \left(\frac{C_{(1.4W,-500,x)}}{C_{(1W,-500,x)}}\right)^n Exp\left(-\frac{E_a}{R}\left(\frac{1}{T_{(1.4W,x)}} - \frac{1}{T_{(1W,x)}}\right)\right) \tag{5.7}$$

Experimental values of these ratios are reported in Figure 5.6 for the 0.6 to 1 watt and 1 to 1.4 watt differentials, granted the former is only available for a shorter range. The respective mean values for the ratios are 1.062 and 1.0006, with respective standard variations of 0.044 and 0.040. While not a formal proof, experimental results strongly agree with hypotheses 1 and 2. It is worth mentioning in this context that the growth

rate ratio of rods grown at 1.4 W and 1.0 W, and 1.0 W and 0.6 W was always greater than one independent of overhang, suggesting that growth happens in the kinetic regime. Having established the basic candidate governing equation, we can now proceed to variational analysis by perturbing each of the process parameters in our control, namely laser power, overhang differential, and tip position.

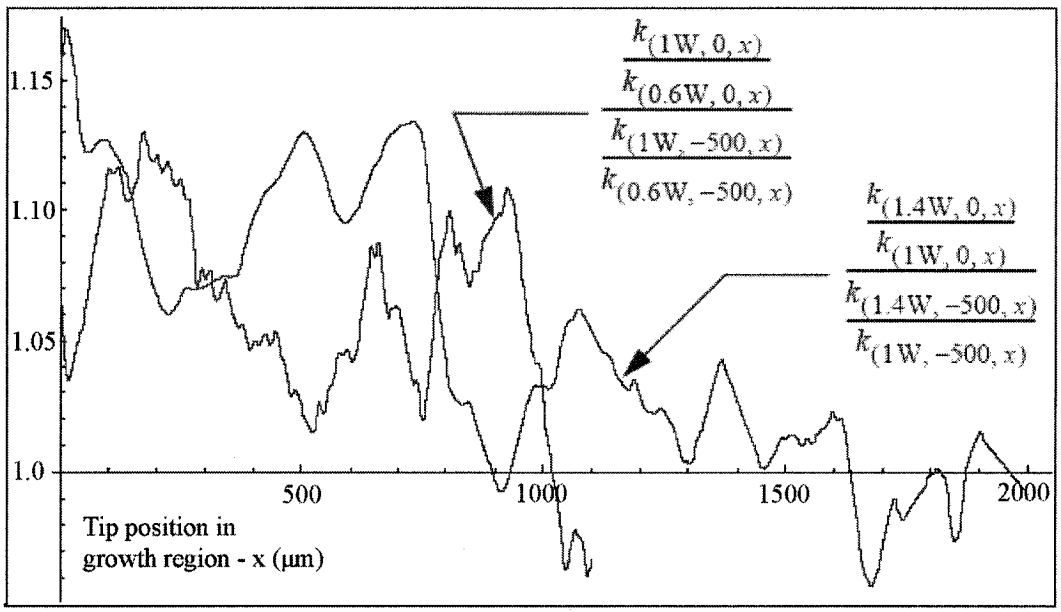

Figure 5.6: Relative differential overhang growth ratios for similar power differentials

5.6.1 Perturbation of laser power

Hypothesis 1 being validated (proportional response of concentration to laser power), we can now proceed with further analysis of the concentration function. Indeed, the ratio of concentrations at different laser powers must be a constant independent of x. In practice, this means that the concentration functions of position (x) and overhang differential (δ) can be decoupled from that of laser power (P).

$$C_{(P,\delta,x)} = {}^{P}C_{(P)}\,{}^{h}C_{(\delta,x)} \tag{5.8}$$

Where ${}^{P}C$ and ${}^{h}C$ represent respectively the fractional component of concentration as a function of power and position, differential overhang. We can therefore take

advantage of the decoupling of variables embodied by (5.8) to simplify the growth ratios of (5.6) and (5.7) for identical overhang differentials, and making those ratios independent of the overhang differential δ. This transformation allows us to extract the temperature sensitivity to a change of laser power.

$$\log\left(\frac{k(P+\Delta P,\delta,x)}{k(P,\delta,x)}\right)=n\log\left(\frac{{}^{P}C_{(P+\Delta P)}}{{}^{P}C_{(P)}}\right)-\frac{E_a}{R}\left(\frac{1}{T_{(P+\Delta P,x)}}-\frac{1}{T_{(P,x)}}\right) \tag{5.9}$$

The ratio in (5.9) can be expressed in first approximation in terms of partial derivatives with respect to laser power:

$$\log\left(\frac{k(P+\Delta P,\delta,x)}{k(P,\delta,x)}\right)\approx n\frac{\partial}{\partial P}\log\left({}^{P}C_{(P)}\right)\Delta P-\frac{E_a}{R}\frac{\partial}{\partial P}\left(\frac{1}{T_{(P,x)}}\right)\Delta P \tag{5.10}$$

Or equivalently

$$\frac{1}{\Delta P}\log\left(\frac{k(P+\Delta P,\delta,x)}{k(P,\delta,x)}\right)\approx\frac{1}{k(P,\delta,x)}\frac{\partial k}{\partial P}\bigg|_{(P,\delta,x)}\approx\frac{n}{{}^{P}C_{(P)}}\frac{\partial}{\partial P}\left({}^{P}C\right)\bigg|_{(P)}+\frac{E_a}{R}\frac{1}{T^2_{(P,x)}}\frac{\partial T}{\partial P}\bigg|_{(P,x)} \tag{5.11}$$

The left hand side of (5.11) can be derived from experimental measurements and thus can be plotted as shown in Figure 5.7. An alternative and instructive representation of the same data is to plot the partial derivative of the growth function with respect to laser power, as a function of rod tip position in the growth region. This is what is done in Figure 5.8. A number of valuable remarks can be drawn from (5.11) and the experimental plots of Figures 5.7 and 5.8 respectively.

First note that the right-hand side of (5.11) does not contain the overhang differential δ. This means that the logarithmic derivative of the growth rate with respect to laser power is independent of overhang. This is supported by the experimental data plotted in Figures 5.7 and 5.8, and it therefore means that the growth function of overhang

differential can only appear as a multiplicative factor; and since it contributes only to the concentration factor, we can write

$$ {}^{h}C_{(\delta,x)} = {}^{\delta}C_{(\delta)}\,{}^{x}C_{(x)} \tag{5.12} $$

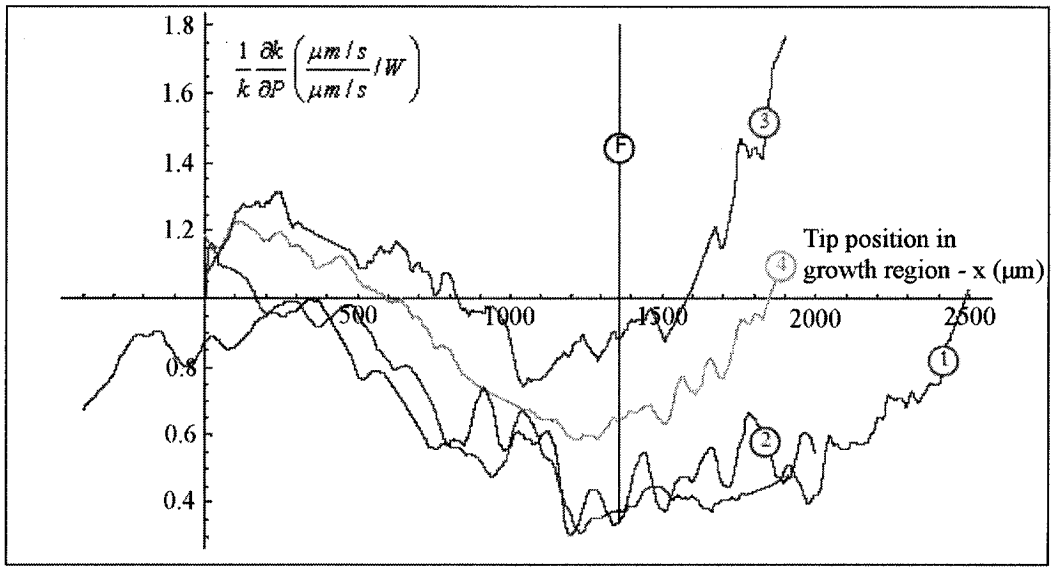

Figure 5.7 Experimental values of $\dfrac{1}{k(P,\delta,x)}\dfrac{\partial k}{\partial P}\Big|_{(P,\delta,x)}$, curves 1, 2, 3, and 4 respectively for values of $(P,\delta,\Delta P)$ equal to (1W, 0, 0.4W), (1W, -500, 0.4W), (0.6W, 0, 0.4W), and (0.6W, 0, 0.8W)

Next we remark that the first term on the right-hand side of (5.11) is a constant in terms of rod tip position x. Hence the graphs in Figure 5.7 are representative of the evolution of inverse temperature with laser power as a function of rod tip position in the growth region. It is therefore remarkable that all curves would appear to reach their minima at about the same value of rod tip position. A cubic curve least square fit followed by a root finding yields an average value of 1356 μm for the common minimum. The standard deviation of 121 μm represents about two-thirds of the focusing optics Raleigh range (161 μm). Seen in terms of the left-hand side of (5.11), Figure 5.7 shows that the sensitivity of the inverse temperature to a change in laser power reaches a minimum at

the same position for all laser powers tested. In other words, the inverse temperature (conversely the temperature) sensitivity to a change in laser power decreases (respectively increases) slowly, then remains near stationary at the common minimum, followed by a rapid increase (respectively decrease).

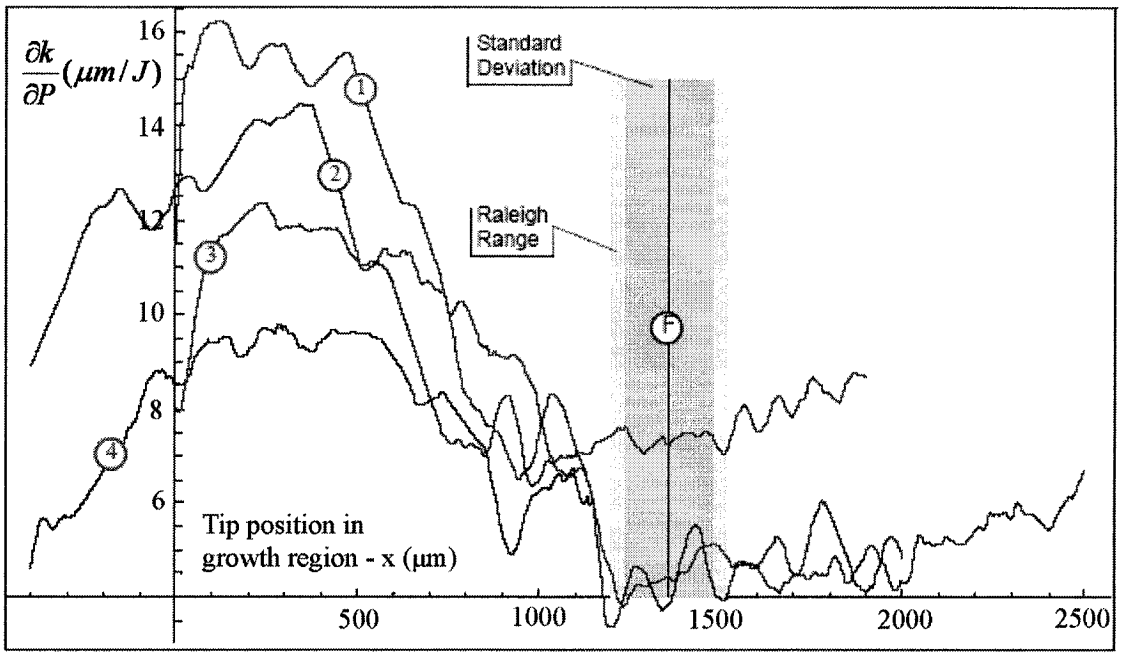

Figure 5.8 Experimental values of $\left.\frac{\partial k}{\partial P}\right|_{(P,\delta,x)}$, curves 1, 2, 3 and 4 respectively for values of $(P,\delta,\Delta P)$ equal to (1W, 0, 0.4W), (1W, -500, 0.4W), (0.6W, 0, 0.4W) and (0.6W, -500, 0.4W)

It should not be surprising that the logarithmic derivatives of the growth rate with respect to laser power (Figure 5.8) reaches their minima at about the same point. But what should the significance of this minimum be? In all evidence, it marks a locus of minimum sensitivity to a change in laser power. And since the only variable is the position along the laser axis in the growth region, there can be only be one such place, the focus. It appears therefore that we have identified a means of localization of the laser focus intrinsic to the process. The line marked Ⓕ in Figures 5.7 and 5.8 (and all

subsequent figures) marks the position of the newly found focal plane. This discovery is important as it now allows us to relate all growth curves to the focal plane, as in Figure 5.9.

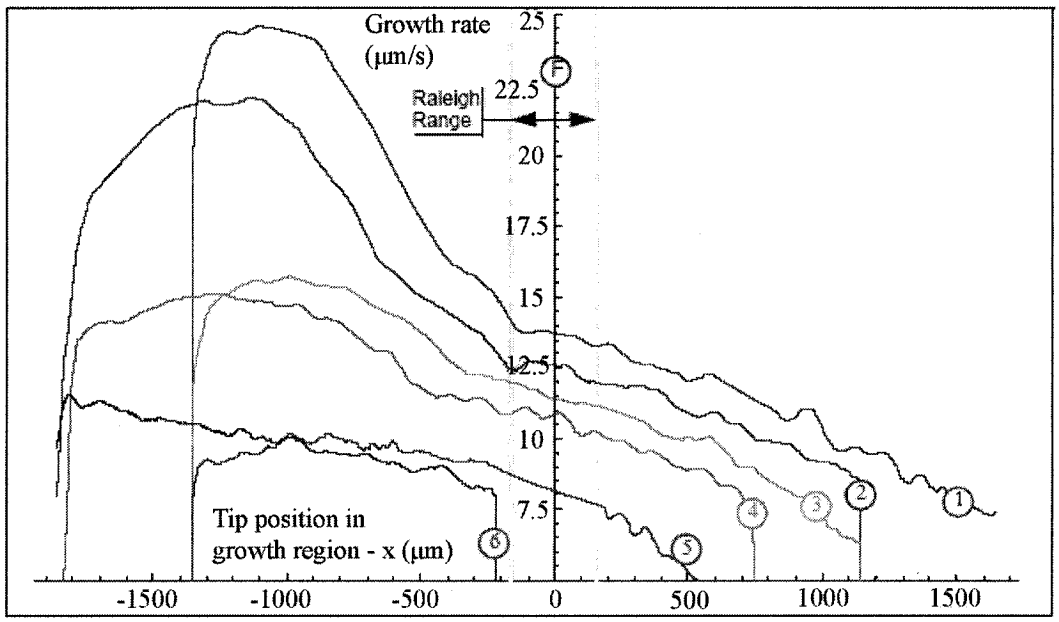

Figure 5.9 Gaussian smoothed average growth curves 1, 2, 3, 4, 5 and 6 respectively for values of (P,δ) (1.4W, 0), (1.4W, -500), (1W, 0), (1W, -500), (0.6W, 0), and (0.6W, -500)

Figures 5.8 and 5.9 carry a great deal of scientific significance and engineering implications. First, as Figure 5.9 shows, the growth rates are nowhere near stationary in the growth region contrary to a long held belief in LCVD literature [62, 79, 81].

Even more puzzling, peak growth rates are consistently obtained far in front of the focal plane, nearly an order of magnitude farther than the Raleigh range, whereas literature [38, 57, 59-62, 79, 81, 84] implicitly assumes that the maximum growth rate should occur at the laser focus. Adding to this confusing observation, note that the growth curves are not symmetric with respect to the focal plane whereas all conditions barred

flow are symmetric. Yet other experiments conducted at various flow rates and with different nozzle architectures all exhibit the same behavior, indicating that we are dealing with an intrinsic property of LCVD rod growth. The reason for this strong asymmetry is yet unexplained.

Similar conclusions hold about Figure 5.8, but in this case they take an especially important significance from an engineering standpoint. Note indeed that the unit of $\partial k/\partial P$ is expressed in microns of rod grown per joule of laser energy. In effect, this quantifies the efficiency of the process. What is most confounding in this picture is that while growth rates generally increase with laser power, efficiency of the process as measured by $\partial k/\partial P$ drops faster with higher powers, and even reverses after crossing the focus. Note indeed that the efficiency of growth at 1.4 W (curves 1 and 2) drops by 75% over 1 mm before the focal plane, and that after the focal plane is crossed, the efficiency of 0.6 W (curve 3) growth is twice that of 1.4 W. From a practical standpoint, the graph in Figure 5.8 shows how critical and sensitive focus tracking is to the optimization of growth rates and material properties [59-60]. To our knowledge, this is the first time that such sensitivity is documented in a quantifiable way.

When combined with rod diameter data, the graphs of Figure 5.8 take on a particularly meaningful form, as it translates into volume deposited per unit of energy, or with appropriate scaling, mass or number of moles deposited per unit energy. A logarithmic plot of the volumetric efficiency of the process ($\mu m^3/J$) is provided in Figure 5.10. The drop in efficiency over the 1000 μm in front of the focal plane is even more marked in this representation. For example, it shows a drop of two orders of magnitude for the 1W (curves 1 and 2) experiments. Note again the asymmetry of the curves with respect to the focus, which cannot be explained on the basis of optics and convective heat transfer alone.

When viewed in terms of molar deposition per unit energy, Figure 5.10 can cast legitimate doubts about published values [61-62, 84] of activation energies derived from growth rate measurements limited to the focal region as in [61, 84] or averaged over the length of the rod using a stationary laser focus and substrate [62]. Indeed, if the molar deposition per Joule is so sensitive to position within the growth region that it can exhibit orders of magnitude variations, the reliability of activation energy measures can be questioned.

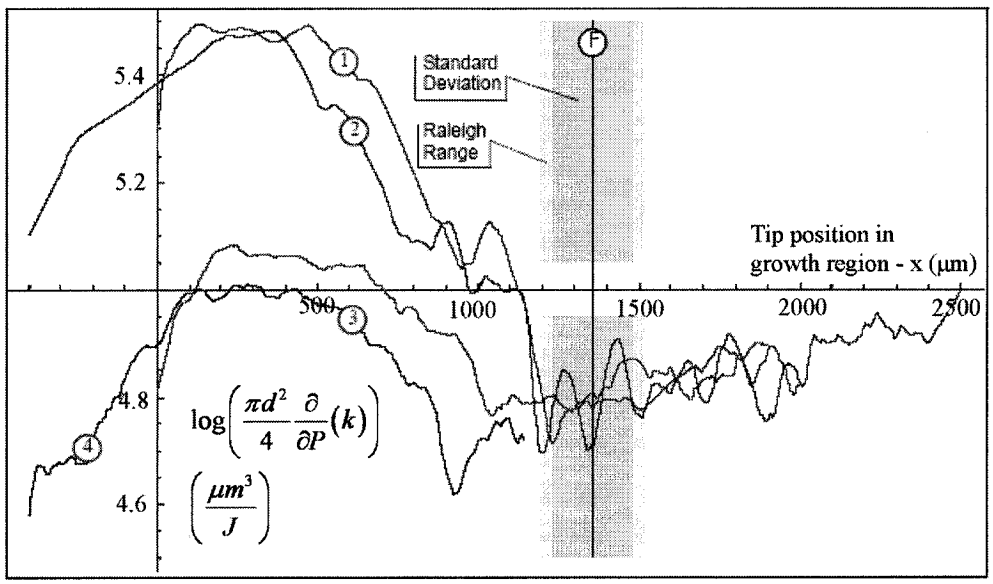

Figure 5.10: Log plot of experimental values of the volumetric efficiency $\log\left(\frac{\pi d^2}{4}\frac{\partial}{\partial P}(k)\right)$, curves 1, 2, 3, and 4 respectively for values of $(P, \delta, \Delta P)$ equal to (1W, 0, 0.4W), (1W, -500, 0.4W), (0.6W, 0, 0.4W), and (0.6W, -500, 0.4W)

Perturbation of laser power was a fruitful procedure. Most important of all, it did yield a method to identify the position of the focal plane that is intrinsic to the process. Hence there is no need for external characterization of the optics focal plane, followed by a precise position transfer procedure to ensure that the focal position is known in the frame of the micro-reactor. This discovery in turn leads to finding that the maximum

growth rate consistently occurs well in front of the laser focal plane. In fact, it occurs about one order of magnitude farther away than the Raleigh range. Perturbation to laser power can also be used to characterize both linear and molar energetic efficiency of the process, namely the number of microns of rod, or number of moles deposited per Joule of energy. We found that both measures of energetic efficiency drop rapidly within the first 10 Raleigh range in front of the focal plane. This is of great practical importance in terms of control of material properties and production rate optimization. But if this analysis made inroads into understanding and controlling the process, it also throws published results concerning growth rates and activation energy into question. Finally it also raises new questions; most intriguing are the reasons for observed asymmetry of growth rate and energetic efficiency with respect to focal plane.

5.6.2 Perturbation of the overhang differential

The overhang differential turns out to be a means to effect fine perturbations over the flow near the primary syringe nozzle.

Hypothesis 3: Numerical simulations indicate that perturbations to the flow brought about by a change in the overhang differential will be confined close to the nozzle and dissipates rapidly. In practice it means that perturbations to the overhang differential will bear relative changes in concentration much smaller than unity.

This hypothesis can be put to test simply by considering the ratio of growth rates for identical laser powers and tip positions (5.13). If hypothesis 3 holds, we should find the ratio to be close to unity. With a mean value of 1.086 (standard deviation 0.083), and despite a small trend associated with power in the region of peak growths, Figure 5.11 is in general agreement with our hypothesis.

$$\frac{k(P,0,x)}{k(P,\delta,x)} = \left(\frac{\delta_{C(0)}}{\delta_{C(\delta)}} \right)^n = \left(\frac{\delta_{C(\delta)} + \delta_{C(0)} - \delta_{C(\delta)}}{\delta_{C(\delta)}} \right)^n \approx \left(1 - \frac{\frac{\partial}{\partial \delta}\left(\delta_C\right)}{\delta_{C(\delta)}} \delta \right)^n \qquad (5.13)$$

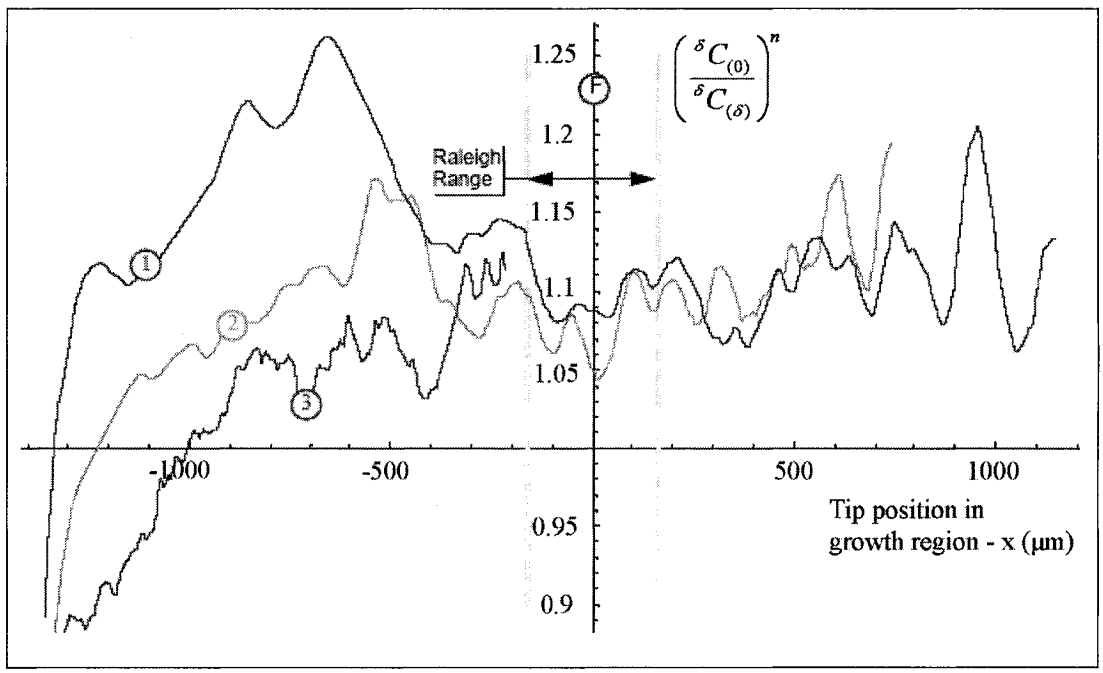

Figure 5.11 Relative concentration change due to overhang differential perturbation as a function of position in growth region. Curves 1, 2, and 3 correspond respectively to the differentials at 1.4, 1.0, and 0.6 W

On the grounds that the ratio is close to unity, we can further simplify (5.13) yielding (5.14); raising the opportunity to map ${}^{\delta}C$ over the region of interest once the reaction order n is determined.

$$\frac{1}{-\delta}\left(\frac{k(P,0,x)}{k(P,\delta,x)}-1\right)\approx n\frac{\frac{\partial}{\partial\delta}\left({}^{\delta}C\right)}{{}^{\delta}C_{(\delta)}}\approx n\frac{\partial}{\partial\delta}\log\left({}^{\delta}C\right) \tag{5.14}$$

For our experimental setup with the stated flow conditions, we find a value of $n\frac{\partial}{\partial\delta}\log\left({}^{\delta}C\right)\Big|_{\delta=0}\approx(0.173\pm0.166)10^{-3}\mu m^{-1}$, testifying to the sensitivity of flow perturbation afforded by the differential overhang, despite a large relative standard deviation.

5.6.3 Perturbation of tip position

Perturbations to the third process parameter within the control of our experiment can be exploited after we notice that the flow situation should be the same for a differential overhang of δ and tip position x, or for an overhang differential 0 and a tip position $x-\delta$. Only power densities, i.e. temperature can be different. Hence we can write:

$$ {}^{\delta}C_{(\delta)}\,{}^{x}C_{(x)} = {}^{\delta}C_{(0)}\,{}^{x}C_{(x-\delta)} \tag{5.15} $$

Note that such a relationship, when brought to bear at the differential level imposes that ${}^{\delta}C$ and ${}^{x}C$ obey exponential laws of the form:

$$ {}^{\delta}C_{(\delta)} = {}^{\delta}C_0 e^{\lambda\delta} \text{ and } {}^{x}C_{(x)} = {}^{x}C_0 e^{-\lambda x} \tag{5.16} $$

(Note that δ is with our axis convention)

The identity (5.15) allows exploiting the ratio of growth rates measured for identical powers, and a differential overhang that is exactly compensated in tip position, leading to the following equation:

$$ \log\left(\frac{k_{(P,0,x-\delta)}}{k_{(P,\delta,x)}}\right) = -\frac{E_a}{R}\left(\frac{1}{T_{(P,x-\delta)}} - \frac{1}{T_{(P,x)}}\right) \approx \frac{E_a}{R}\frac{\partial}{\partial x}\left(\frac{1}{T}\right)\delta = -\frac{E_a}{RT^2}\frac{\partial T}{\partial x}\bigg|_{(P,x)}\delta \tag{5.17} $$

As can be seen from (5.17), the log of the growth rate ratios is proportional to the spatial partial derivative of the inverse temperature. The graph of this function, shown in Figure 5.12, shows that the spatial derivative of the inverse temperature reaches a well defined minimum at about the same point as what we identified in Section 5.6.1 to be the focal plane. As much as this result is counter intuitive, it would appear that the temperature actually decreases rapidly in front of the focal plane, steadies as it crosses into the

Raleigh range, then decreases again but at a slower rate. The reason for this rather strange behavior is still an open question.

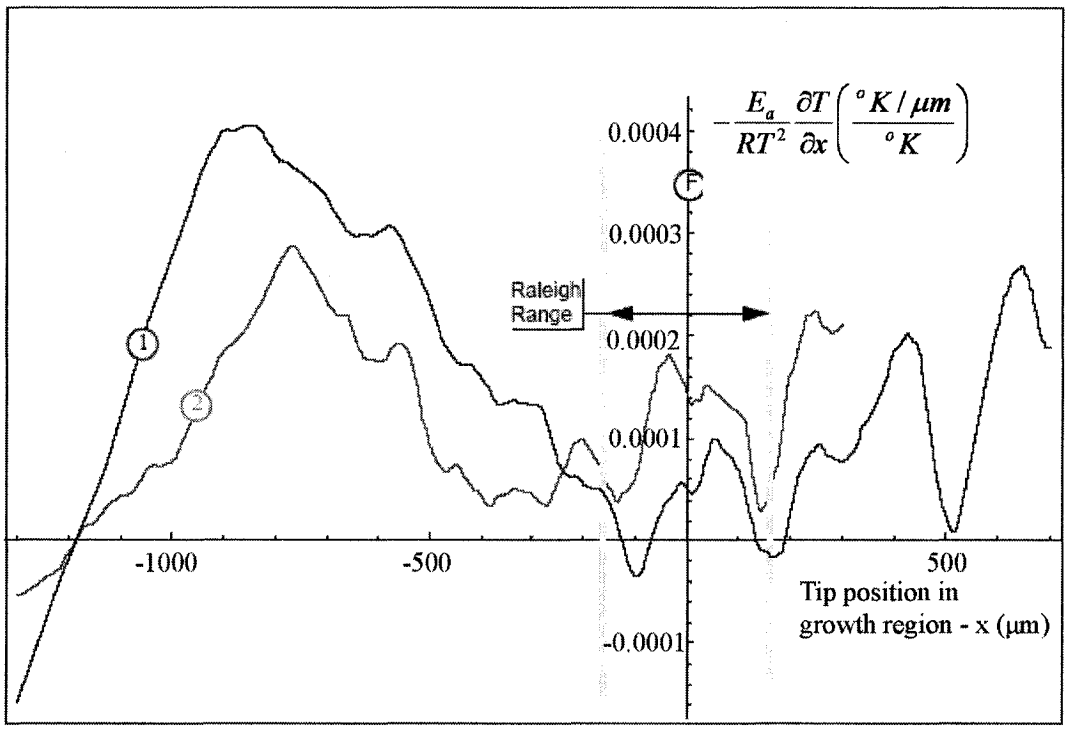

Figure 5.12 Rate of change of the inverse temperature as a function of position at 1.4 and 1W respectively for curves 1 and 2

5.6.4 Other factors

It is obvious that in attempting to map the process described in section 5.3, a number of other parameters ought to be factored in, in particular the effect of flowrates. The initial overhang ω_0, which was measured to have a magnitude of 579 μm, and the reference frame shift from the focal plane s_0, which was found to be at 1356 μm are conspicuously absent from this analysis. Yet their sum $\omega_0 + s_0$ is certain to intervene as a multiplicative factor in the concentration at the tip. Finally, the change in the micro-structure of the deposit with varying temperature along the growth region could result in varying reflectivity and thermal conductivity of the deposit, which influences the

temperature at the rod tip in a cyclical fashion. The change in microstructure of the deposit could also influence the reaction mechanism as documented by Johansson et al. [76], where the change in microstructure from amorphous to crystalline boron changed the reaction mechanism from surface kinetics limited to mass transport limited. Yet, as we concentrated on investigating the sensitivity of the process to a change in reduced number of parameters, the influence of total overhang, distance from the nozzle to the focal plane, flowrates and dependence of rod micro-structure on its position in focus are relegated to further studies, especially now that we have means of identifying the focal position in-situ, and ability to track the rod tip position with enough accuracy to investigate transient growth.

5.7 Conclusions

Whereas a large body of scientific and engineering literature focuses on the characterization of rod growth, this work took advantage of a novel micro-reactor design that made it possible to track rod tip growth in the growth region of a laser with enough precision to investigate variational properties of the process. To our knowledge, this is the first such investigation to be reported. Hence, we do not focus on parameter identification such as activation energy, reaction order, or pre-exponential factor. Rather, our approach uncovers variational relationship pertaining to LVCD growth as a function of position in the growth region and laser power.

This new approach to an old problem points to a number of issues that could not have been easily identified in previous studies.

1. Differential analysis of growth vs. laser power and growth vs. tip position yielded a means of locating the focal plane in-situ.
2. For constant laser power, our measurement shows that the growth rate varies greatly inside the growth region, peaking well in front of the focal plane, at about an order of magnitude greater than the Raleigh range of the optics, then

decreasing rapidly to the focal plane, steadying across the focal plane to decrease again at a lower rate once the focus is crossed.

3. The variability of growth rate with respect to laser power allowed us to push this remark further and define energetic efficiency of the process in terms of microns grown per Joule of laser energy. Variations of this measure accounting for rod diameter, density, and molar mass allow the definition of volumetric $\left(\mu m^3/J\right)$, massic $\left(mg/J\right)$, or molar energetic $\left(Mole/J\right)$ efficiency. These measures point to a great variability of the process within about 10 Raleigh ranges of the focal plane, with the volumetric efficiency dropping nearly two orders of magnitude at 1 W right in front of the focal plane.
4. Similarly, a spatial variational analysis of rod growth indicates that the tip temperature decreases rapidly from the region of peak growth to the focal plane, steadies as it crosses the Raleigh range, and then keeps decreasing at a lower rate.
5. All analyses conducted within the scope of this work point to a strong asymmetry between the front and back of the focal plane though all conditions barred flow, are symmetric with respect to the focal plane. All flowrates used to date exhibit the same pattern. It would seem therefore that this asymmetry is an artifact of the LCVD process, independent of whether convection is forced or not.

As much as the authors would agree that these observations are counterintuitive, they are just experimental facts. Should they be further corroborated, they point to the need to further investigate the phenomena at play in this process. This is especially important if we are to gain enough mastery of the process to gain engineering applications. Another important consequence of corroborating these experimental evidences is that, if confirmed, our work would throw into question a good number of published results reporting growth rates, activation energies, and reaction orders in LCVD, as they can

now be viewed as largely dependent on focus tracking and position inside the growth region.

Acknowledgements

Financial support for this research was provided by the National Science and Engineering Research Council of Canada under grants EQPEQ301036-04 and I2IPJ305768-03, in partnership with Technospin Inc., of Saint-Laurent, Québec. Financial support from Free Form Fibers, L.L.C is greatly acknowledged. The authors also would like to express their gratitude to Dr. Mats Boman for useful discussions, Jun Yu for help with flow modeling and to Christian Fauteux and Rémi Longtin for their valuable comments on the manuscript.

CHAPTER 6: LCVD PROCESS CONTROL

6.1 Closed-loop LCVD: Development of control algorithm and implementation

Prior introduction to the challenges involved in developing LCVD as a fiber production tool (section 1.6, chapter 1) stressed the importance of obtaining LCVD process control, while pointing to the absence of the same. To date, LCVD has been predominantly open-loop. Work done during the course of this work was instrumental in discovering a real-time in-situ positional growth rate measurement technique (Chapter 3). The positional growth rate information yielded by the measurement technique can act as a *growth rate map* (Figure 6.1) for the user to decide the position of the growth front (pixel # in the field of view of the vision system) to be maintained during rod growth. The growth front position in turn determines the growth rate and consequently the microstructure.

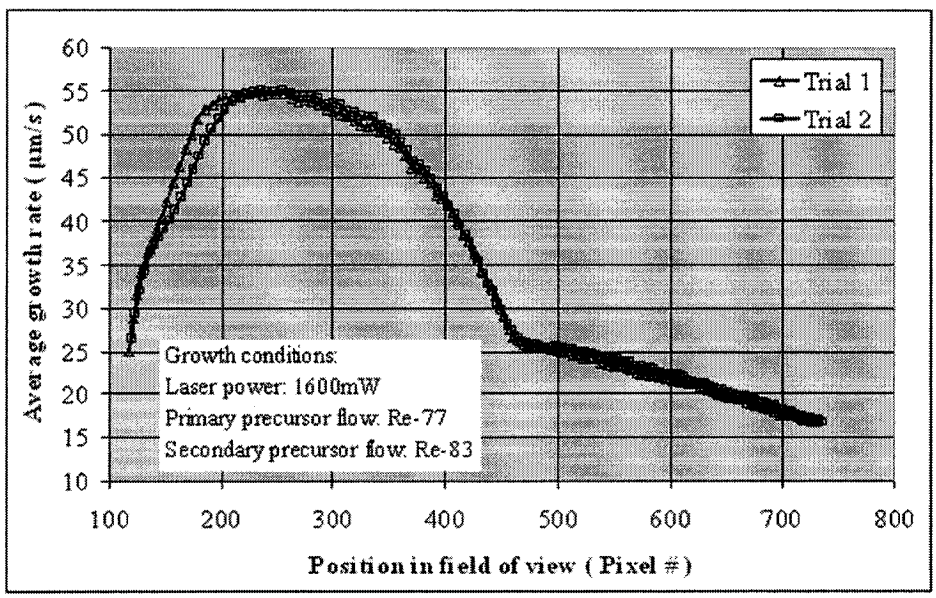

Figure 6.1 Growth rate map

The proposed closed-loop LCVD process control algorithm (Figure 6.2) uses the centroid information of the emission produced during rod growth as a feedback to

control the position of the rod growth front. As shown in the algorithm, the first step towards implementing the closed-loop rod growth system is the determination of the growth rate map in the field of view of the vision system, and selection of the centroid *Set Point (SP)* from the obtained map. Computation of the centroid *Process Value (PV)* follows the same approach presented earlier in chapters 3-5. The PID loop provides appropriate corrective signals in the form of pull velocity to the pickup system interfaced with the growing rod, and maintains the rod growth front at the desired position.

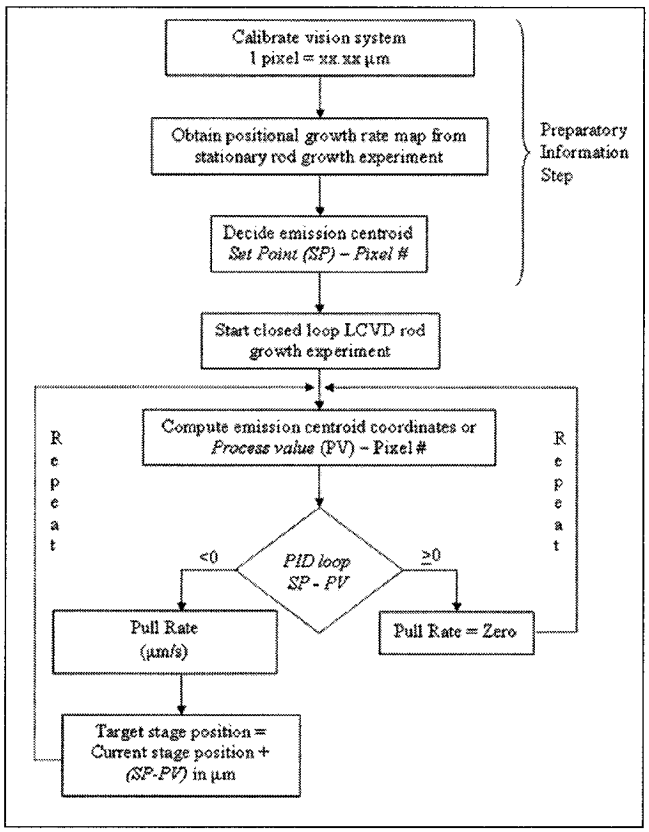

Figure 6.2 Control algorithm for closed-loop LCVD

Figure 6.3(a) gives a pictorial representation to the terminology used in the control algorithm. The proposed closed-loop algorithm is an ON-OFF system as shown in Figure 6.3(b). When the difference (SP-PV)$\geq$0 or in other words, when the current position of the emission centroid (PV) is behind the set point (SP), no correction is made

to reduce the magnitude of the difference (|SP-PV|). The current position of the centroid (PV) is allowed to creep to a value that is equal to the centroid set point (SP) whereupon the control loop is engaged to output a corrective signal. The magnitude of the corrective signal (pull velocity of the pickup system) depends on the magnitude of the difference between the set point and process value (|SP-PV|), and the PID control parameters.

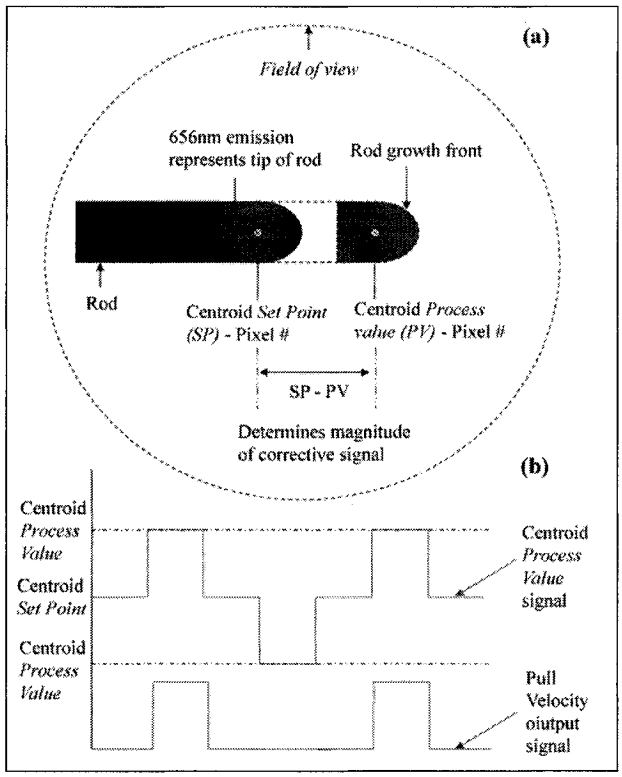

Figure 6.3 Closed-loop LCVD control schematic

The hardware for the closed-loop control system comprises two major components namely:

1. Vision system
2. Pickup or motion control system

The vision system consists of a SONY IEEE-1394 digital camera interfaced with NI-IMAQ for IEEE 1394 camera drivers. The motion control system is a linear servo motor

powered stage interfaced with NI-Motion software. The stage has a travel range of 25 cm with 1 μm resolution. Pull rate of the pickup system can range from 1 μm/s to 25 cm/s. Both the vision and motion control systems were integrated with laser power and gas flow control systems using LabVIEW 7.1 data acquisition, measurement and control software. The front panel of the LabVIEW Virtual Instrument (VI) created for closed-loop rod growth is shown in Figure 6.4.

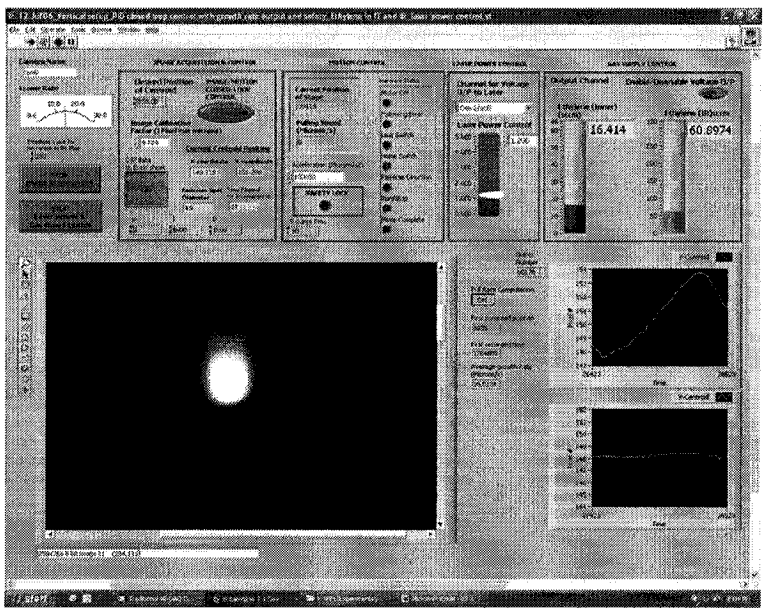

Figure 6.4 Front panel of LabVIEW VI for automated closed-loop control

To test the control algorithm's performance, two different experiments were performed:

1. Growth of a rod at constant laser power, but at different growth front positions.
2. Growth of a rod at constant growth front position, but at varying laser powers.

6.1.1 Closed-loop LCVD rod growth: Constant laser power, varying growth front position experiment

The outcome of this experiment can serve to

1. Test the performance of the closed-loop control in maintaining the rod growth front at desired positions pre-selected using the *growth rate map*.

2. Test the effect of growth front position on the obtained rod growth rate and diameter.

To start the experiment, a rod sample with specifications mentioned in Table 6.1 was designed. The design requires the growth of fifteen 1cm long sections, with each section grown at a different centroid *Set Point (SP)*. The centroid set points were selected from a *growth rate map* such as the one shown in Figure 6.1, obtained from prior experiments at the same growth conditions.

Table 6.1 Design specifications of rod sample for varying growth front experiment

Section #	Section start position (μm)	Section end position (μm)	Laser Power (mW)	Centroid *Set Point (SP) (Pixel #)*
1	0	10000	1600	150
2	10000	15000	1200	150
3	15000	25000	1600	188.45
4	25000	30000	1200	188.45
5	30000	40000	1600	226.9
6	40000	45000	1200	226.9
7	45000	55000	1600	265.35
8	55000	60000	1200	265.35
9	60000	70000	1600	303.8
10	70000	75000	1200	303.8
11	75000	85000	1600	342.25
12	85000	90000	1200	342.25
13	90000	100000	1600	380.7
14	100000	105000	1200	380.7
15	105000	115000	1600	419.15
16	115000	120000	1200	419.15
17	120000	130000	1600	457.6
18	130000	135000	1200	457.6
19	135000	145000	1600	496.05
20	145000	150000	1200	496.05
21	150000	160000	1600	534.5
22	160000	165000	1200	534.5
23	165000	175000	1600	572.95
24	175000	180000	1200	572.95
25	180000	190000	1600	611.4
26	190000	195000	1200	611.4
27	195000	205000	1600	649.85
28	205000	210000	1200	649.85
29	210000	220000	1600	688.3

The design also involves the growth of fourteen 0.5 cm long sections. The purpose of these 14 sections is to merely connect the 15 test sections. Growing the 0.5 cm long

sections at 1200 mW enables one to easily distinguish the test sections (grown at 1600 mW) from one another as a lower laser power produces a smaller diameter rod.

A LabVIEW VI (Figure 6.4) design integrating the vision, motion, laser power, and flow control systems allows the user to track the *Process Value (PV)* of the centroid, pull rate of the pickup system, diameter and length of the produced rod in real-time. Figure 6.5 shows the laser power, centroid *Set Point (SP),* and *Process Value (PV)* monitored throughout the growth of the designed rod sample. The VI clearly demonstrates the ability of the control system to maintain the rod growth front at the desired position. Also, note that the laser power is controlled as per the designed specifications.

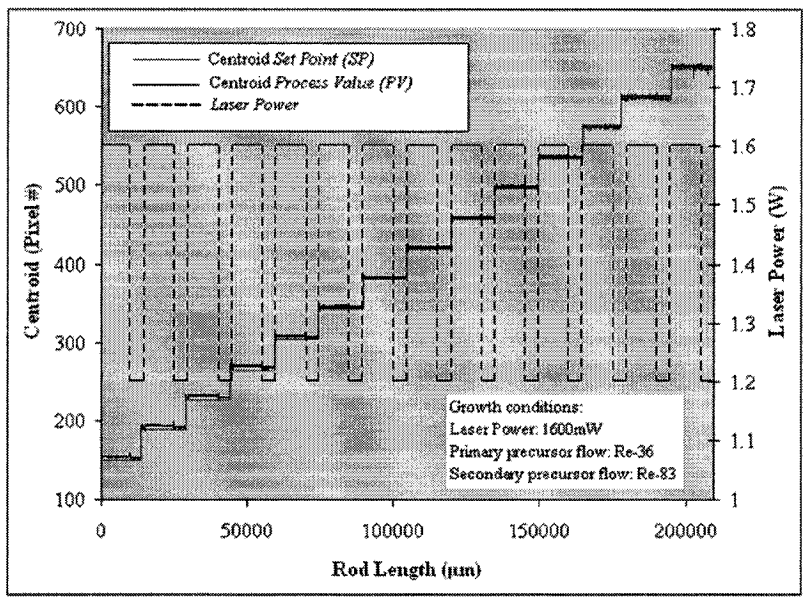

Figure 6.5 Laser power and centroid process value during varying centroid set point experiment

It is important to mention at this venue that although the VI developed for this experiment had a PID loop for process control, only the "proportional parameter" of the PID was used. This led to a constant steady-state error between the centroid set point and process value. Figure 6.6 presents a close-up view of the variation of the centroid

set point (between 90,000 μm and 100,000 μm of the produced rod length) shown in Figure 6.5. As can be seen in Figure 6.6, the steady-state error encountered with the centroid set point at pixel #380.7 is approximately 2.5 pixels. This amounts to approximately 24 μm. Taking the calibration of the vision system into account, the maximum error encountered during the production of the entire sample amounts to approximately 48 μm (with centroid set point at pixel #188.45). The occurrence of the maximum steady-state error at pixel #188.45 is not surprising considering that it is the position of maximum growth rate (Figure 6.7). The steady-state error can be eliminated by appropriate selection of the "integral component" of the PID loop. Further discussion of the PID control parameters can be found in section 6.1.2.

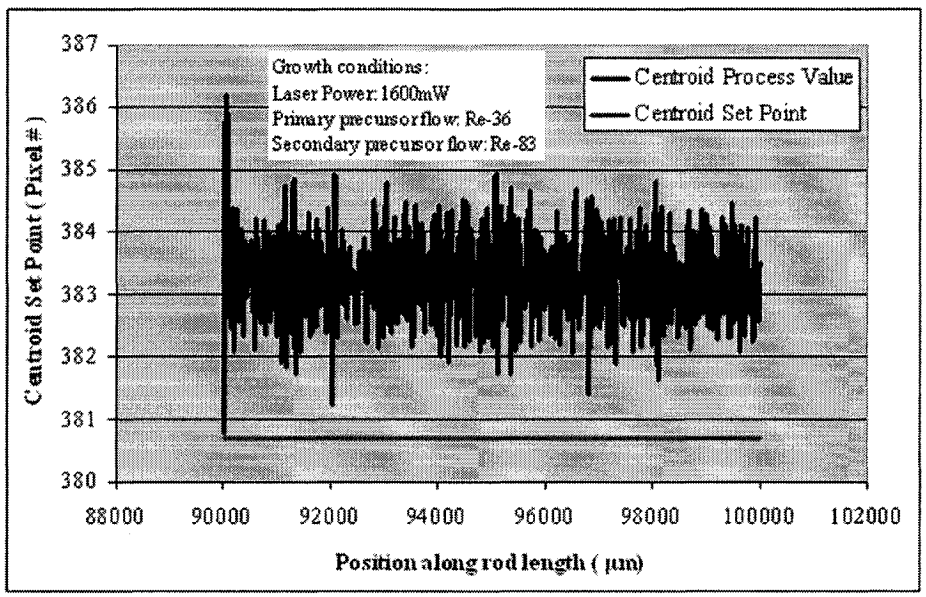

Figure 6.6 Close-up view of centroid set point variation

Growth rate and rod diameter measurements at each of the selected centroid set points are shown in Figure 6.7. To obtain growth rate and rod diameter measurements of the 15 sections at their respective centroid set points, pull rates, and emission size experienced during growth by each of the test sections over their entire length (1 cm) were averaged. It is worth noting that the growth rate values at various centroid

positions when traced by a line yields a profile that is very similar to the typical *growth rate map* (Figure 6.1) obtained using stationary substrate experiments. Finally, the sample grown as per the design specifications is shown in Figure 6.8, with the 1 cm sections numbered (1) through (15) highlighted by their start and end positions.

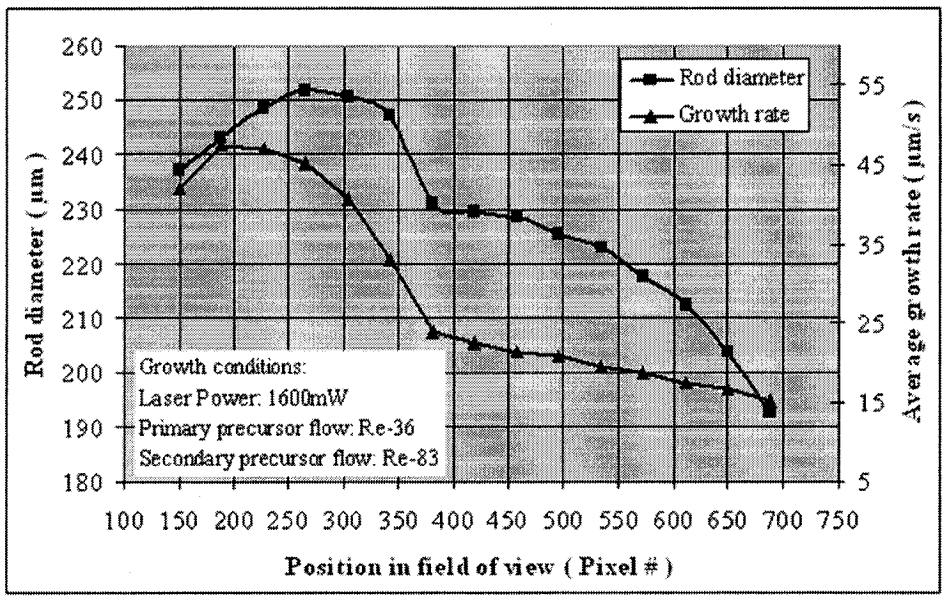

Figure 6.7 Rod growth rate and diameter measurements at selected centroid set points

6.1.2 Closed-loop LCVD rod growth: Constant rod growth front, varying laser power experiment

The outcome of this experiment can provide

1. Information on the effect of laser power on the rod growth rate and diameter at a constant centroid *Set Point* or growth front position.
2. Knowledge of the effect of laser power on the steady-state error when using a closed-loop system with only proportional control.

A test sample was designed as per specifications in Table 6.2. The design requires the growth of 6 rod sections, each grown at a different laser power ranging from 1600 mW to 600 mW while keeping the growth front constant at pixel #210 in the vision system.

The position of the set point was pre-selected from a previously obtained growth rate map at identical growth conditions such that the set point corresponds to the maximum growth rate in the *growth rate map.*

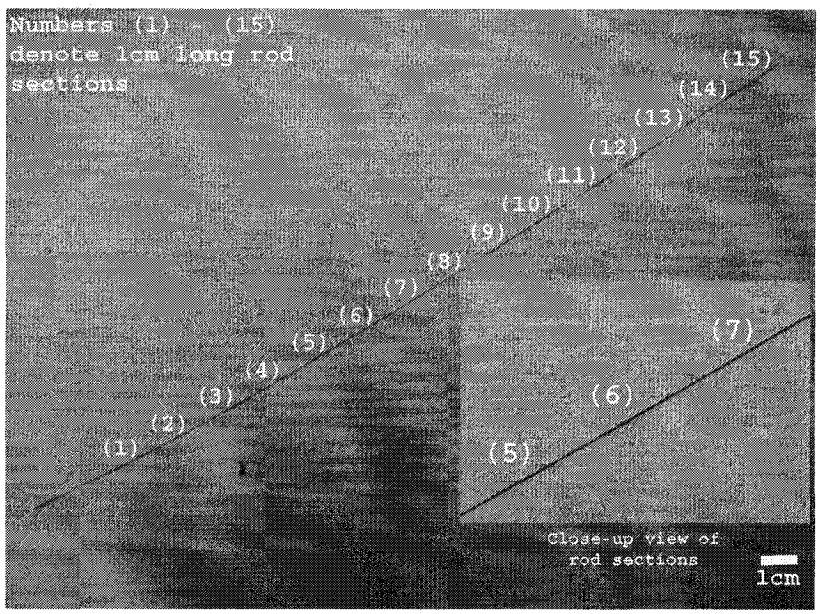

Figure 6.8 Rod sample grown using varying growth front experiment

Table 6.2 Specifications of rod sample for varying laser power experiment

Section #	Section start position (μm)	Section end position (μm)	Laser Power (mW)	Centroid *Set Point* (*SP*) – Pixel #
1	0	40000	1600	210
2	40000	80000	1400	210
3	80000	120000	1200	210
4	120000	140000	1000	210
5	140000	150000	800	210
6	150000	160000	600	210

Real-time rod growth rate and diameter values as a function of laser power output by the LabVIEW VI (Figure 6.4) are shown in Figures 6.9 and 6.10 respectively. The two figures clearly show the sensitivity of the growth rate and rod diameter as a function of laser power. Since the growth front is approximately maintained at the same position

throughout the sample growth, pull rate of the pickup system can be approximated as the growth rate of the produced sample. Average growth rates at each laser power were obtained by averaging the pull rate of the pickup system over the length of each section and plotted in Figure 6.11. Similarly, the average rod diameter at each laser power was computed by averaging the emission size output by the VI over the length of each section and plotted in Figure 6.11.

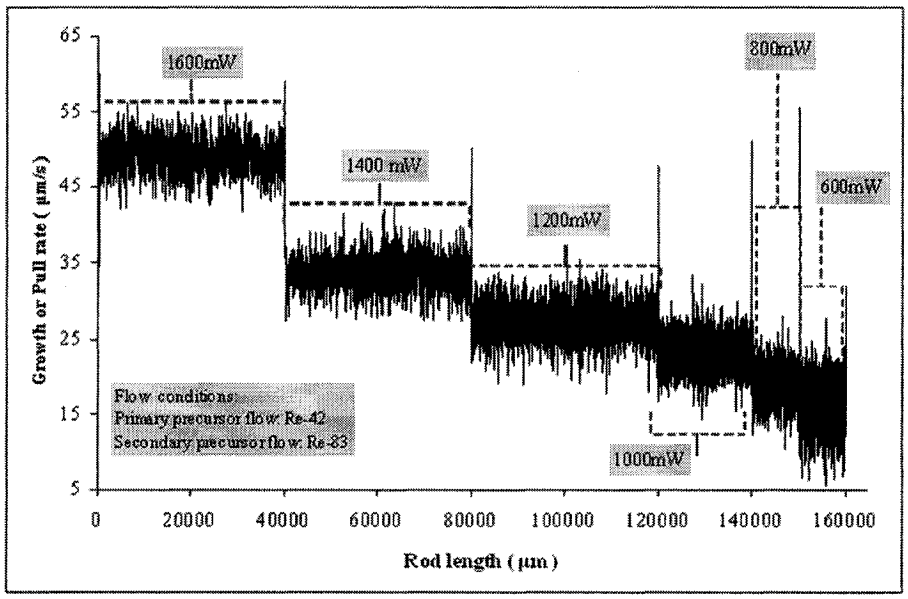

Figure 6.9 Rod growth rate as a function of laser power at a constant centroid set point

As observed during the experiments in section 6.1.1, a steady state error is present in all the experiments conducted at varying laser powers (Figure 6.12). At the highest laser power (1600 mW), an average steady-state error of ~6.5 pixels was evident while at the lowest laser power (600 mW), an average error of ~2 pixels was witnessed. In terms of real-world units, these errors approximate to 48 μm and 15 μm, respectively. Absence of an integral component in the PID loop manifests itself as a steady-state error.

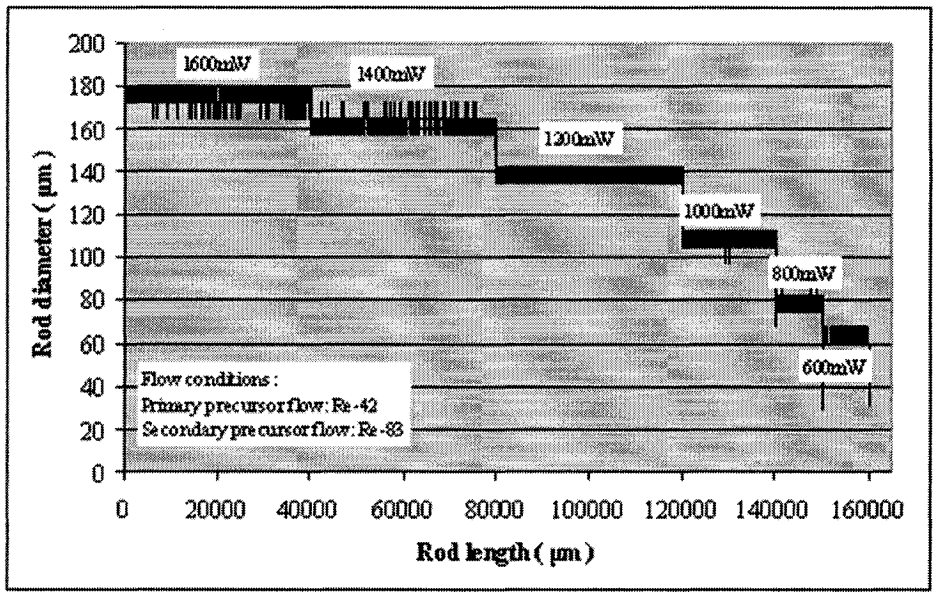

Figure 6.10 Rod diameter as a function of laser power at a constant centroid set point

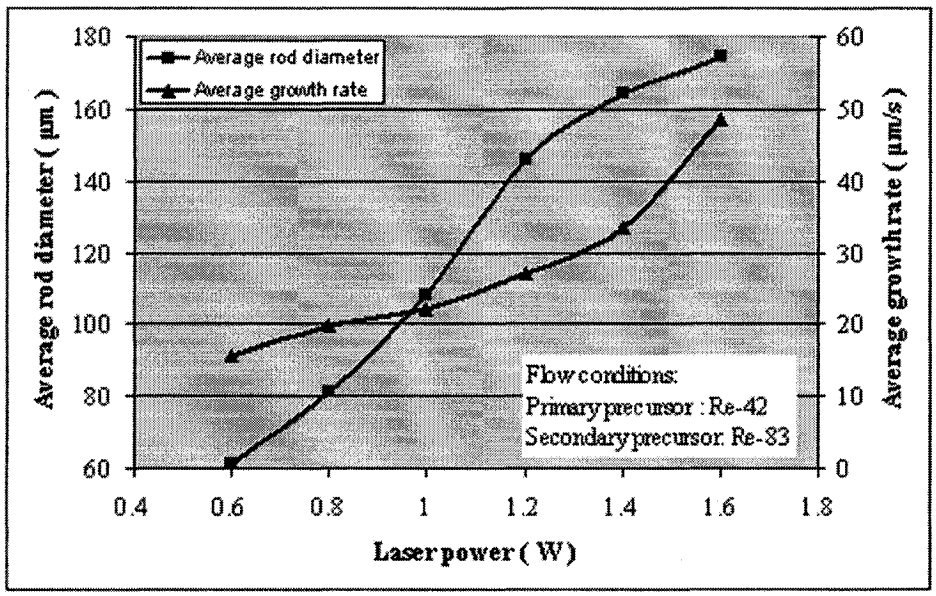

Figure 6.11 Averaged rod growth rate and diameter as a function of laser power at a constant centroid set point

Over the course of this work, some experiments were done using a Proportional Integral (PI) based control. Adding an integral component indeed reduced the magnitude of the

steady-state error. Most of the experiments however were done using a proportional control only, the reason being that the selection of the appropriate control parameters is dependent on the growth conditions of the experiment such as the precursor flow and the laser power. Selection and optimization of PID control parameters as a function of growth parameters is relegated for future work. The sample produced as per specifications in Table 6.2 is shown in Figure 6.13 with section numbers (1) through (6) highlighted by their start and end positions.

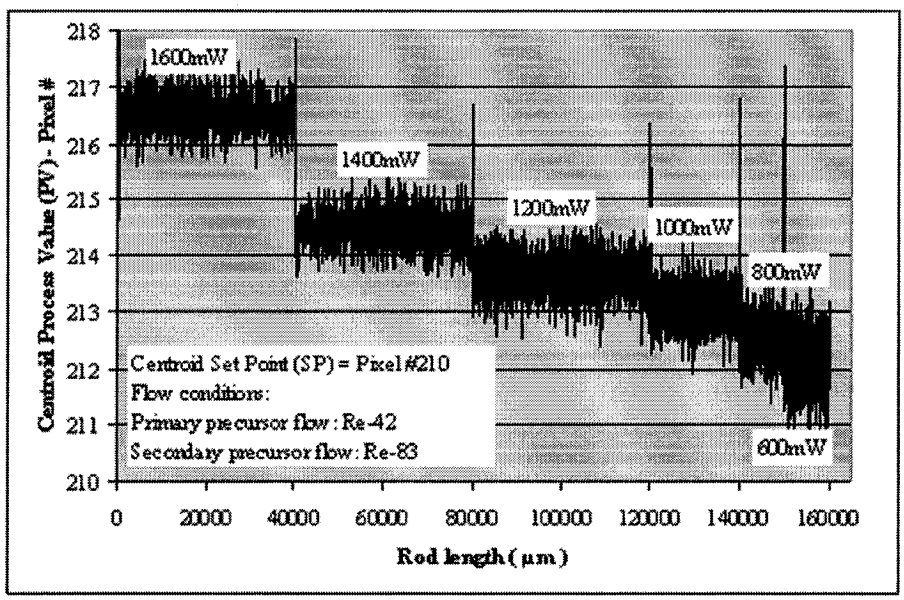

Figure 6.12 Centroid process value as a function of laser power at a constant centroid set point

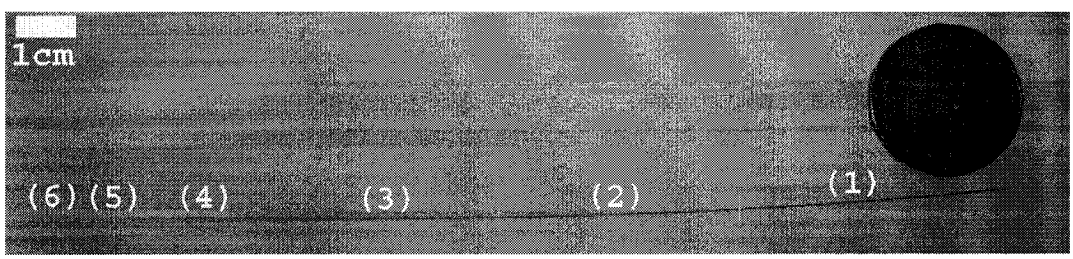

Figure 6.13 Rod sample grown using varying laser power experiment

6.1.3 Final comments on varying growth front position and varying laser power experiments

A final comment on the results presented in sections 6.1.1 and 6.1.2 is regarding the minimal operator intervention during experiments, and length of the produced samples. Both the experiments in sections 6.1.1 and 6.1.2 were completed with minimal operator intervention. For example, in the case of the varying growth front position experiment, the LabVIEW VI monitored the centroid process value, delivered corrective signals to keep the growth front at the desired position, changed the centroid set point to the new position at the completion of growth of each section, provided real-time information on rod diameter, and growth rate. It also maintained the laser power while simultaneously storing data for later use by the operator. In other words, the experiment was completed in one go as opposed to growing independent samples as part of a series of experiments.

Typical length of LCVD carbon rods in literature is less than 0.5 cm. A look at the results in sections 6.1.1 and 6.1.2 reveals rod lengths 22 cm and 16 cm respectively. To the author's knowledge, *this work has achieved the longest LCVD grown carbon rods to date.* In essence, work presented in this chapter so far has successfully tackled two of the challenges presented earlier namely:

1. Achieving better LCVD process control, and
2. Continuous rod growth.

6.2 Turn-key LCVD system for hands-free synthesis of arbitrary rods and rod-based structures

To date, LCVD has predominantly been a laboratory-based tool requiring operator intervention for the majority of its operation steps. An attempt has been made to develop a turn-key LCVD system for production of rod-based structures. To qualify as an automated system, said system must be capable of:

1. Accepting the design or specifications of the structure to be produced and translating the specifications to the actual product.

2. Performing real-time operator-free measurement of process variables such as growth rate and size (diameter and length) of the produced structures.
3. Maintaining process parameters such as laser power and precursor flow and correcting the parameters upon demand.
4. Track process data and output it upon process completion.

Towards this end, a rod-based structure (Figure 6.14) was designed to put the LCVD system to test. The design consists of three 5 cm long and 1 cm long sections grown alternately, with each section connected by a 0.25 cm long tapered structure. The 5 cm and 1 cm long sections are designed to be grown at a laser power of 1600 mW. The tapered sections are designed to undergo an exponential decay from 1600 mW to 1000 mW over their length. The design in Figure 6.14 while simple is sufficient to test the operation of the developed LCVD system because it necessitates proper integration and communication between various components (vision, motion, laser power and flow control) of a typical LCVD system. The vision system acquires data in real-time regarding the position of the rod growth front, growth rate and diameter of the produced structure and communicates the positional information of the growth front to the motion control system.

The motion control system uses this information as an input to position the rod growth front at the desired value while simultaneously computing the growth rate and length of the produced structure. The length information is passed on from the motion control system to the laser power control system, which then decides the laser power to be used to produce the current section of the structure. Similarly, the length information can also be passed to the flow control system if the design requires the use of multiple precursors with different flow compositions or single precursor with varying flow rate. Additionally, a feedback loop can also be established between the vision and laser power control systems to accurately control the shape and diameter of the produced structure.

For example, periodic or tapered structures such as those in [79] can be produced by proper integration of the vision and laser power control systems.

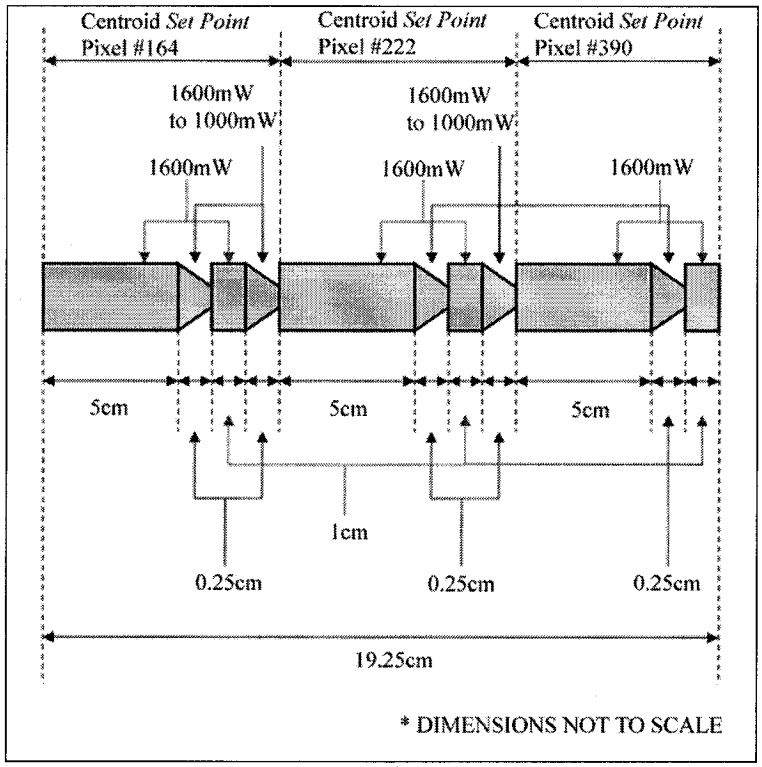

Figure 6.14 Specifications of structure for performance testing turn-key LCVD system

A LabVIEW VI (Figure 6.15) was developed to accept specifications of the structure (length of each section to be grown, and laser power at which each section needs to be grown) as an array input from the operator. The VI also requires the user to input the calibration of the vision system and the desired centroid set points at which the growth front needs to be maintained during the growth of each section. Once all the required inputs are provided, the VI starts producing the sample while recording the required process data into an excel sheet for later analysis by the operator.

The centroid set points were selected from the growth rate map (Figure 6.16) obtained from stationary substrate experiments conducted at the same growth conditions.

Another motivation to the design in Figure 6.14 is the study of the effect of growth front position on the produced deposit's mechanical properties and microstructure. The three 5 cm long sections can serve as test specimens for tensile testing while the three 1 cm long sections can serve as samples for "Micro-Raman spectroscopy."

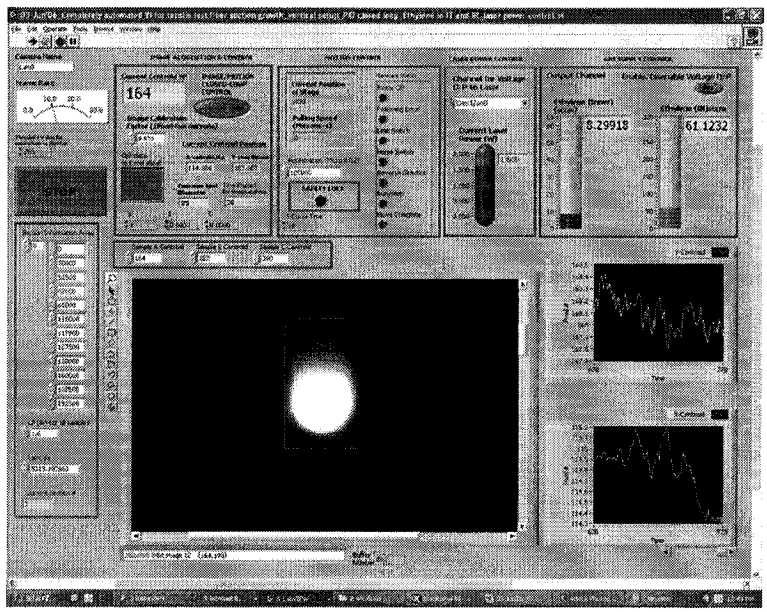

Figure 6.15 Front panel of LabVIEW VI for turn-key LCVD operation

Several experiments were done using the turn-key LCVD system to produce samples similar in dimensional specifications to the sample in Figure 6.14, but grown at different laser powers (1400 mW, 1200 mW, 1000 mW, 800 mW). *In-depth mechanical testing and microstructural analysis of all these samples, and their correlation is however relegated to future study.* Real-time laser power and centroid set point information over the entire sample length is plotted in Figure 6.17.

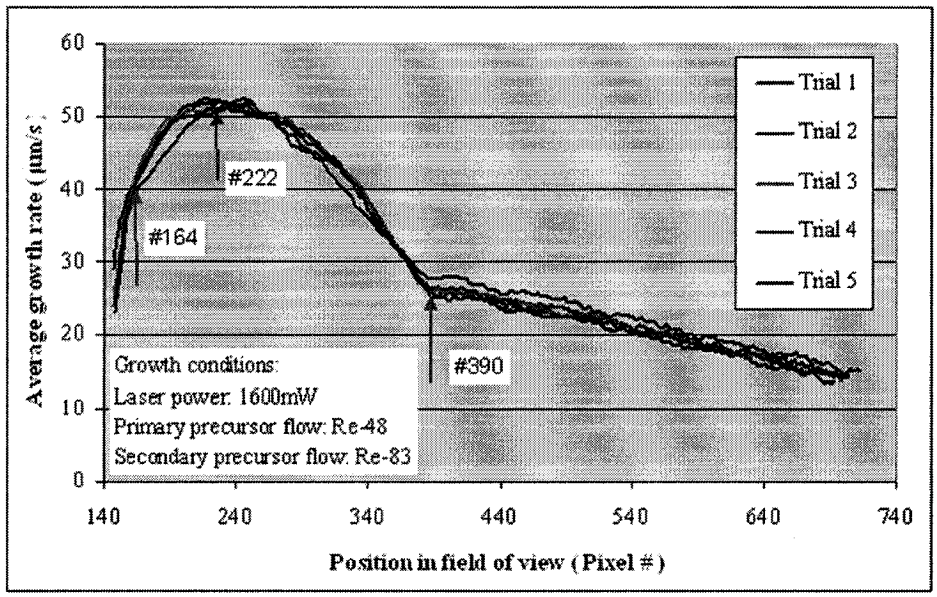

Figure 6.16 Growth rate map for turn-key LCVD experiment

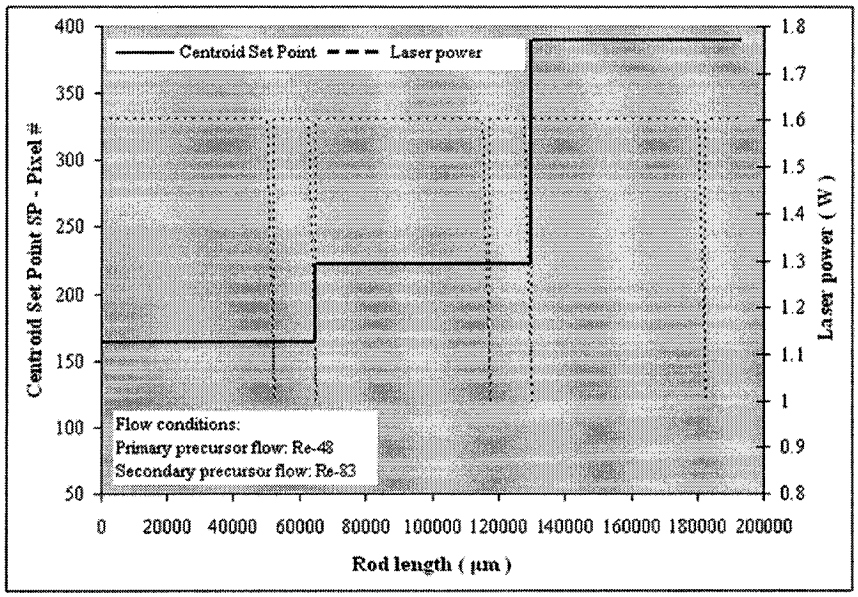

Figure 6.17 Real-time laser power and centroid set point information during turn-key LCVD experiment

The graph (Figure 6.17) clearly shows the successful operation of the LCVD system as per the input design specifications in Figure 6.14. There is a close match between growth rates output in real-time by the VI (Figure 6.18) and those in the growth rate map.

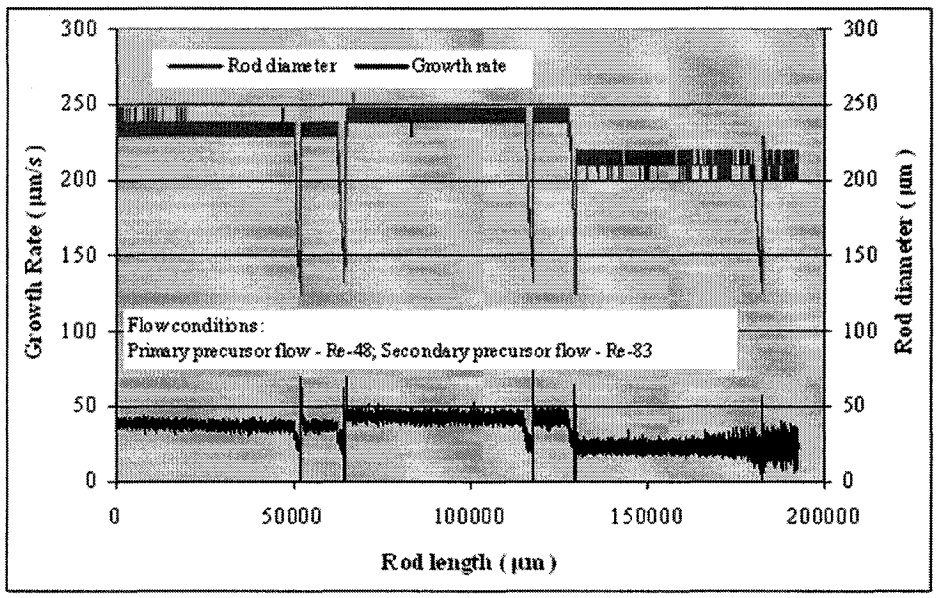

Figure 6.18 Real-time rod growth rate and diameter information during turn-key LCVD experiment

Small mismatches between growth rates output in real-time by the VI and those obtained from the growth rate map can occur, as has been observed during the course of many experiments. It must be noted however that this mismatch is solely a result of calibration errors at the start of the stationary substrate experiments that yield the growth rate map. Pull rates, or in other words, growth rates output by the VI can be trusted as they are transmitted by the optical encoder in the linear servo motor stage. For example, if one were to compare the growth rates obtained at a laser power of 1600 mW in sections 6.1.1 and 6.1.2, a very close growth rate match can be found. On the other hand, if one were to compare the rod diameters obtained at 1600 mW, the calibration mismatch becomes clearly evident as the rod diameter values in section 6.1.2 are much

lower than those in section 6.1.1. The above example is evidence of the dependability of the growth rate output on the pickup system. Calibration errors can occur due to lensing effect created by the quartz tube surrounding the third coaxial flow of argon that acts as a protective shroud to the primary and secondary precursor flows. Addressing this issue can reduce/eliminate growth rate mismatch.

While the work presented in this section represents a significant step towards developing LCVD state-of-the-art, it can certainly benefit from improvement in operations such as positioning the substrate in the vicinity of the focal region and aligning the laser and tube axes. These operations have been done manually during this work and they considerably increase the setup time of the process. Automating these operations can lead to a significant leap in the efficiency of the process, once it is put into use as a production tool. In conclusion, the work presented in this section can act as a stepping stone for further development towards transforming LCVD into a true hands-free turn-key system.

6.3 Open-loop continuous pull rod growth

As mentioned earlier in chapter 1, the vast majority of LCVD work to date has been open-loop. The operator gets the substrate to the vicinity of the laser focal region, induces rod growth, and takes growth rate measurements manually. During this time, the growing rod is either pulled away from the laser focus in small increments or is held stationary. An exception to this methodology, albeit open-loop is the "self-regulating growth mechanism" proposed by Wallenberger et al [57]. In their work, Wallenberger et al proposed positioning the tip of the substrate slightly ahead of the optimum laser focus (towards the laser beam) before rod growth is initiated. Once the laser power is turned on, the substrate is retracted away from the laser focus at a constant rate. They propose that the growth rate will self-regulate itself; if growth rate is larger than the pull rate, the rod would grow out of the laser focal region, and growth comes to a halt. On the contrary, if pull rate is larger than the growth rate, then the growth front will be

pulled away from the laser focal region causing the growth to cease. It must be noted however that Wallenberger et al did not have a means of quantifying the positional growth rate (via a growth rate map) as in this work.

The discovery that the 656 nm emission can be used as a means of measuring the position of the rod growth front (chapter 3) can now allow one to analyze the effectiveness of the "self-regulating mechanism" proposed by Wallenberger et al. Towards this end, two rods were grown using a stationary substrate experiment at 1000 mW to obtain a growth rate map as shown in Figure 6.19. Using the map, it was decided to grow a rod by continuously retracting it at 15 μm/s. Using results in trials #1 and #2 in the growth rate map, a growth rate of 15 μm/s could correspond to a position between pixels #293 and #309. The substrate was brought to the same initial position used for growing rods in Figure 6.19.

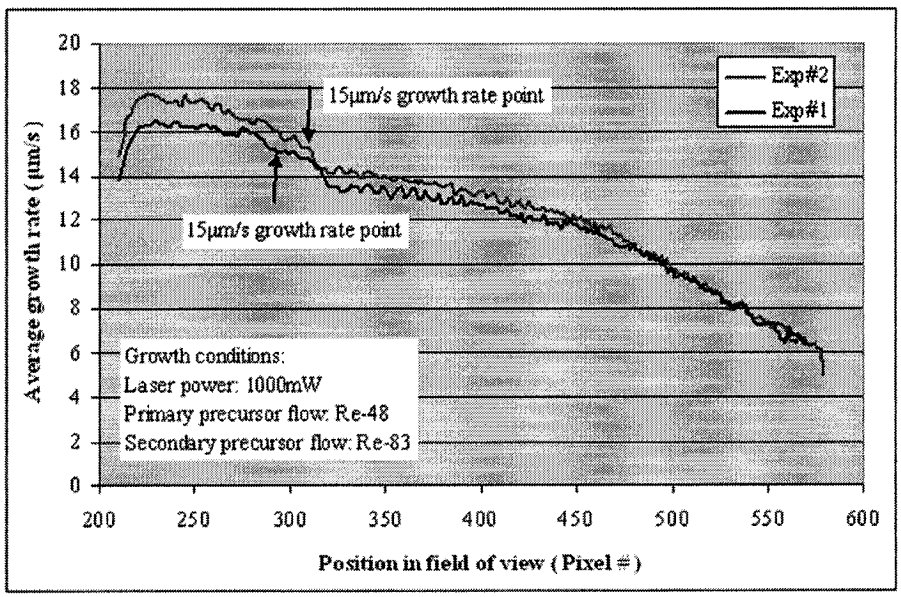

Figure 6.19 Growth rate map for open-loop continuous pull rod growth

A LabVIEW VI was designed to continuously pull the growing rod at 15 μm/s while simultaneously measuring the centroid process value (PV) of the emission at the rod

growth front. If the open-loop system were to work, then the pull rate (15 μm/s) should eventually find a match in the growth rate map at a position corresponding to a growth rate of 15 μm/s. Figure 6.20 tracks the emission centroid position over a time frame of approximately 1500 seconds. The striking feature of the data in Figure 6.20 is the over-damped nature of the centroid position change with time. The initial spike in the growth rate map (Figure 6.19) that peaks at 16.35 μm/s and 17.62 μm/s respectively for trials #1 and #2 causes the rod growth front to cross the centroid position that yields the 15μm/s growth rate.

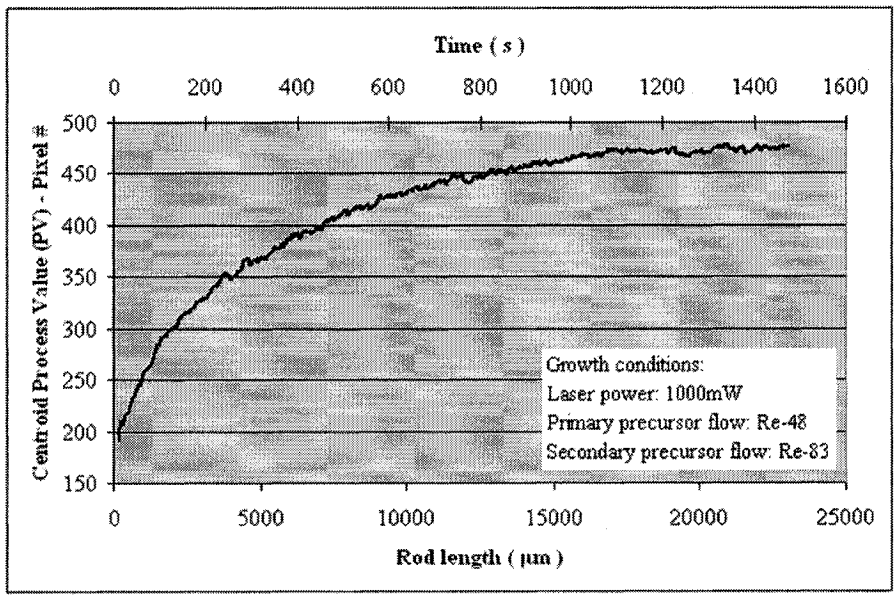

Figure 6.20 Variation of centroid process value during open-loop continuous pull rod growth

It is interesting to note that the emission centroid eventually stabilizes after a considerably long time, owing to the over-damped nature of the system. What is surprising however is that even after 1500 seconds, the emission centroid never reaches its intended position (between pixels #293 and #309) as determined from the growth rate map. *This clearly demonstrates the need for a more proactive approach that can position as well as maintain the emission centroid at the desired set point.* The

identified need for better growth front positioning is satisfied by the closed-loop LCVD system presented in earlier sections (6.1 and 6.2). The proactive nature of the proposed closed-loop algorithm can aid in achieving microstructural reproducibility if the rod growth front position is found to have a significant impact on the obtained rod microstructure.

The effect of pull rate on the obtained microstructure remains to be seen. To the author's knowledge, no analysis of the dependence of pulling rate on the obtained microstructure has been conducted to study the effect of an open-loop continuous pull system. The closed-loop LCVD system developed in this work is not only a proactive approach to rod growth, but can also aid in achieving reproducible microstructure if the pull rate is found to have a significant effect on the obtained microstructural properties.

CHAPTER 7: GENERAL DISCUSSION, CONCLUSIONS, AND SCOPE FOR FUTURE WORK

7.1 General discussion

The primary objective of the thesis at the outset was to get a better understanding of the LCVD process so as to obtain a better control over it. Work done towards this direction has helped push LCVD state-of-the-art further while attempting to bring LCVD closer to the industry as an effective tool for the production of rods and rod based structures. The developed experimental system allowed the study of the impact of axial convection enhancement on the most important process variable, the growth rate. Experiments conducted at all the available laser powers showed no saturation in growth rate with increasing temperature, lending indirect proof to the positive impact of axial convection enhancement. Further theoretical and experimental studies, however, are required to understand and validate the results obtained.

The real-time imaging of the 656 nm atomic hydrogen emission has provided a tool for closely examining the process behavior within the laser-induced growth region, while using a stationary laser focus and substrate setup. It also allowed the first-time quantification of growth rate as a function of position in the laser-induced growth region. Most LCVD systems to date operate either using a stationary substrate and laser focus or a continuously moving laser focus. In the former, the laser power is compensated to ensure identical growth conditions throughout the growth of the rod while in the latter, uniform growth conditions are guaranteed by always maintaining the rod growth tip at the same laser focal condition. It is important to note that both these approaches follow the assumption that the peak axial growth rate occurs at the laser focus.

The variational analysis of LCVD rod growth showed that the peak axial growth rate occurs at about an order of magnitude greater than the Raleigh range of the optics. It

also showed that the process efficiency (energetic, volumetric) varies greatly within the laser-induced growth region. The results therefore bring to light the sensitivity of the LCVD process and the need for improved process control.

As with the peak growth rate, the optimum process efficiency is also not at the focal plane. Surprisingly, the results of the rod tip position perturbation study point to a decrease in the temperature at the focal plane. At this point of time, the explanation for the decrease in growth rate and temperature before the focal plane is speculative, and based on previous LCVD work by Doppelbauer et al [61], and Maxwell et al [82]. Both works suggest the possible occurrence of thermodiffusion (the Soret effect) owing to the extreme temperature gradients present in the gas surrounding the tip of the growing rod. For more information on the Soret effect, one can refer to the review article by Platten [85]. When a sufficiently large temperature gradient (excess of 10^6 to 10^7 K/m) exists, the lighter molecules in the gas mixture (comprised of precursor and by-products) can accumulate near the rod tip. For example, in the case of carbon deposition from ethylene, it is possible that atomic hydrogen can accumulate at the rod tip reducing the concentration of the precursor (ethylene) near the tip. The migration of lighter gas molecules towards the hot zone is further amplified if the gas mixture under consideration contains gases with a large difference in molecular weights. If indeed the Soret effect is present in our experiments, then the decrease in the growth rate as the rod tip gets closer to the laser focus can be explained by the decrease in concentration of ethylene. We speculate the Soret effect to be responsible for the decrease in process efficiency as well, until further studies are carried out.

Another impact of atomic hydrogen accumulation near the rod tip is improved heat dissipation from the reaction zone at the rod tip. Atomic hydrogen has a thermal conductivity of 0.1805 W/mK [86] compared to a thermal conductivity of 0.0168 W/mK [87] for ethylene. As the rod tip gets closer to the focal plane, accumulation of atomic

hydrogen at the rod tip leads to a better heat dissipation from the reaction zone thereby reducing the temperature.

Finally, the developed closed-loop control system while providing improved process control has facilitated the first time demonstration of continuous rod synthesis.

7.2 Conclusions

The key contributions of the thesis are as follows:

1. A novel axial convection enhanced LCVD system capable of producing rods/fibers in chamber-free open-air conditions was realized. *Carbon rods were produced under open-air conditions for the first time* (Chapter 2).
2. The axial flow configuration afforded by the developed LCVD system has *yielded* the *highest carbon rod growth rates to date* at atmospheric conditions. Growth rate studies as a function of laser power point to a trend of continuously increasing growth rate. Under all the available laser powers tested, *no growth rate saturation was witnessed* (Chapter 2).
3. *Real-time in-situ rod growth rate and diameter measurements were made for the first time.* It was made possible by image analysis of the 656 nm hydrogen-alpha emission produced during precursor pyrolysis. The developed technique allowed the determination of growth rate along the rod axis for the first time. It also reduced growth rate measurement errors and improved measurement repeatability (Chapter 3).
4. Contrary to the generally accepted notion of the presence of a steady-state growth region, transient growth rates during rod growth using a stationary substrate and laser focus setup were found to vary greatly inside the laser-induced growth region. The results point to the need to control the position of the rod growth front to obtain reproducible microstructures (Chapter 4).
5. Variational analysis of process parameters brought to light the extreme sensitivity of the LCVD process. It also helped identify the position of the focal

plane intrinsic to the process. Growth rate was found to be asymmetric with respect to the focal plane. The results point to a great variability of the process efficiency: energetic, volumetric, mass, and molar. The reason for the strong asymmetry of growth rate with respect to the focal plane is yet to be determined. Finally, the results stress the importance of LCVD process control (Chapter 5).

6. A closed-loop algorithm was developed and implemented to realize the *first closed-loop LCVD rod growth system.* The closed-loop system *minimized operator intervention* and *produced the longest carbon rods to date* (Chapter 6).
7. An attempt was made to develop the *first turn-key LCVD system for hands-free synthesis of rods and rod based structures.* This was made possible by the effective integration of various LCVD sub-systems such as laser power, vision, gas flow and motion control. The system allows the operator to input the specifications (diameter, length, shape profile) of the desired rod or rod based structure. Upon turning on the system, it measures the process parameters (growth rate, diameter and current length of the structure), and tracks the growth parameters (laser power, precursor flow rate). All acquired data is stored in appropriate form (word or excel documents) for later use by the operator. In essence, the system represents a significant step forward towards developing LCVD into an industrial tool for the production of rods and rod based structures (Chapter 6).

7.3 Scope for future work

The results of the thesis have uncovered further avenues that can be pursued to gain better insight to not only explain the results obtained in this work, but also explore and advance LCVD technology.

1. The growth rate trend (Figure 2.12) witnessed in chapter 2 clearly shows the positive impact of the novel LCVD setup. The trend however is intriguing in that growth rate saturation is visibly absent unlike prior growth rate trends

reported in literature. To probe the reasons for such a behavior, the following studies are recommended:

a. Computational study of the reaction zone around the fiber tip to quantify the effect of convection enhancement.
b. Microstructural study of rods as a function of laser power to uncover the reason for increase in the slope of the growth rate trend (Figure 2.12) after 1400 mW.
c. Optical emission spectroscopic study (at different laser powers) of emission signatures on the rod tip and at different distances from the rod tip to identify the possible reaction mechanism responsible for high growth rates after 1400 mW (Figure 2.12)
d. Develop a means to measure the temperature in the reaction zone. Temperature measurements will aid in correlating temperature with growth rate measurements, obtained microstructure, and emission signatures.

2. Precursor flow (primary and secondary) optimization studies must be done to identify the best flow conditions at each laser power.
3. Variational analysis of rod growth in Chapter 5 revealed the asymmetric nature of the growth rate and efficiency (energetic and volumetric) of the process relative to the focal plane. Further experimental studies would be required to identify the reasons for the asymmetry. The analysis also discovered that the rod tip temperature decreases as the tip gets closer to the focal plane and steadies afterward. Temperature measurement combined with emission spectroscopy of the rod tip as it traverses across the laser-induced growth region can help to corroborate and explain the result.
4. The closed-loop LCVD system can definitely benefit from the optimization of the control parameters (P, I, and D). Optimization can reduce the steady-state errors reported in Chapter 6.
5. Accurate calibration of the field of view of the vision system is crucial for

stationary laser focus and substrate experiments as growth rate measurements rely on the calibration to convert growth rate from pixels/sec to real-world units. It was identified during the course of this work that the quartz tube surrounding the third coaxial flow of argon is responsible for calibration errors. Addressing this issue can eliminate the observed errors.

6. Although the turn-key LCVD system developed in Chapter 6 is a significant step towards minimizing operator intervention, it can certainly benefit from improvement in operations such as positioning the substrate in the vicinity of the focal region and aligning the laser and tube axes. These operations have been done manually during this work and they considerably increase the setup time of the process. Automating these operations can lead to a significant leap in the efficiency of the process, once it is put into use as a production tool.
7. The excellent process control afforded by the closed-loop LCVD system can be used to advantage to study:
   a. The correlation of rod growth front position to the produced microstructure.
   b. The correlation of rod growth front position to the rod mechanical properties.

   Preliminary microstructural analysis of rods produced in section 6.1.1 using the "constant laser power, varying growth front position" experiment indeed points to a change in the microstructure at varying rod growth front positions. Figure 7.1 depicts a correlation between rod growth rate and crystallite size as a function of rod growth front position. A plot like Figure 7.1 would allow the user to utilize the *"growth rate-microstructure map"* to decide the position of the rod growth front to be maintained during deposition to obtain the required microstructure. The closed-loop system in turn guarantees that the rod growth front is maintained at the desired position thereby ensuring microstructural reproducibility.

8. To the author's knowledge, not much is reported in literature on the density of

LCVD rods. Similar to the "rod growth front position-microstructure correlation", one can also work on a "rod growth front position-density correlation" by measuring the density of the produced rods as a function of growth front position.

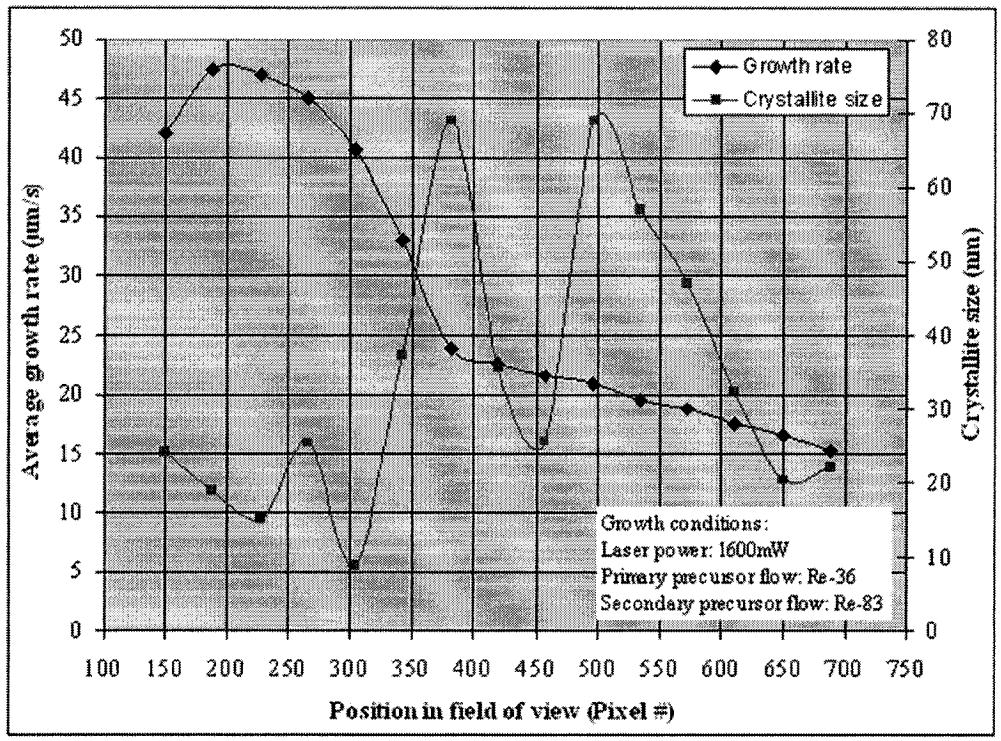

Figure 7.1 Growth rate-crystallite size correlation as a function of rod growth front position

REFERENCES

1. S.T. Peters and G. Lubin, *Handbook of Composites*, 2nd edition, New York: Chapman & Hall, 1998. [Electronic text]. Available in: Knovel Library.
2. F.T. Wallenberger, J.B. MacChesney, R. Naslain and H.D. Ackler, *Advanced Inorganic Fibers: Processes-Structures-Properties-Applications*, Boston: Kluwer Academic Publishers, 1999.
3. W. Watt and B.V. Perov, *Strong Fibers*, Amsterdam: Elsevier Science Publishing, 1985.
4. National Materials Advisory Board. *Ceramic Fibers and Coatings: Advanced Materials for the Twenty-First Century*, Washington: National Academic press, 1998. [Electronic text]. Available in: The National Academic Press.
5. R.A. Lowden and M.A. Karnitz, "A Survey of the Status of Ceramic Reinforcement Technology and its Relationship to CFCCs for Industrial Applications", Metals and Ceramics Division, Oak Ridge National Laboratory, 1995. [On Line]. Available: http://www.ms.ornl.gov/programs/energyeff/cfcc/PRO/fibrep_f.htm [Page consulted on 17 December 2003]
6. C.E. Harris, M.J. Shuart and R. Hugh, "A survey of emerging materials for revolutionary aerospace vehicle structures and propulsion systems", NASA Technical Reports Server, 2002. [On Line]. Available at: http://ntrs.nasa.gov/archive/nasa/casi.ntrs.nasa.gov/20020053644_2002090609.pdf [Page consulted on 24 May 2004]
7. Energetics Incorporated and Richerson and Associates, "Advanced Ceramics Technology Roadmap - Charting Our Course", U.S DOE Energy Efficiency and Renewable Energy, 2000 [On Line]. Available at: http://www.eere.energy.gov/industry/energy_systems/pdfs/ceramics_roadmap.pdf [Page consulted on 29 May 2004]

8. J.W.S. Hearle, *High performance fibers*, Cambridge: Woodhead Publishing, 2001. [Electronic text]. Available in: Knovel Library
9. S. Suresh, A. Mortensen and A. Needleman, *Fundamentals of metal-matrix composites,* Massachusetts: Elsevier, 1993. [Electronic text]. Available in: Knovel Library.
10. K.K. Chawla, *Ceramic matrix composites.* 2nd ed. Boston: Kluwer Academic publishers, 2003.
11. J.J. Hurley and F. George, "Vapor-Liquid-Solid (VLS) SiC Whiskers: Synthesis and Mechanical Properties," in *Fiber Reinforced Ceramic Composites*, Park Ridge, NJ: [On Line]. Park Ridge, NJ: Noyes Publications, 1990, pp. 93-121. [On Line]. Available: http://www.knovel.com/knovel2/Toc.jsp?BookID=364 [Page consulted on 28 May 2006]
12. J.-O. Carlsson, "Techniques for the preparation of Boron fibers," *Journal of Materials Science*, vol.14, no.2, pp.255-264, 1979.
13. Y. Kimura, Y. Kubo and N. Hayashi, "High-performance boron-nitride fibers from poly(borazine) preceramics", *Composites Science and Technology*, vol.51, no.2, pp-173-179, 1994.
14. K. Upadhya and W.P. Hoffman, "Advanced composite microtubes for micro-electromechanical systems," *JOM*, vol.45, no.5, pp.54-56, 1994.
15. L.S. Nelson and N.L. Richardson, "Formation of thin rods of pyrolytic carbon by heating with a focused carbon dioxide laser," *Materials Research Bulletin*, vol.7, no.9, pp.971-975, 1972.
16. K.L. Loewenstein, *The manufacturing technology of continuous glass fibers*, 3rd edition, Amsterdam: Science, 1993.
17. M.L. Nice, "Apparatus and process for fiberizing fluoride glasses using a double crucible and the compositions produced thereby," US patent, US 4,897,100, 1990. [On Line]. Available: Derwent Innovations Index, http://portal.isiknowledge.com/ [Page consulted on 24 May 2004].

18. F.T. Wallenberger, N.E. Weston and S.D. Brown, "Calcium aluminate glass fibers. Drawing from supercooled melts versus inviscid melt spinning," *Materials Letters*, vol.11, no.8-9, pp.229-235, 1991.
19. J.K. Weber, J.J. Felten, B. Cho and P.C. Nordine, "Glass fibres of pure and erbium- or neodymium-doped yttria-alumina compositions," *Nature*, vol.393, no.6687, pp.769-771, 1998.
20. W. Jia, H. Yuan, L. Lu, H. Liu and W.M. Yen, "Crystal growth and characterization of Eu^{2+}, Dy^{3+}: $SrAl_2O_4$ and Eu^{2+}, Nd^{3+}: $CaAl_2O_4$ by the LHPG method," *Journal of Crystal Growth*, vol.200, no.1, pp.179-184, 1999.
21. Y.H. Chiou, M.T. Tsai and H.C. Shih, "Preparation of alumina fibre by sol gel processing," *Journal of Materials Science*, vol.29, no.9, pp.2378-2388, 1994.
22. S. Yajima, Y. Hasegawa, J. Hayashi and M. Iimura, "Synthesis of continuous silicon carbide fibre with high tensile strength and high youngs modulus," *Journal of Materials Science*, vol.13, no.12, pp.2569-2576, 1978.
23. S. Kamimura, K. Watanabe, N. Kasai, T. Seguchi and K. Okamura, "Silicon nitride fiber synthesis from polycarbosilane fiber by radiation curing and pyrolysis under alumina," *Manufacturing and Materials Development*, vol.2, pp.281, 1995.
24. National Materials Advisory Board, *Commercialization of new materials for a global economy*, Washington: National Academic Press, 1993. [Electronic text]. Available in: The National Academic Press.
25. J. Mazumder and A. Kar. *Theory and Application of Laser Chemical Vapor Deposition*, New York: Plenum Press, 1995.
26. K. Björklund, "Microfabrication of tungsten, molybdenum and tungsten carbide rods by laser-assisted CVD," Doctorate thesis, Uppsala University, Uppsala, Sweden, 2001.
27. D. Bäuerle, *Laser Processing and Chemistry*, 1st edition, New York: Springer-Verlag, 1996.

28. C. Duty, D. Jean and W.J. Lackey, "Laser chemical vapour deposition: Materials, modeling, and process control," *International Materials Reviews*, vol.46, no.6, pp.271-287, 2001.
29. Y. Rytz-Froidevaux, R.P. Salathé and H.H. Gilgen, Laser generated microstructures," *Applied Physics A: Solids and Surfaces*, vol.A37, no.3, pp.121-138, 1985.
30. T.H. Baum, C.E. Larson and R.L. Jackson, "Laser-Induced Chemical Vapor Deposition of Aluminum," *Applied Physics Letters*, vol.55, no.12, pp.1264-1266, 1989.
31. M.C. Wanke, O. Lehmann, K. Muller, Q. Wen and M. Stuke, "Laser rapid prototyping of photonic band-gap microstructures," *Science*, vol. 275, pp.1284-1286, 1997.
32. F.A. Houle, C. R. Jones, T. Baum, C. Pico and C. A. Kovac, "Laser chemical vapor deposition of copper," *Applied Physics Letters*, vol.46, no.2, pp.204-206, 1985.
33. T.H. Baum and C.R. Jones, "Laser chemical vapor deposition of gold," *Applied Physics Letters*, vol.47, no.5, pp.538-540, 1985.
34. S. Boughaba and G. Auvert, "Deposition of micron-size nickel lines by argon-ion laser-assisted decomposition of nickel tetracarbonyl," *Applied Surface Science*, vol.69, pp.79-86, 1993.
35. D. Braichotte and H. van den Bergh, "Growth rates and electrical conductivity of microscopic ohmic contacts fabricated by laser chemical vapor deposition of platinum," *Applied Physics A: Solids and Surfaces*, vol.A44, no.4, pp.353-359, 1987.
36. E. Flint, J. Messelhauser and H. Suhr, "Laser-induced chemical vapor deposition of rhodium," *Applied Surface Science*, vol.54, pp.56-59, 1992.
37. J. Maxwell, R. Krishnan and S. Haridas, "High pressure, convectively enhanced-laser chemical vapor deposition of titanium," *Proceedings of the Solid Freeform Fabrication Symposium*, pp. 497-503, 1997.

38. M. Boman and D. Bäuerle, "Laser-assisted chemical vapour deposition of boron," *Journal of Chinese Chemical Society*, vol.42, no.2, pp. 405-411, 1995.
39. F.T. Wallenberger, "Inorganic fibers and microfabricated parts by laser assisted chemical vapour deposition (LCVD): structures and properties," *Ceramics International*, vol.23, no.2, pp.119-126, 1997.
40. H. Westberg, M. Boman, S. Johansson and J. Schweitz, "Free-standing silicon microstructures fabricated by laser chemical processing," *Journal of Applied Physics*, vol.73, no.11, pp.7864-7871, 1993.
41. C. Duty, R. Johnson, S. Bondi and W.J. Lackey, "Pyrolytic laser CVD of boron nitride and molybdenum," *Chemical Vapor Deposition*, vol.9, no.6, pp.298-301, 2003.
42. K.S. Boutros, J.C. Roberts and S.M. Bedair, "Direct writing of GaAs optical waveguides by laser-assisted chemical vapor deposition," *Applied Physics Letters*, vol.68, no.15, pp. 2041-2042, 1996.
43. A. Miehr, R.A. Fischer, O. Lehmann and M. Stuke, "Laser direct writing of β-Co/Ga and Mn/Ga alloy microstructures from organometallic single-source precursors," *Advanced Materials for Optics and Electronics*, vol.6, no.1, pp.27-32, 1996.
44. J.L. Maxwell, J. Pegna, D.A. Deangelis and D.V. Messia, "Three-dimensional laser chemical vapor deposition of nickel-iron alloys," *Materials Research Symposium Proceedings*, vol.397, pp.601-606, 1996.
45. H. Westberg, M. Boman and J.-O. Carlsson, "Kinetics in thermal laser-assisted chemical vapor deposition of titanium carbide," *Thin Solid Films*, vol.218, no.1-2, pp.8-14, 1992.
46. J. Maxwell, J. Shah, T. Webster and J. Mock, "Rapid prototyping of titanium nitride using three-dimensional laser chemical vapor deposition," *Proceedings of the Solid Freeform Fabrication Symposium*, pp.575-580, 1998.

47. H. Westberg, F. Ericson, J. Engqvist and M. Boman, "Laser induced chemical vapor deposition of $TiSi_2$: Aspects of deposition process, microstructure and resistivity," *Thin Solid Films*, vol. 198, pp.279-292, 1991.
48. M.N. Oliveira, A.M. Botelho do Rego and O. Conde, "XPS investigation of $B_xN_yC_z$ coatings deposited by laser assisted chemical vapor deposition," *Surface and Coatings Technology*, vol.100-101, no.1-3, pp.398-403, 1998.
49. R.N. Dean, Jr, P.C. Nordine and C.G. Christodoulou, "3-D helical THz antennas," *Microwave and Optical Technology Letters*," vol.24, no.2, pp.106-111, 2000.
50. J. Pegna, D. Messia and W.H. Lee, "Trussed structures: Freeform fabrication without the layers," *Proceedings of the Solid Freeform Fabrication Symposium*, pp.49-58, 1997.
51. O. Lehmann and M. Stuke, "Laser-driven movement of three-dimensional microstructures generated by laser rapid prototyping," *Science*, vol.270, no.5242, pp.1644-1646, 1995.
52. S. Christiansen, T. Cui, K. Williams, J. Maxwell and M. Boman, "High speed laser chemical vapor deposition of sacrificial cores for three-dimensional microfluidic systems," in *Proceedings of the 4th International Conference on Microreaction Technology (IMRET 4)*, pp.127-132, 2000.
53. O. Lehmann and M. Stuke, "Three-dimensional laser direct writing of electrically conducting and isolating microstructures," *Materials Letters*, vol.21, no.2, pp.131-136, 1994.
54. G. Fuhr, C. Reichle, T. Müller, K. Kahlke, K. Schütze and M. Stuke, "Processing of micro-particles by UV laser irradiation in a field cage," *Applied Physics A: Materials Science and Processing*," vol.69, no.6, pp.611-616, 1999.
55. M. Stuke, K. Mueller, T. Mueller, R. Hagedorn, M. Jaeger and G. Fuhr, "Laser-direct-write creation of three-dimensional OREST microcages for contact-free trapping, handling and transfer of small polarizable neutral objects in solution,"

Applied Physics A: Materials Science and Processing, vol.81, no.5, pp.915-922, 2005.

56. K.L. Williams, "Laser-assisted CVD fabrication and characterization of carbon and tungsten microhelices for microthrusters," Doctorate thesis, Uppsala University, Uppsala, Sweden, 2006.
57. F.T. Wallenberger, P.C. Nordine and M. Boman, "Inorganic fibers and microstructures directly from the vapor phase," *Composites Science and Technology*, vol.51, no.2, pp.193-212, 1994.
58. J.L. Maxwell et al, "Process-structure map of diamond-like carbon fibers form ethane at hyperbaric pressures," *Advanced Functional Materials*, vol.15, no.7, pp.1077-1087, 2005.
59. C. Fauteux, R. Longtin, J. Pegna and M. Boman, "Microstructure and growth mechanism of laser grown carbon microrods as a function of experimental parameters," *Journal of Applied Physics*, vol.95, no.5, pp.2737-2743, 2004.
60. R. Longtin, C. Fauteux, E. Coronel, U. Wiklund, J. Pegna and M. Boman, "Nanoindentation of carbon microfibers deposited by laser-assisted chemical vapor deposition," *Applied Physics A: Materials Science and Processing*," vol.79, no.3, pp.573-577, 2004.
61. J. Doppelbauer and D. Bäuerle, "Kinetic studies of pyrolytic laser-induced chemical processes," in *Laser Proceeding and Diagnostics (II)*, pp.53-56, 1986.
62. D. Jean, C. Duty, R. Johnson, S. Bondi and W.J. Lackey, "Carbon fiber growth kinetics and thermodynamics using temperature controlled LCVD," *Carbon*, vol.40, no.9, pp.1435-1445, 2002.
63. K. Williams, N. Jaikumar, G. Saiprasanna, M. Hegler and J. Maxwell, "The laser micro chemical lathe: Rapid freeform part fabrication from the vapor phase." *Proceedings of the Solid Freeform Fabrication Symposium*, pp.543-551, 1999.

64. R. Longtin, C. Fauteux, J. Pegna and M. Boman, "Micromechanical testing of carbon fibers deposited by low-pressure laser-assisted chemical vapor deposition," *Carbon*, vol.42, no.14, pp.2905-2913, 2004.

65. J.L. Maxwell and J.Pegna. "Method and apparatus for the freeform growth of three-dimensional structures using pressurized flows and growth rate control." US Patent, US 5,786,023, 1998. [On Line]. Available in: Derwent Innovations Index, http://portal.isiknowledge.com/. [Page consulted on 24 May 2004].

66. C. Duty, R. Johnson, J. Gillespie, A. Fedorov and J. lackey, "Heat and mass-transfer modeling of an angled gas-jet LCVD system," *Applied Physics A: Materials Science and Processing*, vol.77, no.5, pp. 697-705, 2003.

67. F.T. Wallenberger and P.C. Nordine, "Strong, small diameter, boron fibers by LCVD," *Materials Letters*, vol.14, no.4, pp.198-202, 1992.

68. D.J. Ehrlich and J.Y. Tsao, "Review of laser-microchemical processing," *Journal of Vacuum Science & Technology: Microelectronics Processing and Phenomena*, vol.1, no.4, pp.969-984, 1983.

69. S.M. Copley, "Mass transport during laser chemical vapor deposition," *Journal of Applied Physics*, vol.64, no.4, pp.2064-2068, 1988.

70. J.L. Maxwell, "Three-dimensional laser-induced pyrolysis: Modelling, growth rate control, and application to micro-scale prototyping," Doctorate thesis, Rensselaer Polytechnic Institute, Troy, New York, USA, 1996.

71. C. Fauteux and J. Pegna, "Radial characterization of 3D-LCVD carbon fibers by raman spectroscopy," *Applied Physics A: Materials Science and Processing*, vol.78, no.6, pp.883-888, 2004.

72. Mathweb. [On Line]. In the site http://mathweb.com/main.php [Page consulted on 28 May 2006].

73. Joseph Pegna, "Archives of LCVD work at the Institute for Micro-manufacturing," 1998. Louisiana Tech University, Ruston, USA.

74. D.S. Kommireddy, "Laser assisted chemical vapor deposition of three-dimensional carbon microstructures," Masters thesis, Louisiana Tech University, Ruston, Louisiana, USA, 2001.

75. K.H Kwok and K.S. Chiu, "Open-air carbon coatings on fused quartz by laser-induced chemical vapor deposition," *Carbon*, vol.41, no.4, pp.673-680, 2003.

76. S. Johansson, J. Schweitz, H. Westberg and M. Boman, "Microfabrication of three-dimensional boron structures by laser chemical processing," *Journal of Applied Physics*, vol.72, no.12, pp.5956-5963, 1992.

77. Personal communication by e-mail with Prof. Dr. Mats Boman, Uppsala University, Sweden [Consulted in July 2006].

78. D.C. Horning, "A study of high-temperature autoignition and thermal decomposition of hydrocarbons," High Temperature Gasdynamics Laboratory, Stanford University, USA, Report No. TSD-135, 2001. [On Line]. Available at: http://navier.stanford.edu/thermosciences/TSD-135.pdf [Page consulted on 30 July 2006].

79. J.L. Maxwell, J. Pegna and D.V. Messia, "Real-time volumetric growth rate measurements and feedback control of three-dimensional laser chemical vapor deposition," *Applied Physics A: Materials Science and Processing*, vol.67, no.3, pp.323-329, 1998.

80. K.L. Björklund, J. Lu, P. Heszler and M. Boman, "Kinetics, thermodynamics and microstructure of tungsten rods grown by thermal laser CVD," *Thin Solid Films*, vol.416, no.1-2, pp.41-48, 2002.

81. J. Senthil Selvan and S. Jeong, "LCVD grown micro carbon rod for MEMS applications: A study on the raman spectroscopic characterization", *Proceedings of SPIE-The International Society for Optical Engineering*, vol.4936, pp.285-292, 2002.

82. J.L. Maxwell, M. Boman, R.W. Springer, J. Narayan and S. Gnanavelu, "Hyperbaric laser chemical vapor deposition of carbon fibers from the 1-alkenes,

1-alkynes, and benzene," *Journal of the American Chemical Society*, vol.128, no.13, pp.4405-4413, 2006.

83. K. Williams, J. Maxwell, K. Larsson and M. Boman, "Freeform fabrication of functional microsolenoids, electromagnets, and helical springs using high-pressure laser chemical vapor deposition," *Proceedings of the IEEE Micro Electro Mechanical Systems (MEMS)*, pp.232-237, 1999.
84. G. Leyendecker, H. Noll, D. Bäuerle, P. Geittner and H. Lydtin, "Rapid determination of apparent activation energies in chemical vapor deposition," *Journal of the Electrochemical Society*, vol.130, no.1, pp.157-160, 1983.
85. J.K. Platten, "The Soret effect: A review of recent experimental results," J Appl Mech Trans ASME, vol.73, no.1, pp.5-15, 2006.
86. WebElements. [Online]. In the site http://www.webelements.com/webelements/elements/text/H/heat.html [Page consulted on 15 December 2006].
87. Air Liquide. [Online]. In the site http://encyclopedia.airliquide.com/Encyclopedia.asp?GasID=29#GeneralData [Page consulted on 15 December 2006].